

Universität  
Rostock



Traditio et Innovatio

Estimation of Coefficients for Modelling Ships from  
Sea Trials Using Stepwise Optimization Methods and  
Considering Trim and Draught Conditions

Dissertation

zur

Erlangung des akademischen Grades

Doktor-Ingenieur (Dr.-Ing.)

der Fakultät für Maschinenbau und Schiffstechnik  
der Universität Rostock

vorgelegt von

M.Sc. Dae Won Kim

geb. am 05.01.1983 in Daegu, Südkorea

Rostock, 2019



Dieses Werk ist lizenziert unter einer  
Creative Commons Namensnennung-Nicht kommerziell 4.0 International Lizenz.

Gutachter:

Prof. Dr.-Ing. habil. Mathias Paschen, Universität Rostock, Lehrstuhl für Meerestechnik

Prof. Dr.-Ing. habil. Knud Benedict, Hochschule Wismar, Institut ISSIMS

Prof. Dr.-Ing. habil. Nikolai Kornev, Universität Rostock, Lehrstuhl für Modellierung  
und Simulation

Tag der Einreichung: 25.09.2018

Tag der Verteidigung: 03.06.2019

# **I. Selbständigkeitserklärung**

Hiermit wird bestätigt, dass die vorliegende Arbeit selbständig verfasst und keine anderen als angegeben Quellen und Hilfsmittel benutzt sowie Zitate und gedankliche Übernahmen kenntlich gemacht wurden.

Rostock, den 25.09.2018

---

Ort/Datum

Unterschrift

## II. List of contents

<b>1.</b>	<b>Introduction .....</b>	<b>1</b>
<b>2.</b>	<b>State of the art in ship manoeuvrability .....</b>	<b>4</b>
2.1	Prediction of ship manoeuvrability.....	4
2.1.1	Coordinate systems.....	4
2.1.2	Equations of a ship's manoeuvring motion .....	5
2.1.3	Representation of hydrodynamic force and moment.....	7
2.1.4	Determination of the hydrodynamic coefficients .....	10
2.2	Manoeuvring characteristics and corresponding tests .....	16
2.3	Influence of trim and draught on ship manoeuvrability .....	23
<b>3.</b>	<b>Fundamentals of mathematical optimization.....</b>	<b>38</b>
3.1	Introduction.....	38
3.2	Unconstrained optimization.....	39
3.2.1	Quasi-Newton Algorithm .....	40
3.2.2	Derivative-free optimization.....	42
3.3	Constrained optimization.....	46
3.3.1	Interior point method .....	47
3.3.2	Sequential quadratic programming method.....	49
<b>4.</b>	<b>Coefficients estimation using mathematical optimization .....</b>	<b>54</b>
4.1	Introduction.....	54
4.2	About the mathematical optimization.....	54
4.3	Setting of optimization problems.....	55



4.4	Sea trial measurements and corrections for reference data .....	59
4.5	Optimization results.....	65
4.6	Conclusion .....	76
<b>5.</b>	<b>Coefficients estimation for various trim and draught conditions .....</b>	<b>78</b>
5.1	Introduction.....	78
5.2	Optimization problems .....	78
5.3	Validation of optimization results using other sea trial data .....	81
5.4	Estimation of hydrodynamic coefficients considering various trim and draught conditions .....	91
5.5	Conclusion .....	96
<b>6.</b>	<b>Conclusion .....</b>	<b>98</b>
<b>7.</b>	<b>References.....</b>	<b>100</b>
<b>Appendix A.</b>	<b>Details of manoeuvres for chapter 5 .....</b>	<b>105</b>

### III. List of figures

Figure 2.1 Coordinate systems .....	5
Figure 2.2 Methods of manoeuvring prediction .....	10
Figure 2.3 Effort/Cost versus accuracy of manoeuvring prediction methods .....	11
Figure 2.4 System identification for estimating hydrodynamic coefficients by Abkowitz ...	14
Figure 2.5 System identification for estimating hydrodynamic coefficients by Rhee et al. ..	15
Figure 2.6 Inherent dynamic stability .....	17
Figure 2.7 Course-keeping ability .....	17
Figure 2.8 Trajectory of the ship during turning .....	20
Figure 2.9 Time histories of rudder angle and heading during zig-zag test .....	21
Figure 2.10 Trajectory of the ship during stopping test .....	21
Figure 2.11 Yaw rate to rudder angle curve from spiral tests .....	22
Figure 2.12 Time histories of the turning rate from pull-out test .....	22
Figure 2.13 User interface for hull coefficients in SIMOPT .....	25
Figure 2.14 Comparison of trajectories for turning manoeuvre with 35 degrees of rudder angle according to changes of mean draught.....	26
Figure 2.15 Comparison of trajectories for zig-zag manoeuvre with 10 degrees of rudder angle according to changes of mean draught.....	28
Figure 2.16 Comparison of heading changes for zig-zag manoeuvre with 10 degrees of rudder angle according to changes of mean draught .....	29
Figure 2.17 Comparison of trajectories for zig-zag manoeuvre with 20 degrees of rudder angle according to changes of mean draught.....	29
Figure 2.18 Comparison of heading changes for zig-zag manoeuvre with 20 degrees of rudder angle according to changes of mean draught .....	30
Figure 2.19 Comparison of trajectories for turning manoeuvre with 35 degrees of rudder angle according to changes of trim.....	31
Figure 2.20 Comparison of trajectories for zig-zag manoeuvre with 10 degrees of rudder angle according to changes of trim .....	32

Figure 2.21 Comparison of heading changes for zig-zag manoeuvre with 10 degrees of rudder angle according to changes of trim .....	33
Figure 2.22 Comparison of trajectories for zig-zag manoeuvre with 20 degrees of rudder angle according to changes of trim .....	33
Figure 2.23 Comparison of heading changes for zig-zag manoeuvre with 20 degrees of rudder angle according to changes of trim .....	34
Figure 2.24 Manoeuvre results with various trim conditions.....	35
Figure 2.25 Concepts of pivot point .....	36
Figure 3.1 Concept of the mathematical optimization .....	38
Figure 3.2 Simplexes for $n = 2$ (left) and $n = 3$ (right).....	44
Figure 3.3 Concept operation for the Nelder-Mead algorithm.....	44
Figure 4.1 Concept of optimization process to estimate hydrodynamic coefficients.....	55
Figure 4.2 Results of sensitivity analysis on hydrodynamic coefficients.....	58
Figure 4.3 Means of data acquisition: S-VDR and ECDIS .....	62
Figure 4.4 Comparisons of measurement data and corrected data .....	64
Figure 4.5 Comparison of optimization algorithms: straight motion .....	68
Figure 4.6 Comparison of optimization algorithms: zig-zag manoeuvre.....	69
Figure 4.7 Comparison of optimization algorithms: turning manoeuvre .....	69
Figure 4.8 Comparison of trajectories: straight motion.....	70
Figure 4.9 Comparison of trajectories: zig-zag motion.....	71
Figure 4.10 Comparison of heading change: zig-zag manoeuvre .....	71
Figure 4.11 Comparison of trajectories: turning manoeuvre.....	72
Figure 4.12 Comparison of heading change for optimization steps 2 and 3: Interior point algorithm with constraint.....	73
Figure 4.13 Comparison of heading change for optimization steps 2 and 3: Interior point algorithm without constraint.....	73
Figure 4.14 Comparison of heading change for optimization steps 2 and 3: Nelder-Mead algorithm.....	74

Figure 4.15 History of iteration: straight motion.....	75
Figure 4.16 History of iteration: zig-zag manoeuvre .....	75
Figure 4.17 History of iterations: turning manoeuvre .....	76
Figure 5.1 Comparison of heading change between sea trial data 2 and simulation results..	83
Figure 5.2 Comparison of trajectories between sea trial data 2 and simulation results ..	83
Figure 5.3 Comparison of heading change between sea trial data 3 and simulation results..	84
Figure 5.4 Comparison of trajectories between sea trial data 3 and simulation results ..	84
Figure 5.5 Comparison of heading change between sea trial data 4 and simulation results..	85
Figure 5.6 Comparison of trajectories between sea trial data 4 and simulation results ..	85
Figure 5.7 Comparison of heading change between sea trial data 1 and various simulations	89
Figure 5.8 Comparison of trajectories between sea trial data 1 and various simulations	90
Figure 5.9 Comparison of heading change between sea trial data 5 and various simulations	90
Figure 5.10 Comparison of trajectories between sea trial data 5 and various simulations....	91
Figure 5.11 Results of curve fitting for $X_{uu}$ and $X_{u4}$ .....	94
Figure 5.12 Comparison of heading change for the simulation results of Clarke estimation and suggested formula .....	96

## IV. List of tables

Table 2.1 Characteristics for methods of manoeuvrability prediction .....	13
Table 2.2 Recommended manoeuvring tests by various organisations.....	19
Table 2.3 Influence of draught changes on turning manoeuvre .....	26
Table 2.4 Influence of draught changes on zig-zag manoeuvre with 10 degrees of rudder angle.....	27
Table 2.5 Influence of draught changes on zig-zag manoeuvre with 20 degrees of rudder angle.....	28
Table 2.6 Influence of trim changes on turning manoeuvre.....	30
Table 2.7 Influence of trim changes on zig-zag manoeuvre with 10 degrees of rudder angle.....	31
Table 2.8 Influence of trim changes on zig-zag manoeuvre with 20 degrees of rudder angle.....	32
Table 4.1 Results of sensitivity analysis on hydrodynamic coefficients .....	57
Table 4.2 Variables on each optimization step.....	59
Table 4.3 Details of the reference vessel for comparing optimization algorithms.....	59
Table 4.4 Summary of conditions for sea trials.....	60
Table 4.5 Time history for zig-zag manoeuvre .....	61
Table 4.6 Time history for turning manoeuvre.....	61
Table 4.7 Detailed conditions of optimization .....	65
Table 4.8 Summarization of Clarke coefficients and optimized coefficients.....	66
Table 4.9 Manoeuvre characteristics of reference data and simulation results .....	67
Table 5.1 Details of the reference vessel.....	78
Table 5.2 Summary of conditions for sea trials.....	79
Table 5.3 Variables on each optimization step.....	79
Table 5.4 Detailed conditions of optimization .....	80
Table 5.5 Summarization of Clarke coefficients and optimized coefficients.....	81

Table 5.6 Manoeuvre characteristics for reference data and simulation results.....	82
Table 5.7 Comparison of optimized coefficients for two sea trial data which have the same trim and draught condition (Case of the data 1 and 2) .....	86
Table 5.8 Comparison of optimized coefficients for two sea trial data which have the same trim and draught condition (Case of the data 4 and 5) .....	87
Table 5.9 Comparison of manoeuvre characteristics for simulation results and sea trial data (Case of the data 1 and 2).....	88
Table 5.10 Comparison of manoeuvre characteristics for simulation results and sea trial data (Case of the data 4 and 5).....	89
Table 5.11 Correction values for estimation formulae which are based on three sea trial measurements .....	93
Table 5.12 Environmental conditions for the sea trial for validation of the estimation formulae .....	94
Table 5.13 Comparison of coefficients between Clarke estimation and suggested formulas .....	95
Table 5.14 Comparison of manoeuvre characteristics for the simulation results of Clarke estimation and suggested formula .....	96

## V. List of abbreviations

ANS	Advanced Nautical Simulator
BFGS	Broyden-Fletcher-Goldfarb-Shanno algorithm
CFD	Computational Fluid Dynamics
DFP	Davidon-Fletcher-Powell formula
DWT	Deadweight Tonnage
EFK	Extended Kalman Filter
G/T	Gross Tonnage
IMO	International Maritime Organization
ISTTES	(Project name) <u>I</u> ntegrative <u>S</u> imulationsanwendung unter Beachtung von <u>T</u> rimm- und <u>T</u> iefgangänderungen zur <u>e</u> ffektiven <u>S</u> chiffssteuerung und Verbesserung der Handlungssicherheit in Gefahrensituationen
ITTC	International Towing Tank Conference
KKT	Karush-Kuhn-Tucker conditions
LCF	Longitudinal Centre of Flotation
LPP	Length Between Perpendiculars
MMG	Mathematical Modelling Group
NMEA	Nautical Marine Electronics Association
RANS	Reynolds-averaged Navier-Stokes equations
SHS	Ship Handling Simulator
SQP	Sequential Quadratic Programming
VDR	Voyage Data Recorder

# 1. Introduction

The development of overall science has been accompanied with the progress of computer technology since the middle of the 20<sup>th</sup> century. Advanced mathematical model on ship's behaviour can explain complex physical phenomena more easily, and the computer technology can introduce various derivative ideas.

This can have a great influence on both a construction and a navigation of a ship. From the ship's design to its actual operation, various forms of application of information processing technology are no longer surprising matters. The improvement of the computer performance can be seen in the estimation of ship's manoeuvrability, more precisely the estimation of hydrodynamic coefficients acting on ship's hull. In the initial ship design stage, it is possible to precheck the ship's manoeuvrability and seaworthiness, and to reflect them in the actual ship construction. This can lead to positive effects such as reliable ship, cost reduction and process innovation.

In 2006, the international towing tank conference (ITTC) provided state-of-art for predicting the manoeuvring behaviour of ships. Most of the methods except for the database method and the free model test are system based manoeuvring simulation or computational fluid dynamics (CFD) based estimation methods. All above methods estimate the ship's hydrodynamic coefficients based on the ship's equations of motion, and these can be utilized to estimate ship's manoeuvrability. Among these, the most popular methods used in the early design stage are the captive model test and CFD based manoeuvring simulation. The above methods are enabling to conduct experiments without using a full-scale sized model, and it is possible to estimate hydrodynamic coefficients and corresponding manoeuvrability of proper reliability.

However, this ship manoeuvrability estimation can be applied differently for existing ships. The system based manoeuvring simulation for the estimation of ship manoeuvrability is applied to various purposes in conjunction with the computer development mentioned above. Simulation based ship handling training has made great progress in the education and training of seafarers. A sailing decision support program, which uses simulations and network technologies, collects data from various navigation equipment to enable safer and more effective ship operation. Unmanned or autonomous vessels, which are currently under active research, reflect this trend well.



Estimation of the ship's hydrodynamic coefficients can also be done through full-scale sea trial. This is the only way to estimate the hydrodynamic coefficients without additional tests such as model tests and CFD. This can be done through a mathematical procedure called system identification. This mathematical process conducts optimization for the hydrodynamic coefficients to represent ship's manoeuvrability in a mathematical way. Abkowitz, Oltmann and Hess conducted representative studies related to this, and the follow-up studies are still carried out at present.

Normally, estimation of hydrodynamic coefficients is conducted according to the specific loading conditions of the ship. In other words, ship's manoeuvrability and its corresponding coefficients can be considered to one specific trim and draught condition of the ship at the time. However, in practice, ships operate with various trim and draught conditions. In some cases, situations may arise where all trim and draught conditions need to be considered, depending on the purpose of the simulation.

Therefore, this thesis proposes a method for estimation of the hydrodynamic coefficients using full-scale sea trial and a method of system identification. Also, based on this, a proposal for a new estimation method that can consider various trim and draught conditions will be given here. The new estimation method will be in the form of suggesting an additional calibration formula that can complement the existing empirical estimation formulas for the hydrodynamic coefficients involving different trim and draught parameters. This makes it possible to estimate a simpler and more efficient estimation of the hydrodynamic coefficients from sea trials.

This thesis is composed as follows. Chapter 2 describes the theoretical background for estimating ship manoeuvrability. The ship's coordinate system, equations of motion, hydrodynamic coefficients acting on the hull, and influence of trim and draught on ship's manoeuvrability are included.

Chapter 3 introduces the mathematical optimization, which is a method for estimating the hydrodynamic coefficients acting on the hull for this thesis. After introducing the basic concepts of the mathematical optimization, an introduction to the representative algorithms of constrained and unconstrained optimization is described in this chapter.

Chapter 4 applies the algorithms introduced in Chapter 3 to actual sea trial data and the optimization results are compared and verified. Details of the sea trial vessel, trial procedures and comparison of optimization results are discussed in this chapter.

Chapter 5 conducts the mathematical optimization with an interior point algorithm, which is finally chosen from the algorithm comparison in Chapter 4. Five sea trial data with three different trim and draught conditions are used for the optimization. Based on the optimization result, the trim and draft correction coefficients are calculated and a correction formula for the final coefficient estimation is suggested.

Chapter 6 describes the final summary and future work based on the previous contents.

## 2. State of the art in ship manoeuvrability

In this chapter concepts, following definitions and corresponding literature study are discussed:

- Coordinate systems
- Equations of motions
- Hydrodynamic coefficients
- Manoeuvring characteristics and trials
- Influence of trim and draught

### 2.1 Prediction of ship manoeuvrability

A ship simulation has been developed with an improvement of computer processing technology. It has become possible to more effectively and simply estimate the manoeuvrability of the ship during its initial design stage. Even in the case of existing vessels, the simulation can be used for various purposes such as training and navigation decision support. Ship modelling in a mathematical way, especially for estimating hydrodynamic coefficients acting on the hull, is one of the most important processes to realize this.

#### 2.1.1 Coordinate systems

Two right-handed three degrees of freedom coordinate systems, the earth-fixed coordinate  $O_0 - x_0y_0z_0$  and the ship-fixed coordinate  $O - xyz$  are selected to estimate ship's manoeuvrability. Both the  $O_0 - x_0y_0$  and the  $O - xy$  horizontal planes placed on the undisturbed free surface and velocities for heave, rolling and pitching are ignored. Figure 2.1 shows an overview of the coordinate systems. Vertical axes  $z_0$  and  $z$  are directed downwards:

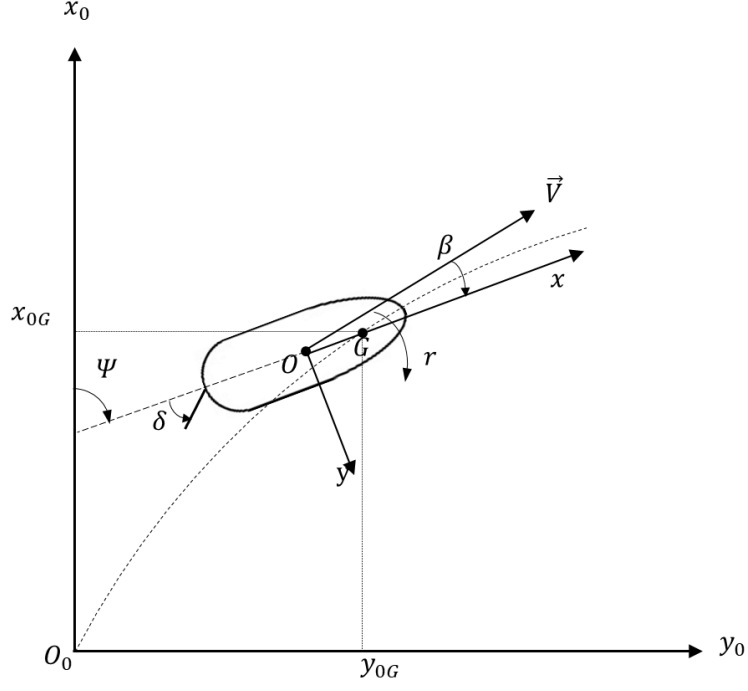


Figure 2.1 Coordinate systems

where  $\Psi$  is a heading angle,  $\beta$  is a drift angle,  $\delta$  is a rudder angle,  $\vec{V}$  is ship's speed and  $r$  is yaw rate, respectively. Heading can be determined by an angle between  $x_0$  and  $x$  axes. A ship's position in each moment is determined by the ship's centre of gravity in the earth-fixed coordinate system. The drift angle is determined by an angle between a direction of speed  $\vec{V}$  and the  $x$  axis. The ship's speed  $\vec{V}$  is expressed by a combination of axial speeds  $u$  and  $v$ . The axial speeds can be calculated as follows:

$$\begin{aligned} u &= |\vec{V}| \cos \beta \\ v &= -|\vec{V}| \sin \beta. \end{aligned} \quad (1)$$

### 2.1.2 Equations of a ship's manoeuvring motion

Equations of a ship's motion are based on the Newton's second law. In the inertial coordinate, the earth-fixed coordinate, the equations can be defined as follows [1]:

$$\begin{aligned} X_0 &= m\ddot{x}_{0G} \\ Y_0 &= m\ddot{y}_{0G} \\ N_0 &= I_{zG}\ddot{\Psi}, \end{aligned} \quad (2)$$

where

$X_0, Y_0$ : component of external force acting on  $x_0$  and  $y_0$  axis, respectively,

$N_0$ : component of external moment for z axis,

$m$ : mass of a ship,

$\ddot{x}_{0G}, \ddot{y}_{0G}$ : component of acceleration acting on  $x_0$  and  $y_0$  axis, respectively,

$I_{zG}$ : moment of inertia of a ship about the z axis and

$\ddot{\Psi}$ : yaw acceleration.

Equation (2), which is focused on the earth-fixed coordinates, can be converted into equations in the body-fixed coordinates. External forces acting on  $x$  and  $y$  axes are the following:

$$\begin{aligned} X &= X_0 \cos \Psi + Y_0 \sin \Psi \\ Y &= -X_0 \sin \Psi + Y_0 \cos \Psi. \end{aligned} \quad (3)$$

The right side of Equation (3) can be transformed to terms of kinetic parameters for the ship-fixed coordinate by applying relations between kinematic parameters for both coordinates. Components of speed in the earth-fixed coordinate are expressed by a ship's longitudinal and lateral speed components,  $u_G$  and  $v_G$ , and heading  $\Psi$ :

$$\begin{aligned} \dot{x}_0 &= u_g \cos \Psi - v_g \sin \Psi \\ \dot{y}_0 &= u_g \sin \Psi + v_g \cos \Psi. \end{aligned} \quad (4)$$

Components of acceleration in the earth-fixed coordinate can be provided by differentiating Equation (4):

$$\begin{aligned} \ddot{x}_0 &= \dot{u}_g \cos \Psi - \dot{u}_g \dot{\Psi} \sin \Psi - \dot{v}_g \sin \Psi - \dot{v}_g \dot{\Psi} \cos \Psi \\ \ddot{y}_0 &= \dot{u}_g \sin \Psi + \dot{u}_g \dot{\Psi} \cos \Psi + \dot{v}_g \cos \Psi - \dot{v}_g \dot{\Psi} \sin \Psi. \end{aligned} \quad (5)$$

Equation (3) can be converted into the equations in the body-fixed coordinate by substituting Equations (2) and (5):

$$\begin{aligned} X &= m(\dot{u}_g - v_g \dot{\Psi}) \\ Y &= m(\dot{v}_g + u_g \dot{\Psi}). \end{aligned} \quad (6)$$

Considering a ship is symmetrical based on a hydrodynamic centre, it is more convenient to place the ship-fixed coordinate on the midship point than the ship's centre of gravity. Then, the ship's new longitudinal and lateral speed components are as follows:

$$\begin{aligned} u_g &= u \\ v_g &= v + x_g \dot{\Psi}. \end{aligned} \quad (7)$$

The equations of motion in the body-fixed coordinate, placed on the midship point, are as follows.

$$\begin{aligned} X &= m(\dot{u} - v\dot{\Psi} - x_g \dot{\Psi}^2) \\ Y &= m(\dot{v} + u\dot{\Psi} + x_g \ddot{\Psi}) \end{aligned} \quad (8)$$

The external moment acting on the z axis and moment of inertia in the ship-fixed coordinate can be modified from the moment acting on the earth-fixed coordinate and the longitudinal centre of gravity position.

$$\begin{aligned} N &= N_0 + Yx_g \text{ and } I_z = I_{zG} + mx_g^2 \\ \text{then, } N &= I_z \ddot{\Psi} + mx_g(\dot{v} + ur) \end{aligned} \quad (9)$$

The first-order differential for the heading can be converted into the yaw rate  $r$ . The equations of motion in the ship-fixed coordinate, lying on the ship's midship point, can be finally provided as follows.

$$\begin{aligned} X &= m(\dot{u} - vr - x_g r^2) \\ Y &= m(\dot{v} + ur + x_g \dot{r}) \\ N &= I_z \dot{r} + mx_g(\dot{v} + ur) \end{aligned} \quad (10)$$

### 2.1.3 Representation of hydrodynamic force and moment

Various studies on expression of hydrodynamic force and moment have been carried out by many researchers. These can be classified into two kinds: a polynomial model and a modular model.

**Model by Abkowitz** Abkowitz presented polynomials for the hydrodynamic force and moment, which is based on the Tayler series. He premises that forces can be determined by instantaneous values of kinematic parameters, without unsteady effects [2]. This

means that the unsteady influences can be ignored when a time step for hydrodynamic changes is extremely smaller than the one for the ship's motion. The polynomials are functions of the kinematic parameters and rudder angle:

$$X, Y \text{ and } N = f(u, v, r, \dot{u}, \dot{v}, \dot{r}, \delta). \quad (11)$$

Abkowitz suggested polynomials based on a third-order Taylor series, as follows [3]:

$$\begin{aligned} X = X_0 &+ \frac{\partial X}{\partial \dot{u}} \dot{u} + \frac{\partial X}{\partial u} \Delta u + \frac{1}{2} \frac{\partial^2 X}{\partial u^2} (\Delta u)^2 + \frac{1}{2} \frac{\partial^2 X}{\partial v^2} v^2 + \frac{1}{2} \frac{\partial^2 X}{\partial r^2} r^2 + \frac{1}{2} \frac{\partial^2 X}{\partial \delta^2} \delta^2 \\ &+ \frac{1}{2} \frac{\partial^2 X}{\partial vr} vr + \frac{1}{2} \frac{\partial^2 X}{\partial v\delta} v\delta + \frac{1}{2} \frac{\partial^2 X}{\partial r\delta} r\delta + \frac{1}{6} \frac{\partial^3 X}{\partial u^3} (\Delta u)^3 + \frac{1}{6} \frac{\partial^3 X}{\partial v^2 u} v^2 \Delta u \\ &+ \frac{1}{6} \frac{\partial^3 X}{\partial r^2 u} r^2 \Delta u + \frac{1}{6} \frac{\partial^3 X}{\partial \delta^2 u} \delta^2 \Delta u + \frac{1}{6} \frac{\partial^3 X}{\partial vru} vr \Delta u + \frac{1}{6} \frac{\partial^3 X}{\partial v\delta u} v\delta \Delta u \\ &+ \frac{1}{6} \frac{\partial^3 X}{\partial r\delta u} r\delta \Delta u \end{aligned} \quad (12)$$

$$\begin{aligned} Y = Y_0 &+ \frac{\partial Y}{\partial \dot{v}} \dot{v} + \frac{\partial Y}{\partial \dot{r}} \dot{r} + \frac{\partial Y}{\partial u} \Delta u + \frac{\partial Y}{\partial v} v + \frac{\partial Y}{\partial r} r + \frac{\partial Y}{\partial \delta} \delta + \frac{1}{2} \frac{\partial^2 Y}{\partial u^2} (\Delta u)^2 \\ &+ \frac{1}{2} \frac{\partial^2 Y}{\partial vu} v \Delta u + \frac{1}{2} \frac{\partial^2 Y}{\partial ru} r \Delta u + \frac{1}{2} \frac{\partial^2 Y}{\partial \delta u} \delta \Delta u + \frac{1}{6} \frac{\partial^3 Y}{\partial v^3} v^3 + \frac{1}{6} \frac{\partial^3 Y}{\partial r^3} r^3 \\ &+ \frac{1}{6} \frac{\partial^3 Y}{\partial \delta^3} \delta^3 + \frac{1}{6} \frac{\partial^3 Y}{\partial vu^2} v (\Delta u)^2 + \frac{1}{6} \frac{\partial^3 Y}{\partial vr^2} vr^2 + \frac{1}{6} \frac{\partial^3 Y}{\partial v\delta^2} v\delta^2 \\ &+ \frac{1}{6} \frac{\partial^3 Y}{\partial ru^2} r (\Delta u)^2 + \frac{1}{6} \frac{\partial^3 Y}{\partial rv^2} rv^2 + \frac{1}{6} \frac{\partial^3 Y}{\partial r\delta^2} r\delta^2 + \frac{1}{6} \frac{\partial^3 Y}{\partial \delta u^2} \delta (\Delta u)^2 \\ &+ \frac{1}{6} \frac{\partial^3 Y}{\partial \delta v^2} \delta v^2 + \frac{1}{6} \frac{\partial^3 Y}{\partial \delta r^2} \delta r^2 + \frac{1}{6} \frac{\partial^3 Y}{\partial vr\delta} vr\delta \end{aligned} \quad (13)$$

$$\begin{aligned} N = N_0 &+ \frac{\partial N}{\partial \dot{v}} \dot{v} + \frac{\partial N}{\partial \dot{r}} \dot{r} + \frac{\partial N}{\partial u} \Delta u + \frac{\partial N}{\partial v} v + \frac{\partial N}{\partial r} r + \frac{\partial N}{\partial \delta} \delta + \frac{1}{2} \frac{\partial^2 N}{\partial u^2} (\Delta u)^2 \\ &+ \frac{1}{2} \frac{\partial^2 N}{\partial vu} v \Delta u + \frac{1}{2} \frac{\partial^2 N}{\partial ru} r \Delta u + \frac{1}{2} \frac{\partial^2 N}{\partial \delta u} \delta \Delta u + \frac{1}{6} \frac{\partial^3 N}{\partial v^3} v^3 + \frac{1}{6} \frac{\partial^3 N}{\partial r^3} r^3 \\ &+ \frac{1}{6} \frac{\partial^3 N}{\partial \delta^3} \delta^3 + \frac{1}{6} \frac{\partial^3 N}{\partial vu^2} v (\Delta u)^2 + \frac{1}{6} \frac{\partial^3 N}{\partial vr^2} vr^2 + \frac{1}{6} \frac{\partial^3 N}{\partial v\delta^2} v\delta^2 \\ &+ \frac{1}{6} \frac{\partial^3 N}{\partial ru^2} r (\Delta u)^2 + \frac{1}{6} \frac{\partial^3 N}{\partial rv^2} rv^2 + \frac{1}{6} \frac{\partial^3 N}{\partial r\delta^2} r\delta^2 + \frac{1}{6} \frac{\partial^3 N}{\partial \delta u^2} \delta (\Delta u)^2 \\ &+ \frac{1}{6} \frac{\partial^3 N}{\partial \delta v^2} \delta v^2 + \frac{1}{6} \frac{\partial^3 N}{\partial \delta r^2} \delta r^2 + \frac{1}{6} \frac{\partial^3 N}{\partial vr\delta} vr\delta, \end{aligned} \quad (14)$$

where  $X_0, Y_0$  and  $N_0$  are derivatives for the initial steady state, where longitudinal speed only exists. Derivatives in Equations (12) to (14) can be shorten as follows:

$$\frac{\partial X}{\partial u} = X_u, \quad \frac{\partial^3 Y}{\partial v r^2} = Y_{vrr}, \quad \frac{\partial^3 N}{\partial v r \delta} = N_{vr\delta}, \dots \quad (15)$$

**Model by Norrbin** Norrbin provided a mathematical model, which is a transitional model between a polynomial and a modular model [4]. The model includes functions for speed components for three axes, a thrust  $T$ , a propeller torque  $Q$  and an inflow velocity to the rudder  $c$ . A wake and thrust deduction factors are independent from the propeller loading. Norrbin's equations are as follows [5]:

$$T = T(u, n) \quad (16)$$

$$Q = Q(u, n)$$

$$c = c(u, n)$$

$$X = X_u \dot{u} + X_{uu} u^2 + X_{vr} vr + X_{vv} v^2 \\ + X_{c|c|\delta\delta} c|c|\delta^2 + X_{c|c|\beta\delta} c|c|\beta\delta + (1 - t)T$$

$$Y = Y_{\dot{v}} \dot{v} + Y_{ur} ur + Y_{uv} uv + Y_{v|v|} v|v| + Y_{c|\delta^2} c|c|\delta^2 \\ + Y_{c|c||\beta||\delta|} c|c||\beta||\delta| + Y_T T$$

$$N = N_{\dot{r}} \dot{r} + N_{ur} ur + N_{uv} uv + N_{v|r|} v|r| + N_{c|\delta} c|c|\delta \\ + N_{c|c||\beta||\beta||\delta|} c|c||\beta||\beta||\delta| + N_T T$$

$$T = T_{uu} u^2 + T_{un} un + T_{n|n|} n|n|$$

$$(I_P - Q_n) \dot{n} = Q_F + Q_{uu} u^2 + Q_{un} un + Q_{n|n|} n|n| + Q_n n + Q_\mu \mu$$

$$c = c_{un} un + c_{nn} n^2, \quad n > 0$$

$$c = 0, \quad n < 0$$

where,  $\mu$  is an engine output ratio. Considering lateral and rotational direction for the symmetrical hull, a form of the absolute value,  $|a|$ , is applied.

**MMG modular model** A research group focused on the 'standardization of a mathematical model for ship manoeuvring predictions' was created by the Japan Society of Naval Architects and Ocean Engineers, and this group provided the current Manoeuvring Modelling Group (MMG) model [6]. Each hydrodynamic force or moment has three



modules, which are acting on the ship hull, the propeller and the rudder, respectively. Each component concerns both individual and interacting effects.

$$X = X_H + X_P + X_R \quad (17)$$

$$Y = Y_H + Y_P + Y_R$$

$$N = N_H + N_P + N_R$$

#### 2.1.4 Determination of the hydrodynamic coefficients

ITTC summarized the state-of-the-art of the ship's manoeuvring prediction methods. Figure 2.2 shows an overview of methods for manoeuvring predictions and Figure 2.3 shows an overview of accuracy against cost. Methods can be categorized into three features: a prediction without simulation, with system based manoeuvring simulation and CFD based manoeuvring simulation.

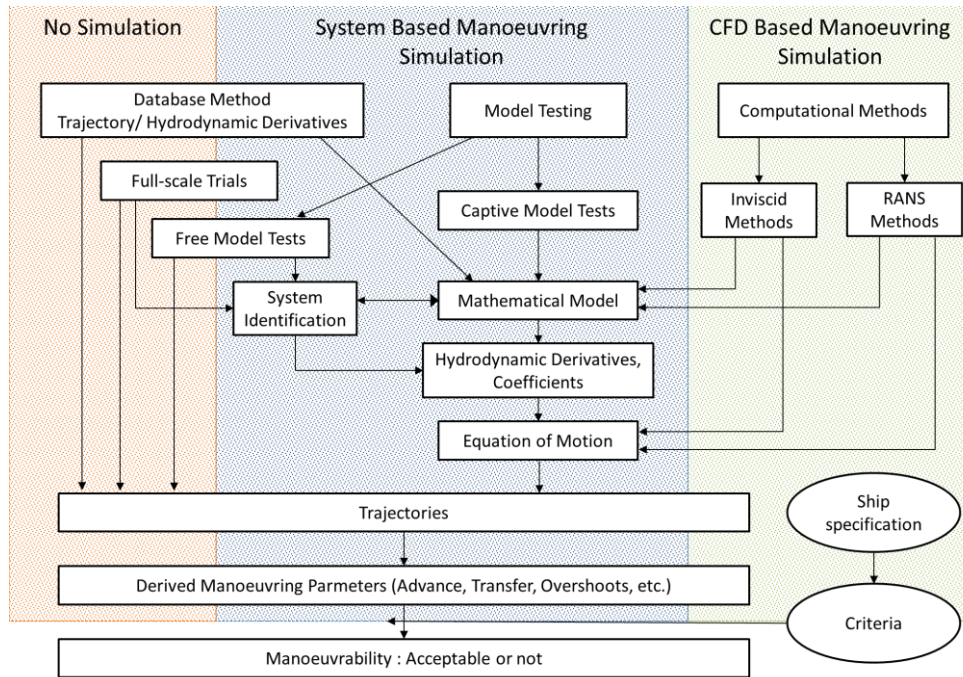


Figure 2.2 Methods of manoeuvring prediction [7]

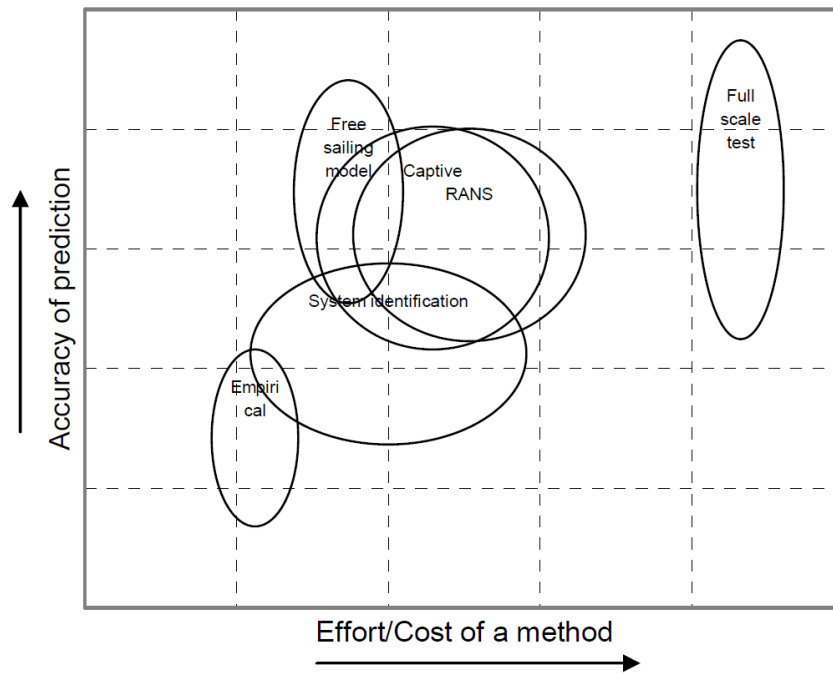


Figure 2.3 Effort/Cost versus accuracy of manoeuvring prediction methods [7]

The full-scale trial is an intuitive way to figure out manoeuvrability of an object. Nomoto estimated indices of  $K$  and  $T$ , which are steering coefficients for rudder effect and ship's reaction inertia, from the analysis of full-scale zig-zag trials, using linear equation of motion [8,9]. Inoue et al. conducted sea trials with various types of vessels and those manoeuvring results were compared to numerical simulation results [10]. The most famous trial is conducted by the 278,000 DWT tanker ESSO Osaka in confined waters by Crane [11]. He showed an impact of the bottom clearance on ship's manoeuvrability and his approach greatly influenced the methods and procedures for sea trial to estimate manoeuvrability. However, this method is not possible to control environmental effects thoroughly and is hard for merchant vessels due to economic reasons.

The model tests are an alternative way to complement deficiencies of the full-scale trial. Forces and kinetic parameters are measured during the trials and there the hydrodynamic coefficients can be derived for certain mathematical model of a vessel. In a model basin, which includes a towing tank and a cavitation tunnel and others, scaled models are tested and resultant forces and corresponding parameters can be measured. A set of model tests can also be applied into empirical regression and corresponding formulas. Norrbin, Inoue et al., Clarke et al., Kijima et al. and Kose proposed foundations of empirical formulas

for the hydrodynamic coefficients of the equations of motion and subsequent researches are still continuing [5,10,12–14].

CFD techniques can provide insight into the ship with the application of computational calculation. Since 1960s, after Hess and Smith introduced three-dimensional CFD model in aviation, CFD has shown outstanding progress with the advancement of computing technology [15]. Compared to the conventional model tests, this method can react to lots of models and external conditions easily. CFD for the shipbuilding industry was introduced later than the aviation, because of the existence of free surface and complex ship geometry [16].

In spite developing a numerical calculation, conventional model tests are still the main source to examine manoeuvring force and moment. As shown in Figure 2.3, the conventional model tests are the best solutions to satisfy both accuracy and cost without bias to either side, when a designated ship is at the early design stage or under construction. On the other hand, the methods above are relatively more expensive than the system identification method.

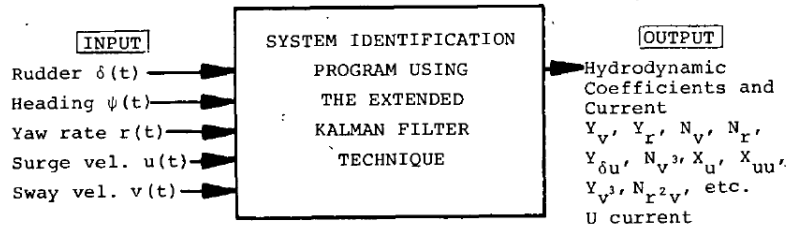
Table 2.1 summarizes characteristics for the predictions methods by ITTC [7]. This study applies a system identification method, which optimizes the hydrodynamic coefficients in a way of mathematical optimization. The optimization procedure requires a set of references and initial conditions. These are delivered from real ship sea trials and existing empirical estimation formulas, which are based on the idea of Norrbin and Clarke [5,12].

The system identification has developed with the progress of computational calculation. Abkowitz used the extended Kalman filter (EKF) to estimate hydrodynamic coefficients for the ESSO Osaka [17]. The resultant coefficients and an effective simulation showed that results of the numerical simulation were fitted to motions during the sea trials.

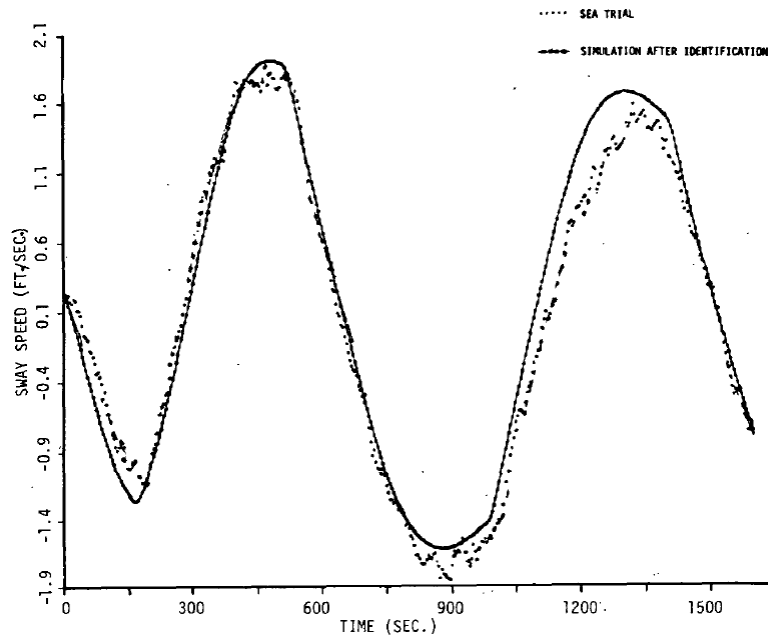
Table 2.1 Characteristics for methods of manoeuvrability prediction

Method	Concept	Advantage	Disadvantage
Free model test	<ul style="list-style-type: none"> <li>- Perform pre-defined manoeuvres, such as zig-zag or turning manoeuvres</li> <li>- Model ship's actuators are controlled by autopilots</li> </ul>	<ul style="list-style-type: none"> <li>- Close to reality</li> <li>- Test results are delivered in real time</li> <li>- Relatively low cost</li> <li>- Possibility for control of environmental conditions in a basin</li> </ul>	<ul style="list-style-type: none"> <li>- Require relatively large test area</li> <li>- Impossible to deliver physical insight</li> <li>- Impossible to connect to mathematical models</li> <li>- Environmental effects also should be considered a scale effect</li> </ul>
Captive model test	<ul style="list-style-type: none"> <li>- Carried out in a tow tank, with planar motion mechanism and rotating arm device</li> <li>- Hydrodynamic coefficients can be obtained from analysing test results</li> </ul>	<ul style="list-style-type: none"> <li>- Perfect control of environmental effects during tests</li> <li>- Created mathematical model can also be utilized for bridge simulators</li> </ul>	<ul style="list-style-type: none"> <li>- Desired result can be delivered after post-processing of test results</li> <li>- Quality of the mathematical model is dependent on the size of test matrix</li> <li>- Test should be carried out by skilled personnel to reduce re-test, which needs a lot of time</li> </ul>
Empirical method	<ul style="list-style-type: none"> <li>- Estimate hydrodynamic coefficients based on multiple previous tests</li> <li>- Test results are utilized in the fast-time and real-time simulators</li> </ul>	<ul style="list-style-type: none"> <li>- Short processing time</li> <li>- Relatively low cost</li> <li>- Easy to change certain parameters of a ship</li> </ul>	<ul style="list-style-type: none"> <li>- The accuracy and reliability are quite low</li> <li>- Sensitive to the shallow water effect</li> <li>- Consideration of hull form detail is missing</li> </ul>
System identification	<ul style="list-style-type: none"> <li>- Estimate hydrodynamic coefficients by mathematical optimization</li> <li>- Utilize sea trial measurements into parameter identification directly</li> </ul>	<ul style="list-style-type: none"> <li>- Apply to generate additional manoeuvres based on results of free model tests</li> <li>- Applicable for both model-scale and full-scale manoeuvres</li> </ul>	<ul style="list-style-type: none"> <li>- Resultant coefficients are not physically correct</li> <li>- Acquired raw data might have noise and this can interfere to a process</li> </ul>
Viscous flow CFD	<ul style="list-style-type: none"> <li>- RANS calculation takes a role of the captive model test</li> </ul>	<ul style="list-style-type: none"> <li>- Physical model is not required</li> <li>- CFD gives physical insight</li> <li>- Applicable for both model-scale and full-scale tests</li> </ul>	<ul style="list-style-type: none"> <li>- Much experience is required for stable test results</li> <li>- A large amount of expertise and coding is required</li> </ul>
Potential flow CFD	<ul style="list-style-type: none"> <li>- CFD methods, which does not apply RANS calculation</li> </ul>	<ul style="list-style-type: none"> <li>- Require less effort than the RANS method</li> </ul>	<ul style="list-style-type: none"> <li>- Reliability is lower than the RANS method</li> </ul>

- "Measurement" or Identification of the Magnitude of the Hydrodynamic Coefficients from the Measurement of the Ship Response to Given Rudder Action.



(a) Concept of the coefficients identification

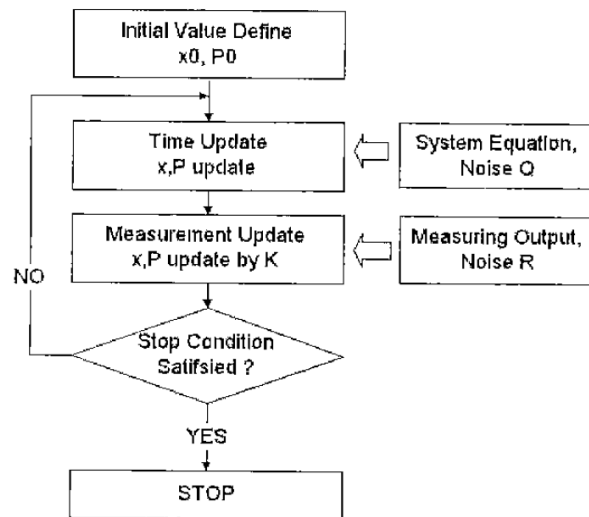


(b) Heading simulation of zig-zag manoeuvre  $20^\circ/20^\circ$  after the identification

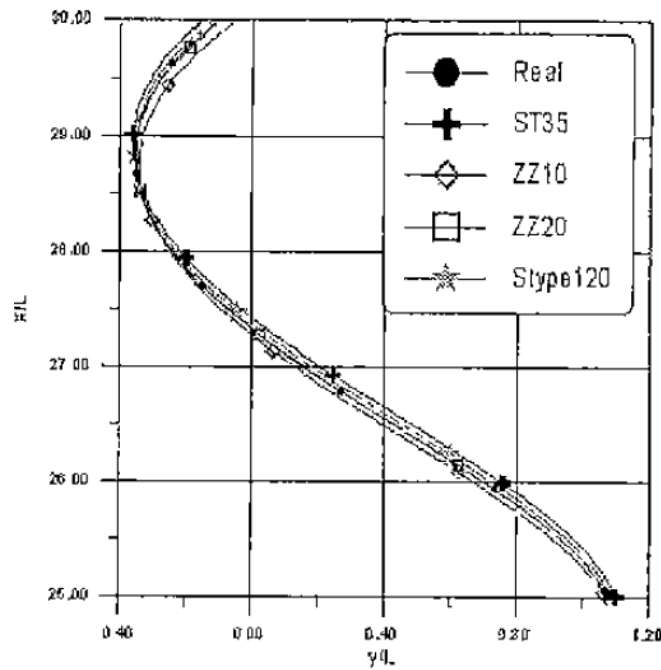
Figure 2.4 System identification for estimating hydrodynamic coefficients by Abkowitz [17]

Rhee et al. also used the EKF with the ESSO Osaka, but this research used the MMG model for the numerical simulations [18]. They implemented an importance of sensitivity for each manoeuvre and conducted coefficients identification according to the result of the sensitivity analysis. Simulations results using estimated coefficients showed satisfactory trajectory and other kinematic parameters compared to the sea trial results.

Zhang and Zou applied  $\varepsilon$ -support vector regression to the coefficients identification [19]. The mathematical model of Abkowitz was applied to the identification process and resultant coefficients were verified by the PMM test results.



(a) Estimation procedure



(b) Trajectory of zig-zag manoeuvre  $20^\circ/20^\circ$  after the identification

Figure 2.5 System identification for estimating hydrodynamic coefficients by Rhee et al. [18]

Tran et al. introduced SQP and BFGS algorithms to obtain optimization results [20]. Coefficients identification was conducted after sensitivity analysis for each manoeuvre and their simulation results were compared with the sea trial data.

Many of previous studies on the system identification were conducted using ESSO Osaka as a reference data and the EKF. It is assumed that these are caused by difficulty of obtaining sufficient sea trial data for estimating hydrodynamic coefficients and limitations of the optimization algorithm at that time. In addition, as mentioned in Table 2.1, it is considered that there has been less research than other methods of manoeuvrability estimation because of the problem of having physical uncertainty about the estimated coefficients.

This study was carried out considering the advantages and disadvantages of the system identification, mentioned above. As a preparation of this thesis, Kim introduced a mathematical optimization process using a simulation result based on Azimuth propulsion ferry ship as a reference [21]. Based on this result, Kim et al. conducted a mathematical optimization by applying sea trial data as a reference, and simulation results using tuned coefficients are closer to the reference compared with simulation results using a basic coefficients estimation of the corresponding simulator [22]. In this study, optimization was performed based on the mathematical models and corresponding hydrodynamic coefficients of Norrbin and Clarke. Reference data required for optimization process were obtained by sea trial.

## **2.2 Manoeuvring characteristics and corresponding tests**

Ship manoeuvrability is an ability of a ship, which presents keeping and altering its state of motion with certain controls. This includes straight motions with constant speed or increasing speed and changing course manually. IMO provided standards for ship manoeuvring characteristics to evaluate qualities of the manoeuvrability [23].

**Inherent dynamic stability** A ship is dynamically stable on a straight course if it can fix a new straight course after a disturbance without any steering actions by a helmsman. Figure 2.6 shows a concept of the inherent dynamic stability. An unstable ship moves continuously into an irrational course in contrast with a stable ship, which can reset its course after an interruption. The consequent deviation from the original heading relies on the extend of inherent stability and on the weight and length of the disturbance.

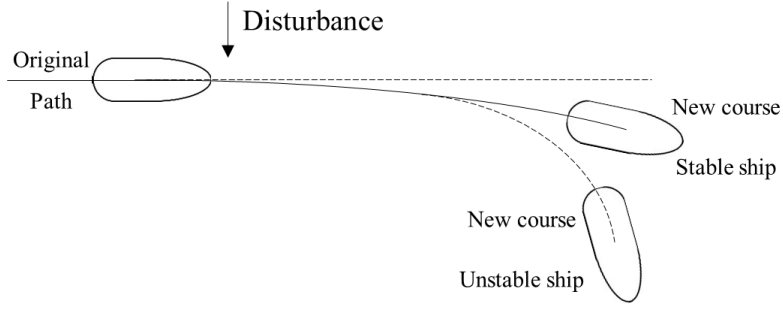


Figure 2.6 Inherent dynamic stability

**Course-keeping ability** The course-keeping ability is a means of a steered ship, which keeps a straight path toward a prearranged course without inordinate oscillations of rudder or heading. As shown in Figure 2.7, a ship with inherent dynamic stability can only keep its original course with certain control action. However, a ship with an inherent dynamic instability can also maintain its original course if it applies a frequent control action.

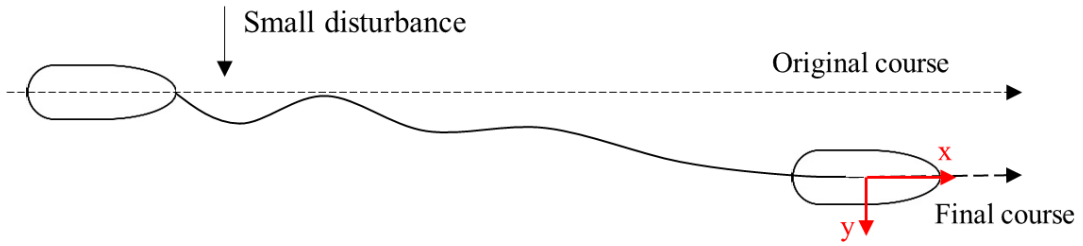


Figure 2.7 Course-keeping ability

**Initial turning / course-changing ability** The initial turning ability is described by the change-of-heading response to a control action. A ship which has good initial turning ability can alter to its original course. This can be expressed by the ‘P number’, which represents the rate of heading change as to the helm angle [24]. Norrbin defines this index as follows:

$$P = \frac{\psi'(t' = 1)}{\delta'(t' = 1)} \quad (18)$$

where  $\psi'$ ,  $\delta'$  and  $t'$  are the nondimensionalised heading, rudder angle and time, respectively [9]. Norrbin studied the P number for different ships and proposed the value  $P=0.3$  as a lower limit for proper manoeuvrability of a ship [25].



**Yaw checking ability** The yaw checking ability is a ship performance measurement of how fast a turning motion defeats and settles a course [26]. It can be measured from the response to counter-rudder in a certain state of turning manoeuvre. The overshoot angle or time to yaw-check of course change test and zig-zag test can examine the yaw checking ability.

**Turning ability** The turning ability is an ability to turn a ship with a hard-over rudder. Corresponding results are an advance, a tactical diameter and a transfer. Details are discussed later.

**Stopping ability** The stopping ability is measured from ‘track reach’ and ‘time to dead in water’ by a stop engine-full astern manoeuvre after a steady motion with full engine speed. Normally a ship deviates due to environmental disturbances and initial test conditions.

As shown in Table 2.2, ITTC summarized a total of 19 manoeuvring tests, which are recommended by various organisations. 15 of these provide information on manoeuvring characteristics, which are mentioned above [27].

The standard of IMO resolution MSC.137(76) is chosen for this dissertation. Test details and their satisfactory criteria are as follows [28].

**Turning test** A turning test evaluates a ship’s turning ability. It performs to both starboard and port with a 35-degree rudder angle or designed maximum angle at the test speed. Command for rudder execution comes after the ship is at a steady state with zero yaw rate. Figure 2.8 shows a concept and kinematic parameters of the turning test. The standard requires that the advance should not be more than 4.5 ship lengths and the tactical diameter should be more than 5 ship lengths in the manoeuvre.

Table 2.2 Recommended manoeuvring tests by various organisations [27]

	Type of test	IMO A.601	IMO A.751	IMO 137(76)	ITTC 1975	SNAME 1989	Norse Standard	Japan RR	ISO	ITTC 2002	Remarks (*)
1	Turning circle	✓	✓	✓	✓	✓	✓	✓	✓	✓	5
2	Z-manoeuvre	✓	✓	✓	✓	✓	✓	✓	✓	✓	3,4
3	Modified Z-manoeuvre							✓		✓	1,3
4	Z-manoeuvre at low speed	✓				✓		✓		✓	1,2
5	Direct spiral			✓	✓	✓	✓	✓		✓	1,2
6	Reverse spiral			✓	✓	✓	✓	✓		✓	1,2
7	Pull-out	✓		✓	✓	✓			✓	✓	1
8	Stopping	✓	✓	✓	✓	✓	✓	✓	✓	✓	6
9	Stopping inertia	✓					✓	✓		✓	6
10	Man-overboard	✓							✓	✓	4,5
11	Parallel course manoeuvre	✓							✓	✓	4,5
12	Initial turning					✓				✓	3
13	Accelerating turning	✓			✓				✓	✓	5
14	Thruster	✓			✓	✓	✓			✓	4,5
15	Crabbing									✓	3
16	New course keeping	✓						✓			
17	Acceleration/ deceleration	✓									
18	Crash stop ahead	✓				✓	✓	✓			
19	Minimum revolution	✓				✓	✓				
(*)	1) inherent dynamic stability 2) course-keeping ability 3) initial turning/course-changing ability 4) yaw checking ability 5) turning ability 6) stopping ability										

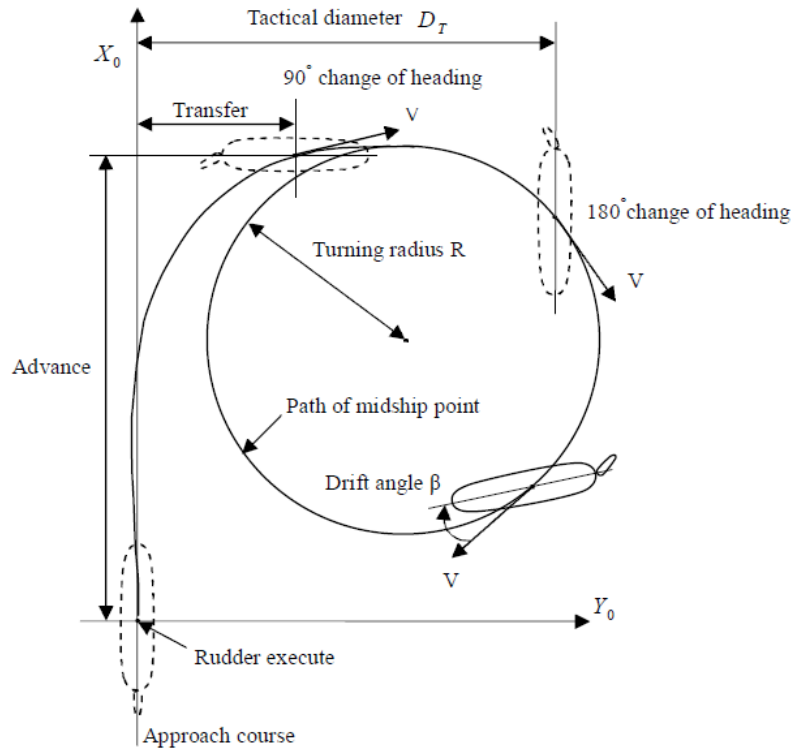


Figure 2.8 Trajectory of the ship during turning [1]

**Zig-zag test** A zig-zag test evaluates the ship's initial turning, the yaw checking and the course-keeping abilities. It begins by executing a certain amount of rudder angle from an initial straight manoeuvre, called 'first execute'. When a specified deviation from the ship's original heading occurs, the rudder angle is altered to the opposite side, called 'second execute'. Normally two kinds of zig-zag tests,  $10^\circ/10^\circ$  and  $20^\circ/20^\circ$  tests are applied. Each test has  $10^\circ$  and  $20^\circ$  of heading deviation, respectively. Figure 2.9 shows characteristic parameters and time histories for the rudder angle and heading during the test. Overshoot angles and initial turning time to second execute are chosen as manoeuvrability parameters. For the initial turning ability, with the  $10^\circ/10^\circ$  test, the ship should not travel more than 2.5 ship lengths by the time for  $10^\circ$  of heading deviation. For the yaw checking and course-keeping ability, satisfactory criteria is as follows:

- The first overshoot angle for the  $10^\circ/10^\circ$  test should not exceed
  - $10^\circ$  if  $L/V$  is less than 10s;
  - $20^\circ$  if  $L/V$  is 30s or more; and
  - $(5+1/2(L/V))^\circ$  if  $L/V$  is 10s more, but less than 30s.
- The second overshoot angle for the  $10^\circ/10^\circ$  test should not exceed
  - $25^\circ$  if  $L/V$  is less than 10s;
  - $40^\circ$  if  $L/V$  is 30s or more; and

$(17.5 + 0.75(L/V))^\circ$  if  $L/V$  is 10s or more, but less than 30s.

- The first overshoot angle for the  $20^\circ/20^\circ$  test should not exceed  $25^\circ$ .

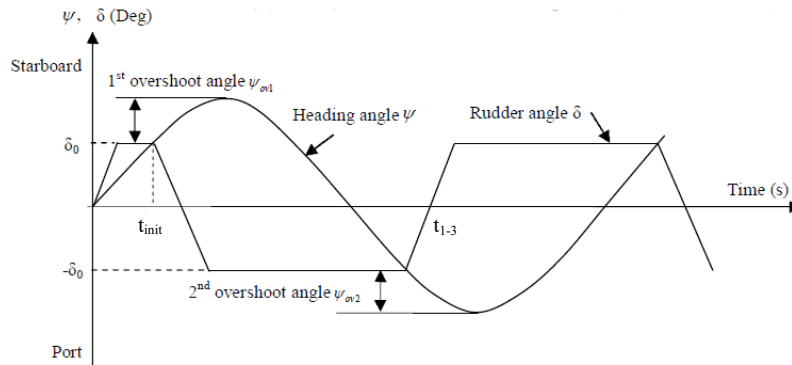


Figure 2.9 Time histories of rudder angle and heading during zig-zag test [1]

**Stopping test** A stopping test evaluates the stopping ability. A full astern stopping test is conducted to measure the track reach of a ship from the moment of full-astern order to the place ship is stopped. Figure 2.10 shows a concept of the test. The standard requires that the track reach should not exceed 15 to 20 ship lengths, considering a ship's displacement.

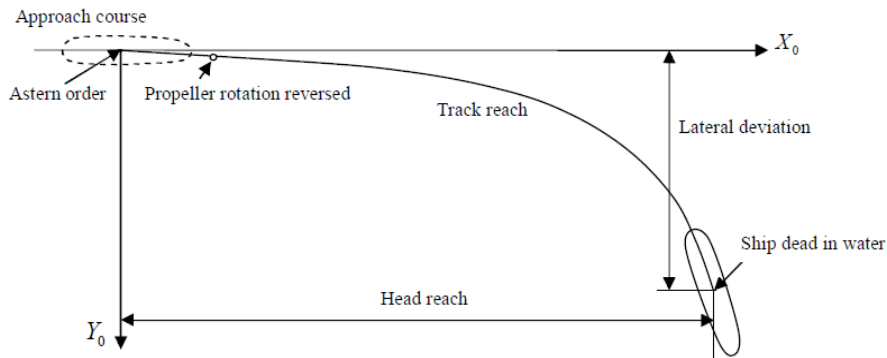


Figure 2.10 Trajectory of the ship during stopping test [1]

**Spiral test** A spiral test is included as additional manoeuvres in the standard of IMO. It evaluates the inherent dynamic stability and the course-keeping ability. A direct spiral test conducts a series of turning manoeuvres. Rudder commands for the turning change every 5 degrees from 15 degrees of one side to 0 degrees. This is repeated for both the port and starboard side. Each turning manoeuvre should be recorded at least one minute

after the yaw rate remains constant. A reverse spiral test can substitute the direct spiral test to define an instability loop. In the test, a ship is steered to obtain a constant yaw rate and the mean rudder angle is required to measure the yaw rate. Then the yaw rate versus rudder angle can be plotted on the area of the instability. Figure 2.11(a) and Figure 2.11(b) show results of spiral tests for a stable ship and unstable ship, respectively.

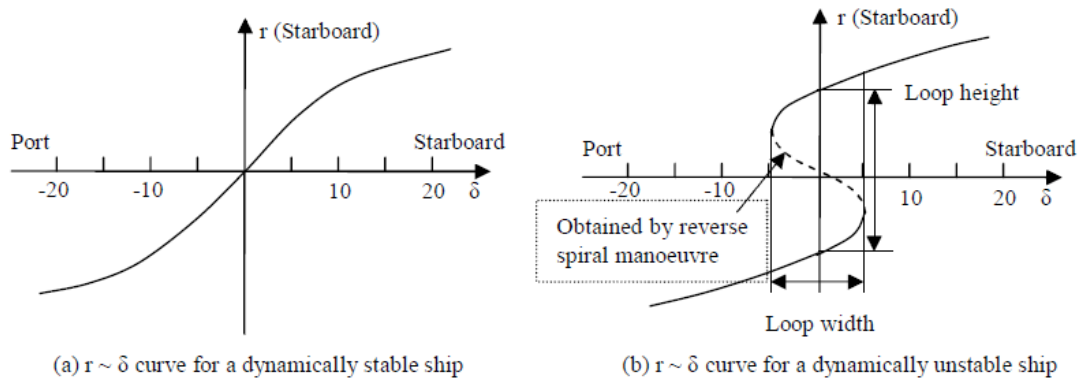


Figure 2.11 Yaw rate to rudder angle curve from spiral tests [1]

**Pull-out test** A pull-out test evaluates a ship's dynamic stability on a straight course. After the completion of the turning manoeuvre, the rudder is set to midship position, and from there a steady yaw rate is obtained. If the ship is stable, the rate of turn decreases to zero. The continuing rates of turn indicates the degree of instability at the  $0^\circ$  of the rudder angle. Figure 2.12(a) and Figure 2.12(b) compare results of the pull-out tests for a stable and an unstable ship.

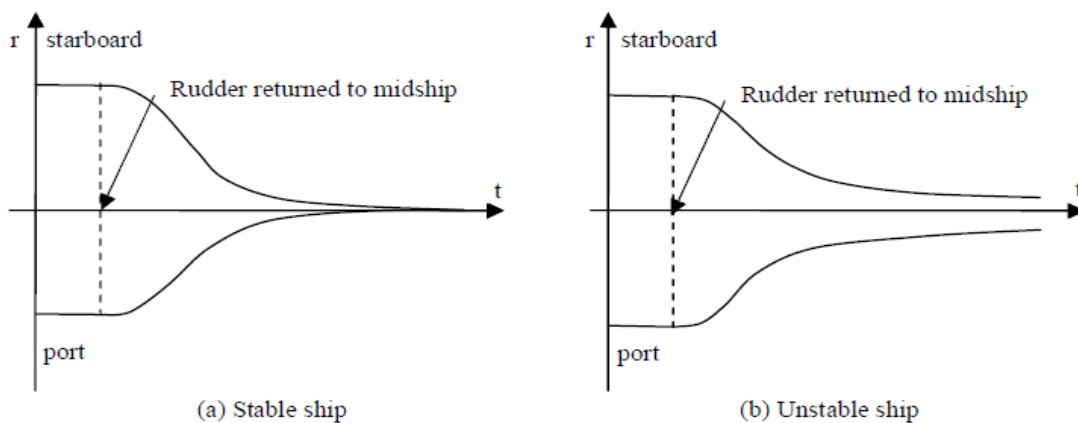


Figure 2.12 Time histories of the turning rate from pull-out test [1]

### 2.3 Influence of trim and draught on ship manoeuvrability

Since IMO adopted a guideline, “Interim Guidelines for Estimating Manoeuvring Performance in Ship Design”, in 1985, many studies about estimation and evaluation of the manoeuvrability have been provided and this enhanced accuracy of prediction at the design stage. While the guideline gives a criterion only for ship’s full loaded even keel condition, most of sea trials are carried out in ballast conditions for practical reasons.

Changes of trim and draught have a remarkable effect on a ship’s manoeuvrability due to the change of multiple corresponding ship’s conditions, such as displacement, a location of the centre-of-pressure for the sway force, rudder inflow angle and so on. It is easily shown that a ship with a trim by stern is common when the ship is in ballast condition due to its relatively stable manoeuvrability than other trim and draught conditions.

Most studies on manoeuvrability regarding loading conditions are focusing on the corresponding changes of displacement, stern shape and rudder area. Kijima et al. and Kose studied an influence and an importance of trim and draught conditions on a ship’s manoeuvrability. In order to estimate a ship’s manoeuvrability in different trim and draught conditions, they conducted captive model tests with various types of ships and four trim and draught conditions: fully loaded, half loaded, ballast with even keel and ballast aft trim conditions [13,14,29]. The prediction results based on the estimation agreed well with the measured results of free running model tests. Yasukawa et al. investigated an influence of the load condition on the effect of rudder force [30]. Inoue et al. suggested a set of empirical formulae from model experiments considering both in even keel and trimmed conditions using the aspect ratio  $k$  as follows [31]:

$$\begin{aligned} Y'_\beta &= \left( \frac{1}{2} \pi k + f \left( C_B \frac{B}{L} \right) \right) \left( 1.0 + \frac{2t}{3d_m} \right) \\ Y'_r &= \frac{1}{4} \pi k \left( 1.0 + \frac{0.80t}{d_m} \right) \\ N'_\beta &= k \left( 1.0 - \frac{0.27t}{l_\beta d_m} \right) \\ N'_r &= (0.54k - k^2) \left( 1.0 + \frac{0.30t}{d_m} \right) \\ \text{where, } l_\beta &= k / \left( \frac{1}{2} \pi k + f \left( C_B \frac{B}{L} \right) \right) \end{aligned} \tag{19}$$

Influence of ship manoeuvrability due to changes in draught and trim can be confirmed using fast time simulator. For this experiment, a fast time simulator SIMOPT of ISSIMS GmbH and a G/T 6686t model ship were used for the simulations. Details of the model ship will be referred in Chapter 4. A ship's dynamic capabilities of the SIMOPT are based on the mathematical models of Norrbin and Clarke [5,12] which is in between the polynomial model and modular model. Clarke's formulae are reduced from the same form of Inoue et al. [31]. Figure 2.13 presents an example of user interface for SIMOPT. Hull forces and moment of the equations consist of the following components:

$$\begin{aligned}
X_h &= X_{up}(\dot{u} - \dot{u}_g) + X_{vr}vr + X_{uu}u|u| + X_{u4}u^3|u| \\
&\quad + X_{uvv}u|v|v^2 + f(u_{threshold}) \\
Y_h &= Y_{vp}(\dot{v} - \dot{v}_g) + Y_{rp}\dot{r} + Y_{ur}ur + Y_{uv}|u|v + Y_{nonlinear} \\
N_h &= N_{rp}(\dot{r} - \dot{r}_g) + N_{rv}\dot{v} + N_{ur}|u|r + N_{uv}uv + N_{nonlinear},
\end{aligned} \tag{20}$$

where  $u, v, r$  are speed components through water, and  $\dot{u}, \dot{v}, \dot{r}$  and  $\dot{u}_g, \dot{v}_g, \dot{r}_g$  are acceleration components through water and over ground, respectively. The term  $f(u_{threshold})$  is only active when a pre-defined threshold velocity is greater than a ship's velocity. Sets of nonlinear coefficients  $Y_{nonlinear}$  and  $N_{nonlinear}$  can be composed by the following coefficients:

$$\begin{aligned}
Y_{nonlinear} &= [Y_{rr}, Y_{vv}, Y_{vr}, Y_{vrt}, Y_{vvvr}, Y_{rrt}, Y_{vvt}, Y_{4v2rt}, Y_{non\_turning\_point}] \\
N_{nonlinear} &= [N_{vr}, N_{rrt}, N_{vvt}, N_{rr}, N_{vv}, N_{v4r2}, N_{vrt}, N_{5v3rt}, N_{non\_turning\_point}].
\end{aligned}$$

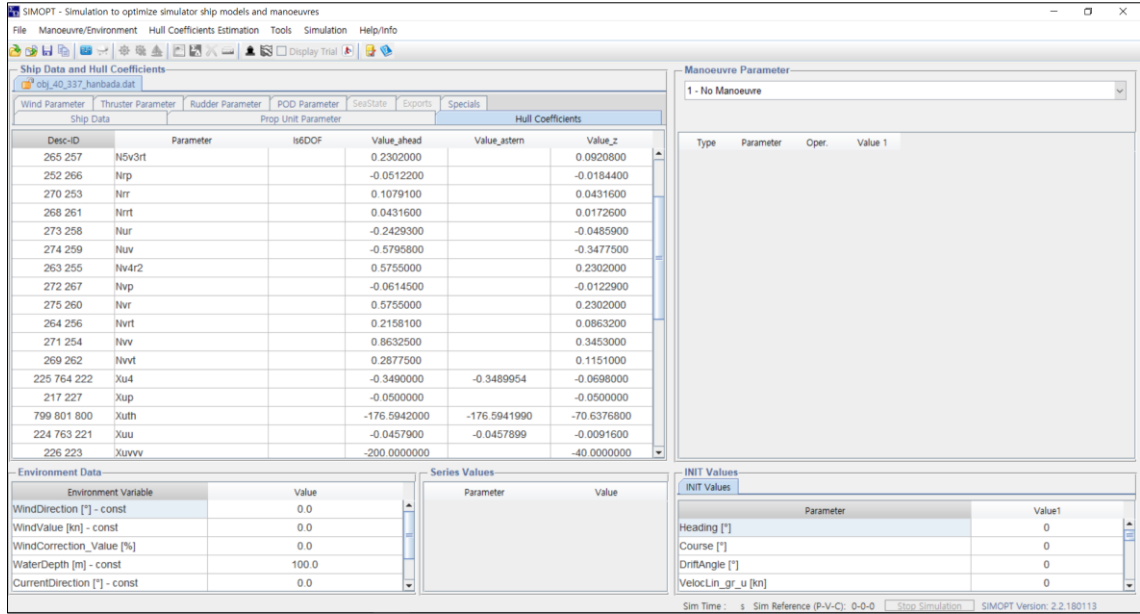


Figure 2.13 User interface for hull coefficients in SIMOPT

The coefficients,  $Y_{non\_turning\_point}$  and  $N_{non\_turning\_point}$  can vary according to a turning point. The standard estimation for the SIMOPT system, named ‘Clarke estimation’, uses the following ship parameters:

- Length
- Breadth
- Draught, fore
- Draught, aft
- Displacement
- Block coefficient
- Nominal power
- Nominal speed

The experimental method is as follows. In comparing the manoeuvrability according to the draught change, trim is fixed to the even keel condition. On the contrary, simulations for the comparison of the manoeuvrability with the change of the trim are carried out by changing only the trim at the same mean draught. The mean draughts were set in five conditions, ranging from 3.9m to 5.9m with every 0.5m. The trims are total of 5 conditions, from -2m to +2m per meter. Because the sign of the trim differs from related organizations and industries, this thesis uses the trim by stern as positive and trim by head as minus based on the document of IMO [28].

$$Trim = Draught_{aft} - Draught_{forward}$$



Table 2.3 shows simulation results of the turning manoeuvre with the change of the draught. Advance, tactical diameter and kinematic parameters were selected for manoeuvre characteristics to be compared. Turning manoeuvre results show that as the draught increases, the advance and the tactical diameter also increases. This leads to increased distance of straight motion before turning and larger turning radius. Tendencies of distance parameters relate also to corresponding kinematic parameters. Figure 2.14 shows comparison for trajectories, based on the corresponding simulation results.

Table 2.3 Influence of draught changes on turning manoeuvre

Mean draught [m]	TC35P				
	Advance [m]	Tactical di- ameter [m]	Final speed [kts]	Final ROT [deg/min]	Final drift angle [deg]
3.9	304.43	157.54	7.42	-75.849	13.77
4.4	316.8	167.19	7.12	-71.896	13.21
4.9	328.33	177.14	6.83	-68.527	12.75
5.4	338.18	182	6.61	-66.055	12.36
5.9	347.51	186.63	6.33	-63.552	12.09
Remark	ROT: Rate of Turn				

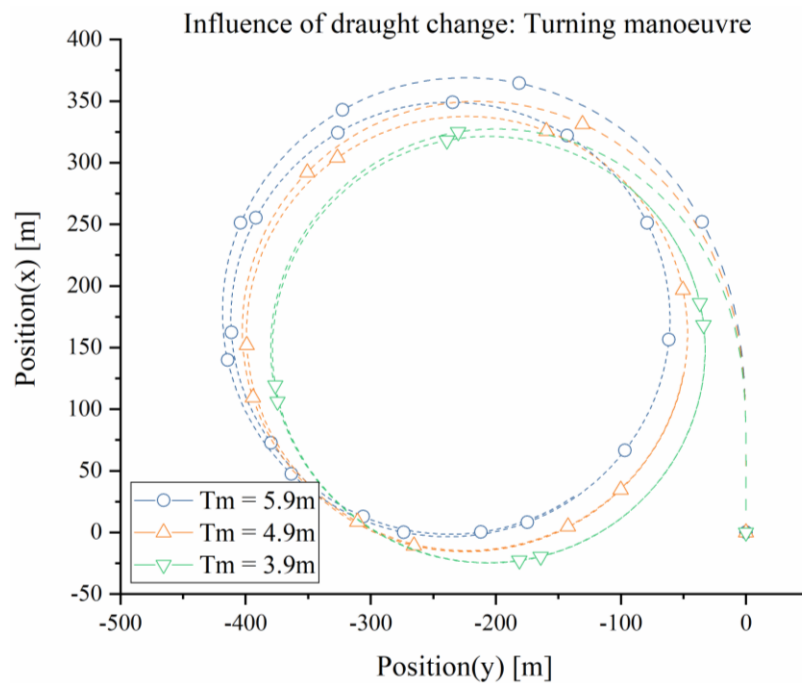


Figure 2.14 Comparison of trajectories for turning manoeuvre with 35 degrees of rudder angle according to changes of mean draught

Table 2.4 and Table 2.5 show influence of draught change for zig-zag manoeuvre with 10 degrees and 20 degrees of rudder angle, respectively. First and second overshoot angles, dimensionless parameters and elapsed time for certain amount of heading change were selected for the characteristics to be compares. Definitions for manoeuvre characteristics are as follows:

- **Initial turning parameter:** dimensionless distance between starting point and the first point ( $x_{init}$  in Figure 2.9) where ship's heading meets rudder command, in relation to ship's length;
- **Turning & checking parameter:** dimensionless period of time ( $x_{1-3}$  in Figure 2.9) between first and third zero crossing of heading, in relation to ship speed performance ( $L/V$ );
- **Initial response time:** initial time of ship's heading response to rudder command.

Comparison shows that the overshoot angles increase consistently as the draught increases. Although the first overshoot at 5.9m for zig-zag with 10 degrees does not follow the trend with others, the rest parameters at that draught maintain a steady trend. This is considered to be due to the increase of ship's displacement and resistance, which is caused by the increase of the underwater portion of the hull. Figure 2.15 to Figure 2.18 show comparison for trajectories and heading changes, based on the corresponding simulation results.

Table 2.4 Influence of draught changes on zig-zag manoeuvre with 10 degrees of rudder angle

Mean draught [m]	ZZ10S				
	First overshoot [deg]	Second overshoot [deg]	Initial turning parameter	Turning & checking parameter	Initial response time [s]
3.9	3.3	3.1	1.38	7.35	16
4.4	3.4	4.1	1.47	8.04	17
4.9	3.7	4.1	1.56	8.47	18
5.4	3.9	5.1	1.64	9.16	19
5.9	3.4	5.2	1.73	9.5	20

Table 2.5 Influence of draught changes on zig-zag manoeuvre with 20 degrees of rudder angle

Mean draught [m]	ZZ20S				
	First overshoot [deg]	Second overshoot [deg]	Initial turning parameter	Turning & checking parameter	Initial response time [s]
3.9	8.4	7.2	1.64	9.6	19
4.4	8.8	8.1	1.73	10.2	20
4.9	9.2	9.1	1.81	10.89	21
5.4	9.6	8.8	1.9	11.4	22
5.9	10.2	9.8	1.99	12.09	23

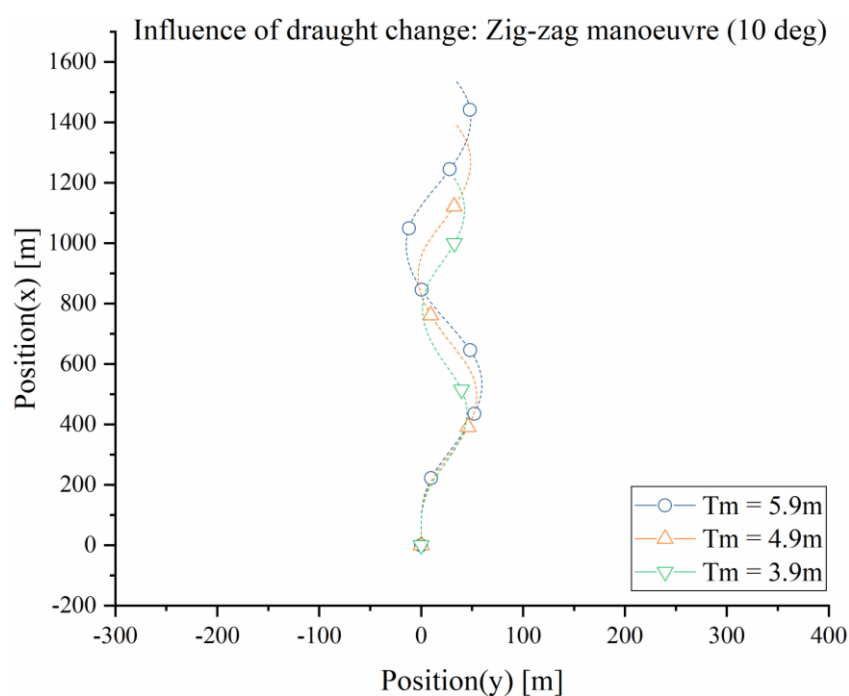


Figure 2.15 Comparison of trajectories for zig-zag manoeuvre with 10 degrees of rudder angle according to changes of mean draught

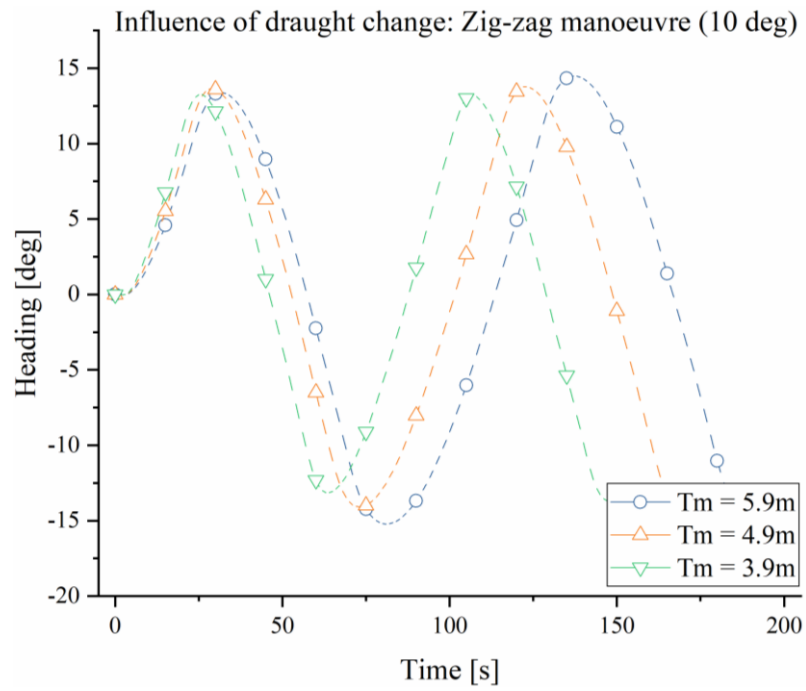


Figure 2.16 Comparison of heading changes for zig-zag manoeuvre with 10 degrees of rudder angle according to changes of mean draught

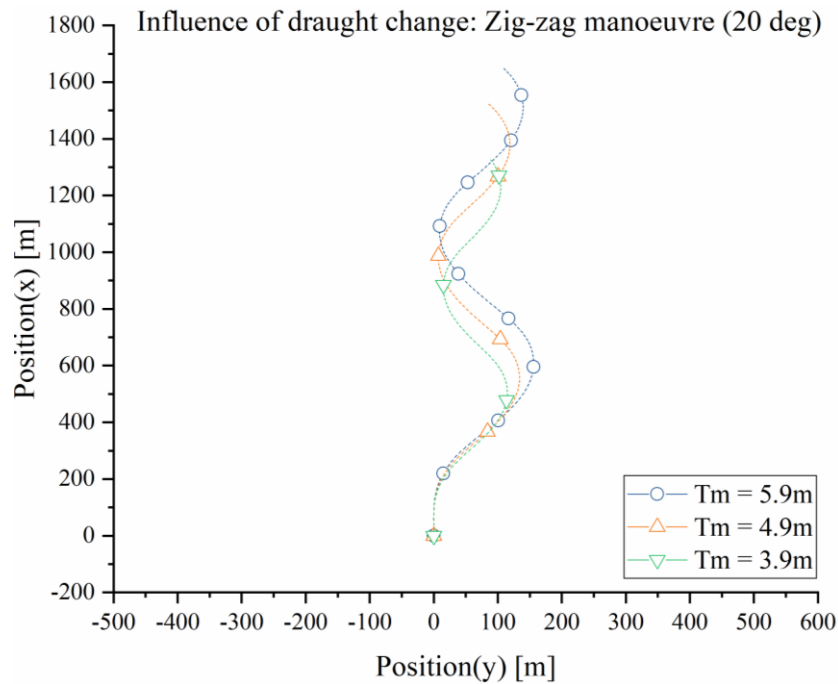


Figure 2.17 Comparison of trajectories for zig-zag manoeuvre with 20 degrees of rudder angle according to changes of mean draught

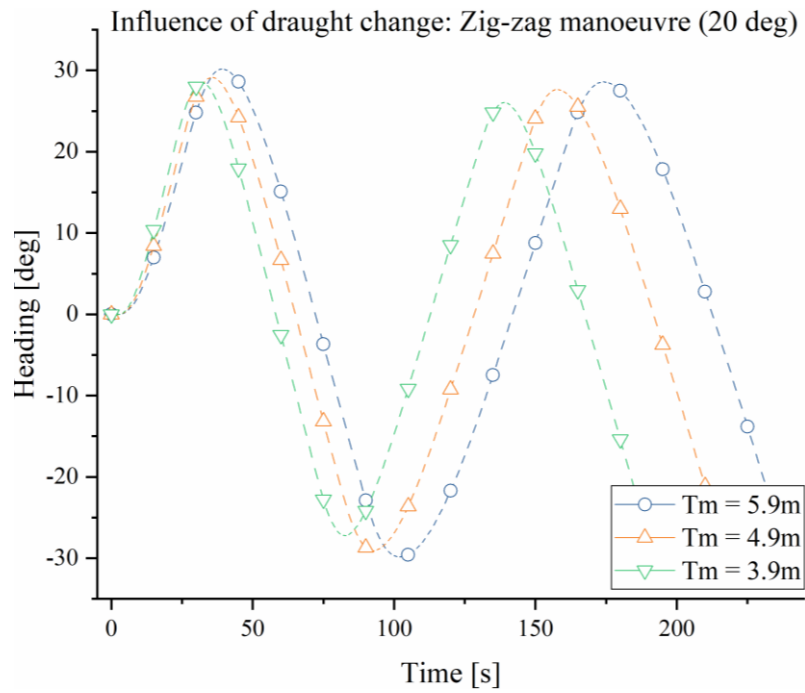


Figure 2.18 Comparison of heading changes for zig-zag manoeuvre with 20 degrees of rudder angle according to changes of mean draught

Table 2.6 and Figure 2.19 show the changes of manoeuvre characteristics for turning manoeuvre according to the trim changes. As the trim changes from ‘by the head’ to ‘by the stern’, the turning circle increases and the corresponding kinetic parameters are also consistent.

Table 2.6 Influence of trim changes on turning manoeuvre

Trim [m]	TC35P				
	Advance [m]	Tactical di- ameter [m]	Final speed [kts]	Final ROT [deg/min]	Final drift angle [deg]
-2	289.96	116.12	4.26	-67.194	18.72
-1	317.2	150.43	5.19	-65.444	15.12
0	347.51	186.63	6.33	-63.552	12.09
+1	381.95	229.03	7.55	-61.037	9.73
+2	419.91	277.72	8.72	-57.975	7.94
Remark	ROT: Rate of Turn				

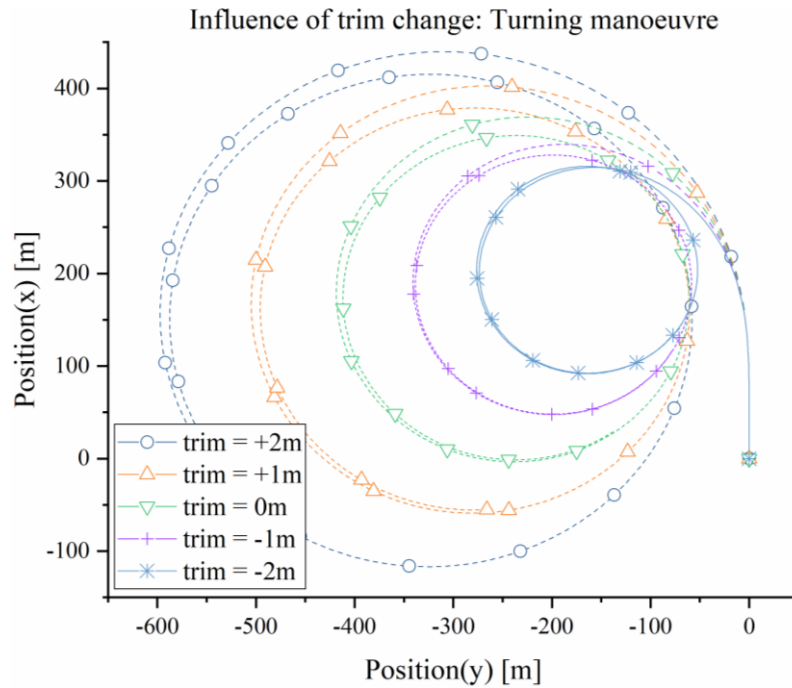


Figure 2.19 Comparison of trajectories for turning manoeuvre with 35 degrees of rudder angle according to changes of trim

Table 2.7 and Table 2.8 show changes in the zig-zag manoeuvre as the trim changes. The characteristics to be compared are the same as those of the previous draught change. As the trim changes from 'by the head' to 'by the stern', the initial turning ability decreases but the yaw checking ability becomes better. Figure 2.20 to Figure 2.23 show comparison for trajectories and heading changes, based on the corresponding simulation results.

Table 2.7 Influence of trim changes on zig-zag manoeuvre with 10 degrees of rudder angle

Trim [m]	ZZ10S				
	First overshoot [deg]	Second overshoot [deg]	Initial turning parameter	Turning & checking parameter	Initial response time [s]
-2	8.1	17.2	1.55	12.09	18
-1	5.2	9.3	1.64	10.36	19
0	3.4	5.2	1.73	9.5	20
+1	2.7	3.3	1.81	9.41	21
+2	2.1	2.8	1.9	9.67	22

Table 2.8 Influence of trim changes on zig-zag manoeuvre with 20 degrees of rudder angle

Trim [m]	ZZ20S				
	First overshoot [deg]	Second overshoot [deg]	Initial turning parameter	Turning & checking parameter	Initial response time [s]
-2	19.1	21.2	1.81	14.08	21
-1	13	13.6	1.9	12.52	22
0	10.2	9.8	1.99	12.09	23
+1	6.8	7.1	2.16	11.75	25
+2	6	7.3	2.25	12.26	26

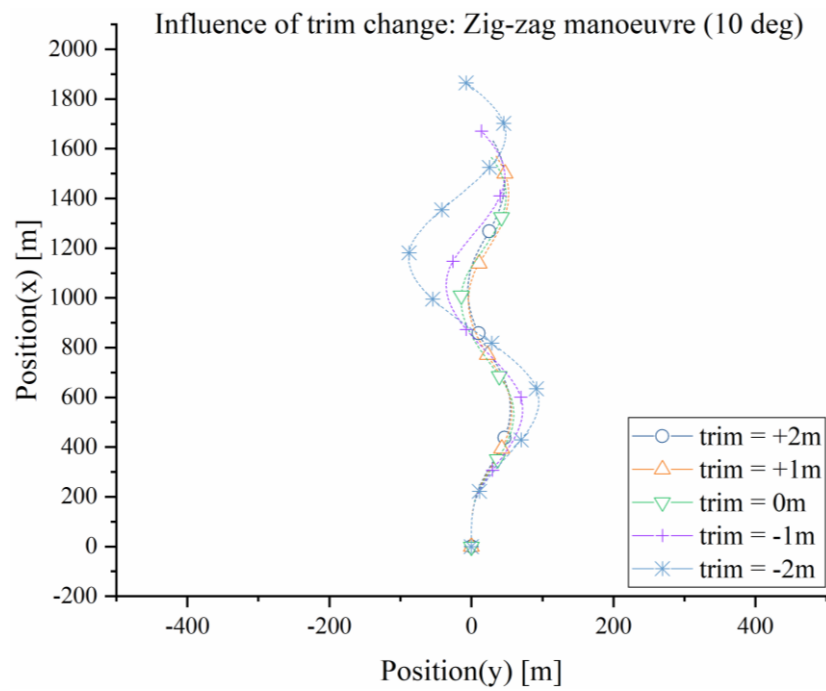


Figure 2.20 Comparison of trajectories for zig-zag manoeuvre with 10 degrees of rudder angle according to changes of trim

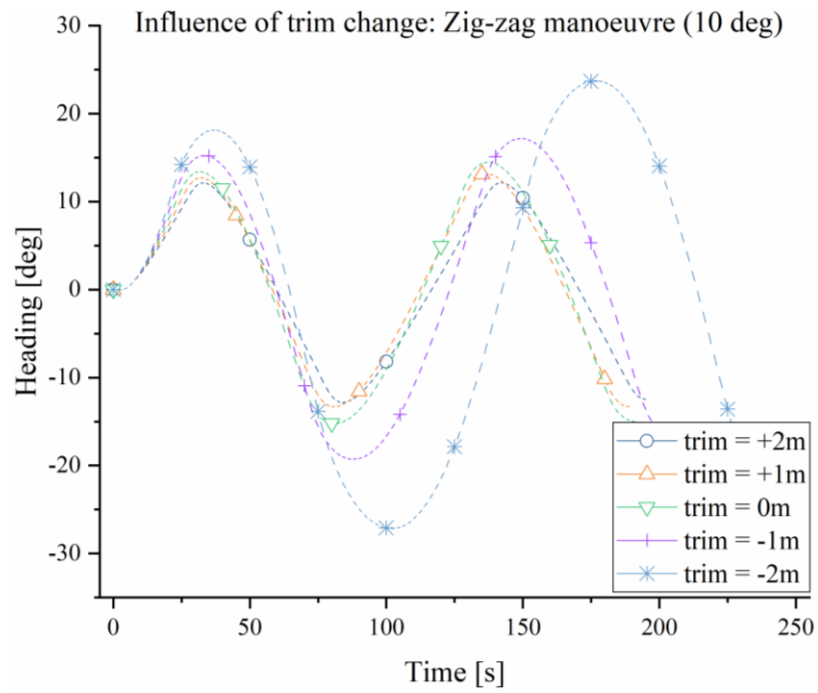


Figure 2.21 Comparison of heading changes for zig-zag manoeuvre with 10 degrees of rudder angle according to changes of trim

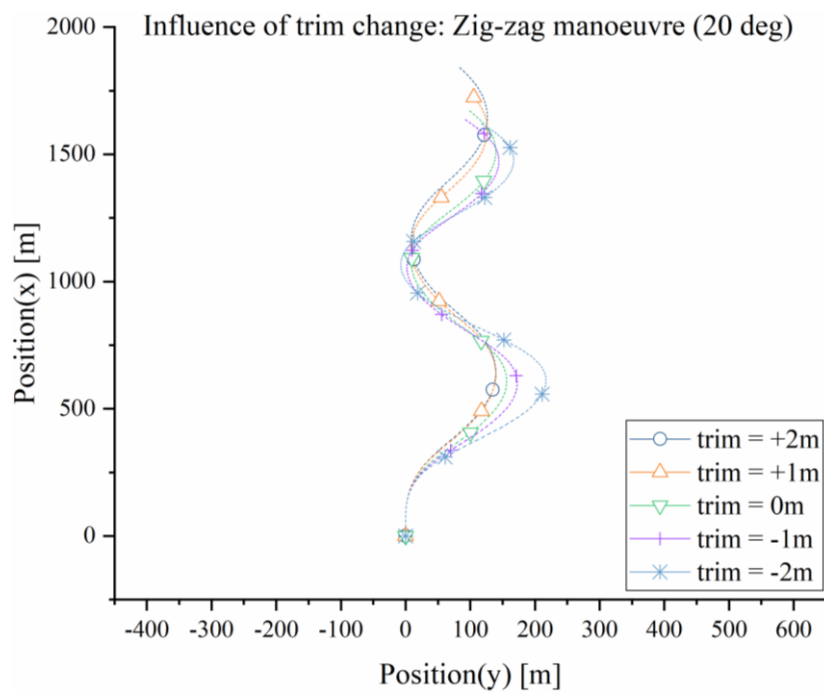


Figure 2.22 Comparison of trajectories for zig-zag manoeuvre with 20 degrees of rudder angle according to changes of trim



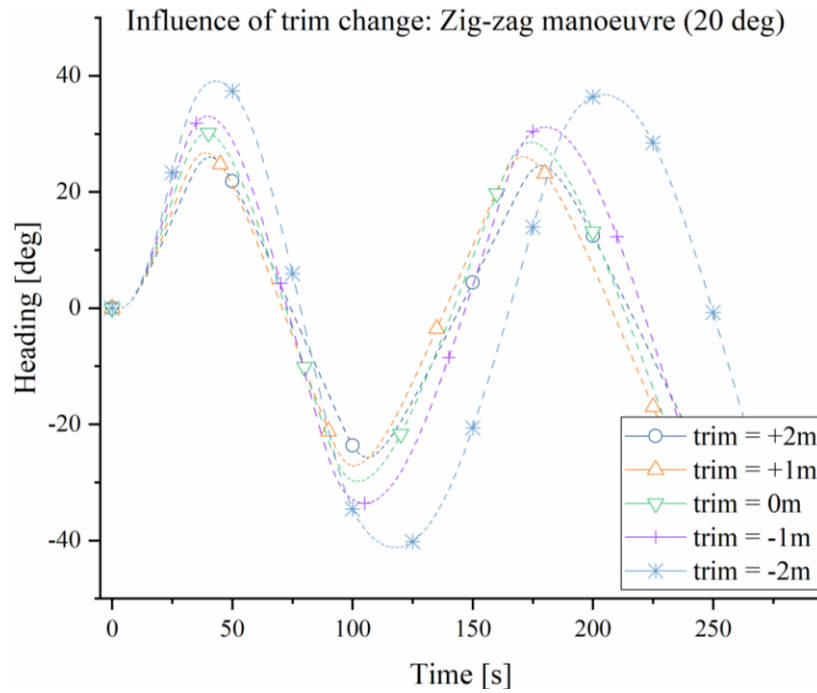


Figure 2.23 Comparison of heading changes for zig-zag manoeuvre with 20 degrees of rudder angle according to changes of trim

Krüger introduced comparison for a ship's manoeuvrability with various trim condition by Benedict [32,33]. He found that a change of trim is subject to major changes of a ship's manoeuvrability, but this influence is not subject to the linear laws. Figure 2.24 shows simulation results for a turning manoeuvre and a zig-zag manoeuvre for a fully loaded 2,500 TEU container ship. All manoeuvres are conducted under the same mean draught, and trim is the only control variable for the comparison. Trim conditions are provided every 1 metre from the even keel condition to 3 metres by the head. Results confirm that increased trim by the head affects to greater overshoot angle and to decrease turning circle. These are consistent with the effect of trim changes, shown in the Table 2.6 to Table 2.8.

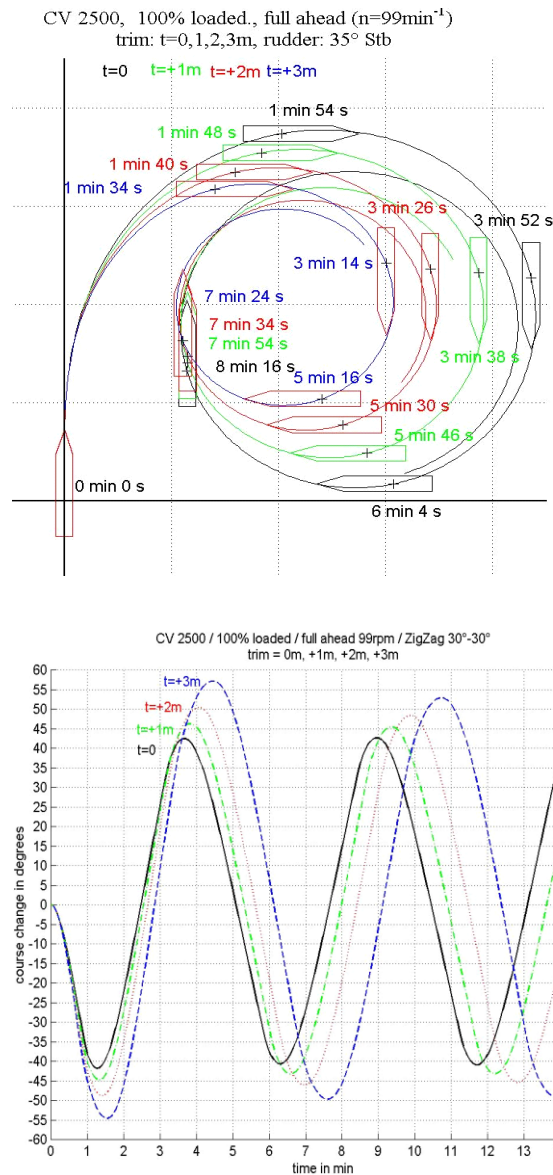


Figure 2.24 Manoeuvre results with various trim conditions [33]

These experimental results can be explained by theoretical considerations. The position of the pivot point, also as known as the apparent centre of rotation, has a close correlation with the ship's manoeuvrability, especially in the turning of the ship. As shown in Figure 2.25, Seo and Mishu stated that the pivot point is not the actual centre of ship's yaw motion, but it is a useful concept to explain the movement of ship [34].

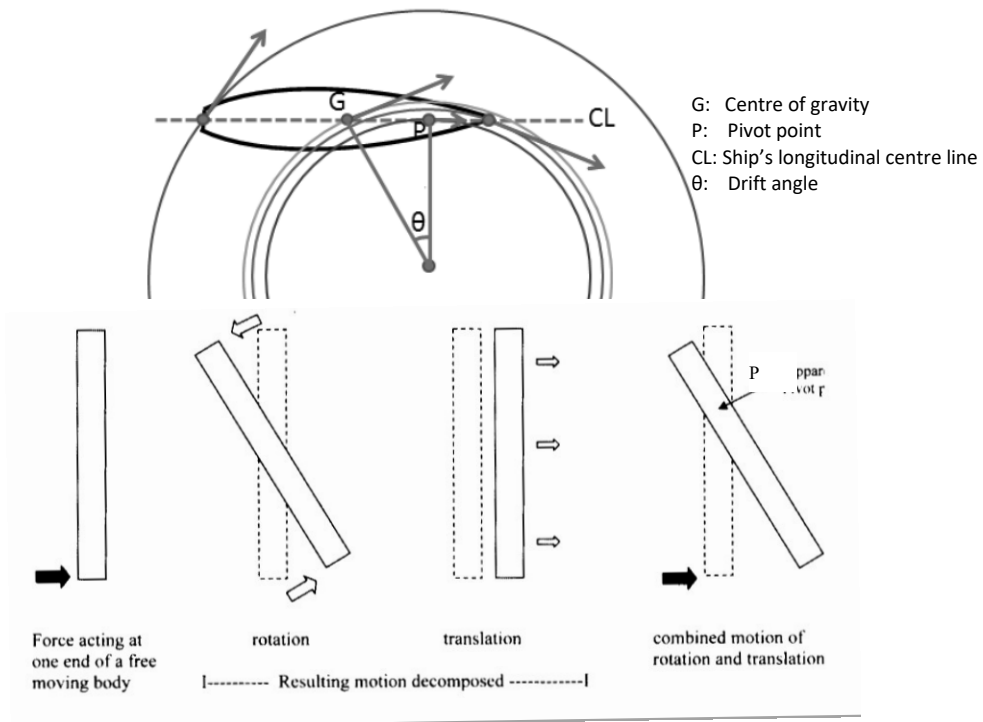


Figure 2.25 Concepts of pivot point [34]

A research project ISTTES introduces two approaches for the coefficient estimation regarding various trim and draught conditions [36]. A traditional approach is a kind of direct tuning of parameters, which are presented in the form of polynomials to describe the response of the ship's body to external forces. It is simple to demonstrate and to understand, however the optimized parameters are no longer consistent with others because of linear dependency of the whole parameters. Another approach, which the author contributed, is to change the geometric data of the ship. The premise of this approach is that it should be possible to optimize hydrodynamic coefficients by varying the geometric ship characteristics which affects "Clarke estimation" for the polynomials. However, the change of the geometric dimensions does not consider the further physical effects. Also, this idea is a simple and efficient idea, but as the estimation formulas for all the coefficients are bound to the ship's dimension, changing one parameter causes all the coefficients to change. As a result, there was a problem in obtaining the desired tuning value.

In consideration of the above results, this study conducts the optimization only for specific coefficients, which have a particularly large influence on the specific manoeuvre

used in the sea trial, through the sensitivity analysis. The correction formula of the existing Clarke estimation formula according to influence of the trim and draught condition is as follows.

$$C_{new} = C_{reference.condition} + \Delta C_{trim\ and\ draught} \quad (21)$$

### 3. Fundamentals of mathematical optimization

#### 3.1 Introduction

A mathematical optimization is a method to determine scientific solutions and to analyse physical systems [37]. Also, it is a process for the formulation and for the solution of an optimization problem [38]. This method minimizes or maximizes an objective function on its variables. Sometimes the variables should also be restricted by constraints. The basic optimization problem can be expressed as follows:

$$\begin{aligned} \min f(x) \quad , \text{subject to} \quad (22) \\ c_E(x) = 0 \\ c_I(x) \leq 0 \end{aligned}$$

where  $x$  is the vector of variables,  $f$  is the objective function ( $f: \mathbb{R}^n \rightarrow \mathbb{R}$ ), a function of the variable(s)  $x$  to be minimized or maximized,  $c_E$  is an equality constraint ( $c_E: \mathbb{R}^n \rightarrow \mathbb{R}^m$ ) and  $c_I$  is an inequality constraint ( $c_I: \mathbb{R}^n \rightarrow \mathbb{R}^p$ ).

Figure 3.1 illustrates a concept of the mathematical optimization. Contour refers to a set of points whose values of the objective function are constant. The feasible region is an area that satisfies all constraints and contains an optimum point. This optimum point can be either a local optimum or a global optimum.

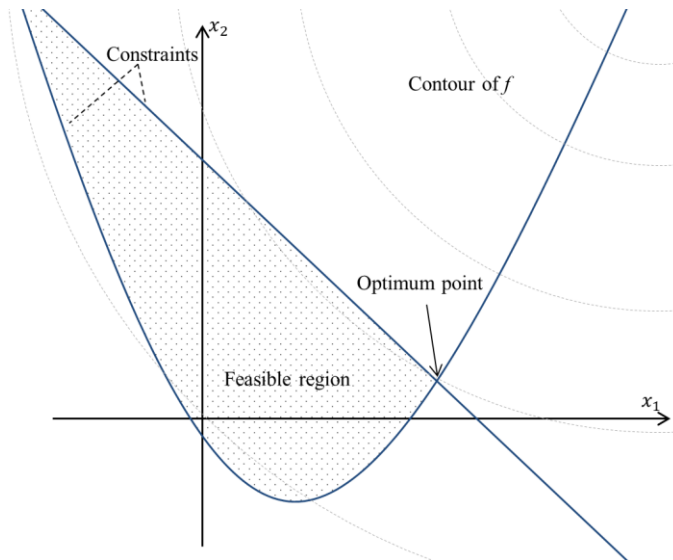


Figure 3.1 Concept of the mathematical optimization

Determining a proper problem—which is a process of modelling to find an objective function, variables and constraints—is the most important thing for successful mathematical optimization. A designed optimization problem can be solved by an optimization algorithm. An appropriate algorithm for a certain problem is determined according to the types of the objective function and the constraints. This may determine a quality of an optimization result, an elapsed time and so on.

During the optimization process, the algorithm observes its optimality conditions at each iteration. If a current optimality condition is not satisfactory, the algorithm finds a new set of variables, and this strategy distinguishes each algorithm. Some algorithms utilize first- and/or second-order derivatives information from previous. In contrast, others use information only at the current point.

Optimization problems can be classified into four categories: a continuous versus a discrete optimization, a constrained versus an unconstrained optimization, a global versus a local optimization and a stochastic versus a deterministic optimization. In this study, we only focus on continuous, local and deterministic optimizations. Based on this, constrained and unconstrained optimizations will be discussed, and the optimal algorithm for estimating hydrodynamic derivatives will be suggested.

### **3.2 Unconstrained optimization**

An unconstrained optimization solves a problem without restrictions for all variables. The optimization algorithm produces a set of iterates and it terminates a sequence when a change of particular conditions is relatively small or when it may be a solution. Most algorithms are based on two fundamental strategies to decide movement toward the next iteration: the line search method and the trust region method. Briefly the line search method determines a direction for a new iteration, whereas the trust region method determines a maximum distance, which is called as a trust region radius, for a new iteration. This study chooses the Quasi-Newton algorithm, which is a kind of the line search method, and the Nelder-Mead simplex algorithm, which is a kind of a derivative-free method. The trust region method is not chosen because it requires a gradient vector and a Hessian matrix – a square matrix of second-order partial derivatives - for determining a next iteration, and the optimization process for estimating hydrodynamic coefficients is not able

to provide them manually. Details will be discussed in the next chapter with a demonstration of an entire optimization process.

### 3.2.1 Quasi-Newton Algorithm

The line search method determines a direction  $p$  and explores a new iteration, which has a smaller value of the objective function, along this direction from the current iteration  $x_k$ . This method can be distinguished by a strategy of search direction, especially for use of the Hessian: the steepest descent method, Newton's method and the Quasi-Newton method. The steepest descent method is a kind of first-order method and it has advantages of simplicity and good theoretical guarantee of convergence for weak problem conditions [39]. Newton's method obtains a direction, if the calculated Hessian is positive. This second-order method performs better than the steepest descent method, however it requires an 'exact' Hessian information, which is a very expensive computation, and some optimization problems are not able to meet this condition [40,41].

The Quasi-Newton method covers disadvantages for both the steepest descent method and Newton's method, and it is still the most popular algorithm in nonlinear optimization. It does not require computation of the Hessian, but it can present a convergence as a superlinear rate. The basic idea for the Quasi-Newton method is to replace the true Hessian  $\nabla^2 f$  to an approximation  $B$ , which is updated at each step considering the latest step information. The updated approximation is used for checking whether a provided gradient is still changing.

A common minimizer for the mathematical optimization can be expressed by the Taylor's theorem. Suppose that an objective function  $f$  is twice continuously differentiable and for  $t \in (0,1)$ , a formula can be as follows:

$$\begin{aligned} f(x + p) &= f(x) + \nabla f(x + tp)^T, \\ \nabla f(x + p) &= \nabla f(x) + \int_0^1 \nabla^2 f(x + tp) p dt. \end{aligned} \tag{23}$$

These can be converted into the following:

$$f(x + p) = f(x) + \nabla f(x)^T p + \frac{1}{2} p^T \nabla^2 f(x + tp) p, \quad (24)$$

where  $p = x_{k+1} - x_k$  and  $\nabla f$  is the gradient. By substituting the Hessian  $\nabla^2 f$  to an approximation  $B$  and  $x = x_k$ , Equation (24) is the following:

$$f(x_k + p) \approx f(x_k) + \nabla f(x_k)^T p + \frac{1}{2} p^T B_k p. \quad (25)$$

The corresponding gradient, which is in respect to  $p$ , is the following:

$$\nabla f(x_k + p) \approx \nabla f(x_k) + B_k p. \quad (26)$$

When points  $x_k$  and  $x_{k+1}$  are close to each other and near at a local optimum  $x^*$ , the Newton step is the following:

$$p = -B_k^{-1} \nabla f(x_k). \quad (27)$$

The newly updated Hessian should satisfy the secant equation, which is a kind of Newton method:

$$B_{k+1} s_k = y_k, \quad (28)$$

where  $s_k = p = x_{k+1} - x_k$  and  $y_k = \nabla f(x_k + p) - \nabla f(x_k) = \nabla f_{k+1} - \nabla f_k$ . For the successive optimization, the updated approximation  $B_{k+1}$  should meet particular conditions: low rank updated, symmetry matrix and positive definiteness [42].

The Quasi-Newton method can be distinguished into several sub algorithms according to ways of updating the Hessian approximation. The Davidon-Fletcher-Powell (DFP) formula, Broyden-Fletcher-Goldfarb-Shanno (BFGS) algorithm and Symmetric rank one (SR1) are well known methods and this study applies the BFGS method for the optimization.

To update an approximate Hessian, two matrices are required as follows [43]:



$$B_{k+1} = B_k + U_k + V_k \quad (29)$$

where  $U_k$  and  $V_k$  are symmetric rank one matrices. For the successful approximation for the next step, the update form should be converted as follows:

$$B_{k+1} = B_k + \alpha uu^T + \beta vv^T. \quad (30)$$

From the secant condition in Equation (28) and substituting  $u = y_k$  and  $v = B_k s_k$  into Equation (30), components  $\alpha$  and  $\beta$  are the following:

$$\begin{aligned} \alpha &= \frac{1}{y_k^T s_k} \\ \beta &= -\frac{1}{s_k^T B_k s_k}. \end{aligned} \quad (31)$$

Finally, an approximation formula for the BFGS algorithm is as follows:

$$B_{k+1} = B_k + \frac{y_k y_k^T}{y_k^T s_k} - \frac{B_k s_k s_k^T B_k^T}{s_k^T B_k s_k} \quad (32)$$

The BFGS has a property of self-correction [44]. By using the inverse Hessian approximation, incorrect approximates, which cause slow calculation, are ignored and corrected in the next few steps.

### 3.2.2 Derivative-free optimization

Derivative-free optimization is a kind of mathematical optimization which does not require derivative information. Though the derivative-free optimization is not popular and is not as advanced as derivative-based methods, they perform well with certain functions, such as non-smooth, noisy and time-consuming to get derivatives [45]. One class of methods sets a linear or a quadratic model up for the objective function and it defines an updated iteration by searching to minimize this model inside a trust region [37]. Since Hooke and Jeeves introduced a direct search solution, the derivative-free optimization has been grown by many applicants and has been applied in wide area, such as scientific problems, medical problems and engineering design and facility location problems [46]. However,

this method cannot guarantee an optimality, especially for an optimization problem with more than a few tens of variables [47]. Also, it is relatively slower to converge than gradient-based algorithms.

This study chooses the Nelder-Mead algorithm, which is a kind of direct local search method. The direct search method is a sequential process which solves a problem by comparing trials in the same iteration to find the best one [48]. The Nelder-Mead method searches an optimal in  $n$ -dimensional space using heuristic ideas. It is also called a ‘non-linear simplex’, but it has nothing doing with the simplex method for linear optimization programming. As mentioned, it does not require any pre-defined derivatives. This means that a corresponding objective function must not be smooth during an optimization process.

A term ‘simplex’ is a geometric figure in  $n$ -dimensional space and it is produced by  $n + 1$  vertices, each iteration of the algorithm starts with a simplex and an objective function for  $n + 1$  sets of variables, and the algorithm reshapes the simplex using four simple operations in the same iteration.

The algorithm firstly finds  $n + 1$  points of the simplex based on a given initial point  $x_0$ . It is preferable for arranging the simplex to make with equal length edges. Figure 3.2 presents examples of the simplex. Consider all the lengths are set to be  $c$  and  $x_0$  is the  $(n + 1)$ th vertex. Resting vertices for the simplex can be calculated by adding a vector to  $x_0$ , and their elements are all  $b$ , except one component, which is set to  $a$  [49]:

$$b = \frac{c}{n\sqrt{2}}(\sqrt{n+1} - 1) \quad (33)$$

$$a = b + \frac{c}{\sqrt{2}}.$$

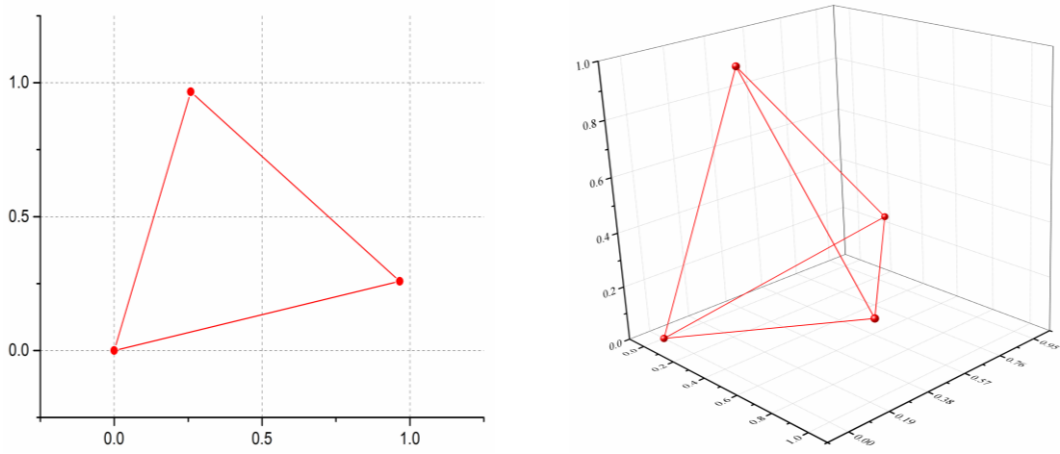


Figure 3.2 Simplexes for  $n = 2$  (left) and  $n = 3$  (right)

A process for the optimization is as follows:

**Order** After setting the initial simplex, objective function values for all vertices are compared and three of them are selected: the highest(“worst”)  $x_w$ , the second highest(“lousy”)  $x_l$  and the lowest(“best”)  $x_b$ . The Nelder-Mead algorithm performs the optimization process with four scalar parameters: reflection ( $\rho$ ), expansion ( $\chi$ ), contraction ( $\gamma$ ) and shrinkage ( $\sigma$ ). Figure 3.3 shows concept operations for the Nelder-Mead algorithm.

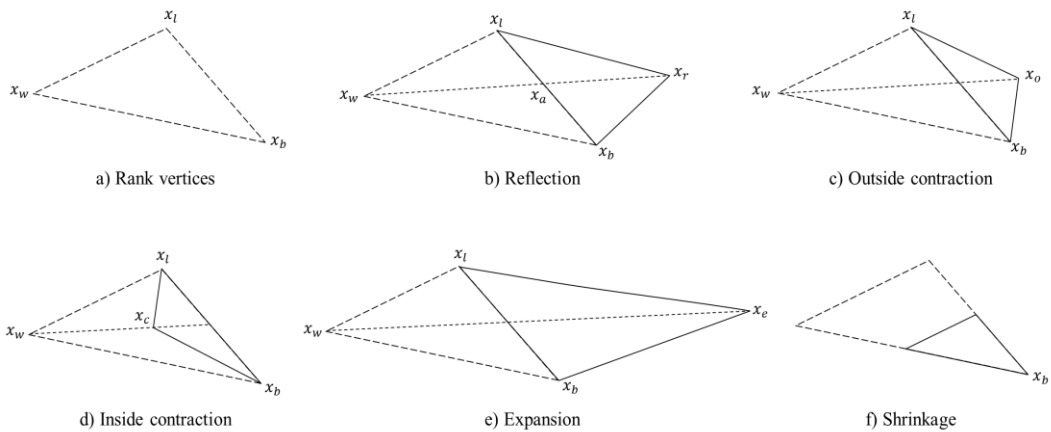


Figure 3.3 Concept operation for the Nelder-Mead algorithm

Nelder and Mead provided criteria for satisfactory as follows [50]:

$$\rho > 0, \quad \chi > 1, \quad \chi > \rho, \quad 0 < \gamma < 1 \text{ and } 0 < \sigma < 1.$$

Lagarias et al. suggested a universal standard for the algorithm [51]:

$$\rho = 1, \quad \chi = 2, \quad \gamma = \frac{1}{2} \text{ and } \sigma = \frac{1}{2}.$$

An operation for each parameter calculates a new vertex and sequences of operations in the same iteration rely on values of the new vertex. The first operation calculates an average of the  $n$  points,  $x_a$ , which do not include a value for  $x_w$ :

$$x_a = \frac{1}{n} \sum_{i=1, i \neq w}^{n+1} x_i \quad (34)$$

**Reflection** A new vertex is located on the line from  $x_w$  to  $x_a$ , which is a descent direction:

$$x_r = x_a + \rho(x_a - x_w). \quad (35)$$

If  $f(x_b) \leq f(x_r) < f(x_l)$ , accept the reflected vertex  $x_r$  and proceed to the next iteration.

**Expansion** If the value at the reflected point is better(lower) than the best point, the reflection is acceptable, and the algorithm calculates the expansion point  $x_e$ :

$$x_e = x_r + \chi(x_r - x_a). \quad (36)$$

If  $f(x_e) < f(x_r)$ , accept the expansion vertex  $x_e$  and proceed to the next iteration. On the other hand, if  $f(x_e) \geq f(x_r)$ , accept  $x_r$  and proceed the next iteration.

**Outside contraction** If  $f(x_l) \leq f(x_r) < f(x_w)$ , perform an outside contraction:

$$x_o = x_a + \gamma(x_a - x_w). \quad (37)$$

If  $f(x_o) \leq f(x_r)$ , accept  $x_o$  and proceed to the next iteration.

**Inside contraction** If  $f(x_w) \leq f(x_r)$ , perform an inside contraction:

$$x_c = x_a - \gamma(x_a - x_w). \quad (38)$$

If  $f(x_c) \leq f(x_w)$ , accept  $x_c$  and proceed to the next iteration.

**Shrinkage** A new vertex is accepted only after the expansion is successful. Otherwise previously reflected points are accepted for the next iteration. If reflection, expansion and contraction fail, an operation shrinkage performs. This operation absorbs all vertices excluding the best one:

$$x_i = x_b + \rho(x_i - x_b). \quad (39)$$

### 3.3 Constrained optimization

Many optimization problems have certain variables which must be satisfied before evaluating an optimality condition and before reliability is ensured. The physical laws for the conservation of mass and Kirchhoff's voltage and current are representative constraints [52]. These can be either equality or inequality conditions. The constrained optimization is relatively more difficult and expensive to get an optimization result than the unconstrained optimization. Forms of the equality and inequality constraints are the same as Equation (22).

The constrained optimization can be largely distinguished by the type of objective and constraint functions and solution methods: linear, integer, quadratic, nonlinear and dynamic programming. It is most common for algorithms to be required to convert an optimization problem with simple constraints into unconstrained problems.

This study only considers the nonlinear constrained optimization, due to a type of objective function for the estimating hydrodynamic dynamics. The interior point method and the sequential quadratic programming method are especially discussed in the following subchapters.

### 3.3.1 Interior point method

The interior point method is a group of algorithms which solves both linear and nonlinear convex optimization problems. This method finds solutions with the barrier function, which is based on the penalty method, to make constraints simple.

As many algorithms do so, an idea is initiated from solving linear problems. The simplex method, which handles vertices of the polytope defined by the constraints, had been the only available one for decades since the 1940s [53]. Because the simplex method does not use a polynomial, it requires a lot of time to reach an optimal value through visiting many vertices [54]. Since Neumann introduced a concept of the interior point method, it has been continuously updated and progressed. Karmarkar applied a polynomial into his algorithm, which is based on Khachiyan's ellipsoid algorithm and is 50 times faster than the simplex method [55,56]. Gill et al. found that the classical barrier function is similar with the Karmarkar's equation and it can be applied to not only to linear problems but also other problems, such as quadratic and nonlinear programming [57].

An overview of the interior point method for nonlinear optimization is described in the following. Equation (22) can be transformed by applying the slack variables  $s$  [58]:

$$\begin{aligned} \min f(x) \quad , \text{subject to} \\ c_E(x) = 0 \\ c_I(x) - s = 0 \\ s \geq 0. \end{aligned} \tag{40}$$

The general inequality constraints  $c_I(x) \leq 0$  is replaced by the slack variables  $s \geq 0$ . However, the constraints are still complex and it is required to be simpler using the barrier problem:

$$\begin{aligned} \min_{x,s} f(s) - \mu \sum_{i=1}^m \log s_i \quad , \text{subject to} \\ c_E(x) = 0 \\ c_I(x) - s = 0 \end{aligned} \tag{41}$$

where  $\mu$  is a positive penalty parameter and the slack variable  $s$  is assumed to be positive. The barrier problem finds a solution for a sequence of positive barrier parameters, which converges to zero.

The algorithm applies one of two types of searching directions at each iteration [59]:

- A direct step, also known as in the Newton step, in  $(x, s)$ , by using the KKT equations and the primal-dual method for the linear approximation.
- A conjugate gradient step, by using a trust-region method.

The ‘fmincon’ solver attempts to take a direct step firstly. However, if it is not successful, it searches direction with a conjugate gradient step. This process happens when the approximate problem is not locally convex.

The KKT equation for the nonlinear programming is [37]:

$$\begin{aligned} \nabla f(x) - A_E^T(x)y - A_I^T(x)z &= 0 \\ Sz - \mu e &= 0 \end{aligned} \quad (42)$$

$$\begin{aligned} c_E(x) &= 0 \\ c_I(x) - s &= 0, \end{aligned}$$

with  $\mu = 0$ ,  $s \geq 0$  and  $z \geq 0$ . Where  $\nabla f(x)$  is the gradient of  $f$ :

$$\nabla f(x) = \left( \frac{\partial f(x)}{\partial x_1}, \frac{\partial f(x)}{\partial x_2}, \dots, \frac{\partial f(x)}{\partial x_n} \right)^T \quad (43)$$

$A_E(x)$  and  $A_I(x)$  are the Jacobian matrices, first-order partial derivatives for matrices, for functions of equality constraints and inequality constraints, respectively:

$$\begin{aligned} A(x) = \nabla c(x) &= (\nabla c_1(x), \nabla c_2(x), \nabla c_3(x), \dots, \nabla c_m(x)), \\ \text{with } c: \mathbb{R}^n &\rightarrow \mathbb{R}^m, \end{aligned} \quad (44)$$

and  $y$  and  $z$  are corresponding Lagrange multipliers.  $S$  and  $Z$  are diagonal matrices and  $e$  is a vector of ones, with the same size as the inequality constraint.

The primal-dual system for equation (42) by applying Newton’s method is

$$\begin{bmatrix} \nabla_{xx}^2 \mathcal{L} & 0 & -A_E^T(x) & -A_I^T(x) \\ 0 & Z & 0 & S \\ A_E(x) & 0 & 0 & 0 \\ A_I(x) & -I & 0 & 0 \end{bmatrix} \begin{bmatrix} p_x \\ p_s \\ p_y \\ p_z \end{bmatrix} = - \begin{bmatrix} \nabla f(x) - A_E^T(x) - A_I^T(x) \\ Sz - \mu e \\ c_E(x) \\ c_I(x) - s \end{bmatrix} \quad (45)$$

where  $\mathcal{L}$  is the Lagrangian equation for corresponding variables (41):

$$\mathcal{L}(x, s, y, z) = f(x) - y^T c_E(x) - z^T (c_I(x) + s). \quad (46)$$

Next iterations can be calculated after determining the corresponding steps  $p = (p_x, p_s, p_y, p_z)$ :

$$\begin{aligned} x^+ &= x + \alpha_s^{max} p_x \\ s^+ &= s + \alpha_s^{max} p_s \\ y^+ &= y + \alpha_z^{max} p_y \\ z^+ &= z + \alpha_z^{max} p_z, \end{aligned} \quad (47)$$

where  $\alpha_s^{max}$  and  $\alpha_z^{max}$  are boundary rules, which monitor descent directions toward lower bounds, known as the boundary rule:

$$\begin{aligned} \alpha_s^{max} &= \max\{\alpha \in (0,1): s + \alpha p_s \geq (1 - \tau)s\} \\ \alpha_z^{max} &= \max\{\alpha \in (0,1): z + \alpha p_z \geq (1 - \tau)z\}, \\ &\text{with } \tau \in (0,1). \end{aligned} \quad (48)$$

The equations above are a concept of the interior point method. In a real situation, the algorithm is struggling with nonconvexities and nonlinearities.

### 3.3.2 Sequential quadratic programming method

The sequential quadratic programming (SQP) method is an effective technique for small- and medium-sized nonlinear programming problems. It generates steps by solving quadratic subproblems [37]. Since Wilson proposed the first SQP method, this method has become one of the most successful methods for constrained nonlinear optimization problems [60]. As with most optimization methods, the SQP is a huge concept, which is composed of multiple specific algorithms [61].



Unlike the interior point method, which mainly applies the barrier function as a kind of penalty method, the SQP method applies the Lagrange multiplier to solve an optimization problem with equality and inequality constraints. The advantages and disadvantages of the SQP method and the interior point method counter to each other [62]. The interior point method is efficient if users can deliver reliable and correct second derivatives. With that, the interior point method can converge within a few iterations, no matter if corresponding problems are small or large. However, the interior point method is not efficient to solve sequence-related nonlinear programming problems. Also, this method requires a lot of iterations when constraints are infeasible.

Otherwise, the SQP method can distinguish infeasibility. As a quadratic programming (QP) method, sophisticated matrix factorization updating techniques are applied to make a problem simple. However, it is difficult for SQP method to deliver exact second derivatives due to theoretical properties of the QP subproblem. Adding to this problem, the SQP method, which employs empty convex quasi-Newton approximation, can be slow when it solves large scale problems [63].

The SQP method is a sequential process, which finds a solution from a given iteration  $x^k, k \in \mathbb{N}$  by the QP subproblem. A solution at each iteration is delivered to a new iteration  $x^{k+1}$ . As the iteration  $k$  increases, corresponding variable  $x^k$  is close to a local minimum, or this can be a global minimum. Contrary to the interior point method, which finds a solution at each iteration only in the feasible area, iterations of the SQP method need not to be in the feasible area, except the optimal solution. This is a major advantage of this method [64].

An objective function  $f$  and constraints  $c$  in equation (22) can be replaced by QP subproblems. At each iteration, the subproblem must find a local optimal of the nonlinear problem:

$$\begin{aligned} f(x) &\approx f(x^k) + \nabla f(x^k)(x - x^k) + \frac{1}{2}(x - x^k)^T Hf(x^k)(x - x^k) \\ c_E(x) &\approx c_E(x^k) + \nabla c_E(x^k)(x - x^k) \\ c_I(x) &\approx c_I(x^k) + \nabla c_I(x^k)(x - x^k), \end{aligned} \quad (49)$$

where  $Hf(x^k)$  is Hessian for the variables at each iteration:

$$(Hf(x))_{ij} = \frac{\partial^2 f(x)}{\partial x_i \partial x_j}, \quad 1 \leq i, j \leq n, \quad (50)$$

and it will be replaced by an approximation  $B_k$  as the Quasi-Newton method. Based on Equation (49) and substituting  $B_k = Hf(x^k)$  and  $d(x) = x - x^k$ , the QP subproblem can be written as follows:

$$\min \nabla f(x^k)^T d(x) + \frac{1}{2} d(x)^T B_k d(x) \quad (51)$$

$$\text{over } d(x) \in \mathbb{R}^n$$

$$\text{subject to } c_E(x^k) + \nabla c_E(x^k)^T d(x) = 0$$

$$c_I(x^k) + \nabla c_I(x^k)^T d(x) \leq 0.$$

The objective function in Equation (51) can be converted to a function of Lagrangian equation  $\mathcal{L}$ :

$$\min \nabla \mathcal{L}(x^k, y^k, z^k)^T d(x) + \frac{1}{2} d(x)^T H \mathcal{L}(x^k, y^k, z^k) d(x) \quad (52)$$

$$\text{over } d(x) \in \mathbb{R}^n$$

$$\text{subject to } c_E(x^k) + \nabla c_E(x^k)^T d(x) = 0$$

$$c_I(x^k) + \nabla c_I(x^k)^T d(x) \leq 0.$$

$$\mathcal{L}(x, y, z) = f(x) + y^T c_E(x) + z^T c_I(x) \quad (53)$$

where  $y^k$  and  $z^k$  are the corresponding Lagrange multipliers for equality and inequality constraints, respectively. When variables at a certain iteration  $x^k$  are a local minimum  $x^*$ , Equation (22) is

$$\begin{aligned}
& \min \mathcal{L}(x^*, y^*, z^*) \\
& \text{over } x \in \mathbb{R}^n, \text{ subject to} \\
& c_E(x) = 0 \\
& c_I(x) \leq 0
\end{aligned} \tag{54}$$

To ensure equivalence between Equation (51) and Equation (52), the following conditions must be satisfied:

- If there are no inequality constraints, both equations are equivalent.
- In case of the fully constrained case, the Lagrange multiplier for the inequality constraint  $z^k$  must be 0.

The first-order necessary optimality conditions, which are important to determine a local minimum are:

$$\begin{aligned}
& \nabla \mathcal{L}(x^*, y^*, z^*) = \nabla f(x^*) + \nabla c_E f(x^*) y^* + \nabla c_I f(x^*) z^* = 0 \\
& \text{with } x^* \in \mathbb{R}^n, y^* \in \mathbb{R}^m \text{ and } z^* \in \mathbb{R}^p,
\end{aligned} \tag{55}$$

and the second order sufficient optimality conditions are the following:

- The columns of  $G(x^*)$  are linearly independent,
- Strict complementary slackness holds at  $x^*$ , and
- The Hessian of the Lagrangian is positive definite, when  $x$  is positive definite on the null space of  $G(x^*)^T$

where  $G(x^*)$  is a matrix of first derivatives for equality constraints  $c$  and strict complementary slackness  $g$ :

$$\begin{aligned}
G(x^*) &= \left( \nabla c_{E1}(x), \nabla c_{E2}(x), \dots, \nabla c_{Em}(x), \nabla g_{i1}(x), \dots, \nabla g_{iqx}(x) \right), \text{ subject to} \\
g_i(x^*) z^* &= 0, \quad 1 \leq i \leq p \\
z^* &> 0, \quad i \in
\end{aligned} \tag{56}$$

where  $I_{ac}(x^*)$  is known as a set of active constraints:

$$I_{ac}(x^*) = \{i \in \{1, \dots, p\} \mid c_{Ii}(x) = 0\}. \quad (57)$$

The optimization process terminates and returns an optimal solution  $x^*$  when the iteration  $x^k$  for the QP subproblem is the same with the active constraints at the iteration  $x^k$ :

$$\begin{aligned} \min \quad & \nabla f(x^k)^T d(x) + \frac{1}{2} d(x)^T B_k d(x), \\ \text{subject to} \quad & \nabla c_I(x^k)^T d(x) + c_I(x^k) = 0. \end{aligned} \quad (58)$$

## **4. Coefficients estimation using mathematical optimization**

### **4.1 Introduction**

This chapter introduces an overall procedure to estimate hydrodynamic derivatives for a ship's hull using mathematical optimization algorithms and a ship's equations of motion which are described in previous chapters. Optimization problems, such as variables, and objective function and constraints, are demonstrated according to the sequence of the mathematical optimization. Also, basic information on reference data and ways to acquire them will be provided.

Aims of this chapter can be mainly distinguished into two parts. The first one is that sea trial data can be suitable for reference data for the optimization process. Success of this aim can be determined how simulation data using optimized coefficients are close to the reference data. If it is satisfactory, the second aim finds which algorithm is the most proper one to the mathematical optimization using sea trial data. With preparation and verification of the optimization, estimation of hydrodynamic coefficients considering trim and draught conditions are tried in the next chapter.

### **4.2 About the mathematical optimization**

The mathematical optimization finds minimums or maximums of an objective function with certain constraints. Especially for the optimization of hydrodynamic coefficients, this is a series of processes to acquire optimized coefficients which return similar manoeuvring characteristics with certain reference data. These data can be measured from sea trials and are essential to set up an objective function and constraints, to compare with simulation results at each iteration.

Figure 4.1 shows a concept for the optimization process, especially for estimating hydrodynamic coefficients. When a user provides reference data, initial coefficients and lower/upper bounds, an optimization solver finds an optimal solution according to a designated optimization algorithm. The algorithm calculates a set of hydrodynamic coefficients, satisfying all constraints, and checks an optimality of the objective function which compares simulation data using the coefficients with the reference data. If the objective

function satisfies certain criteria, the optimization process stops and returns an optimal solution.

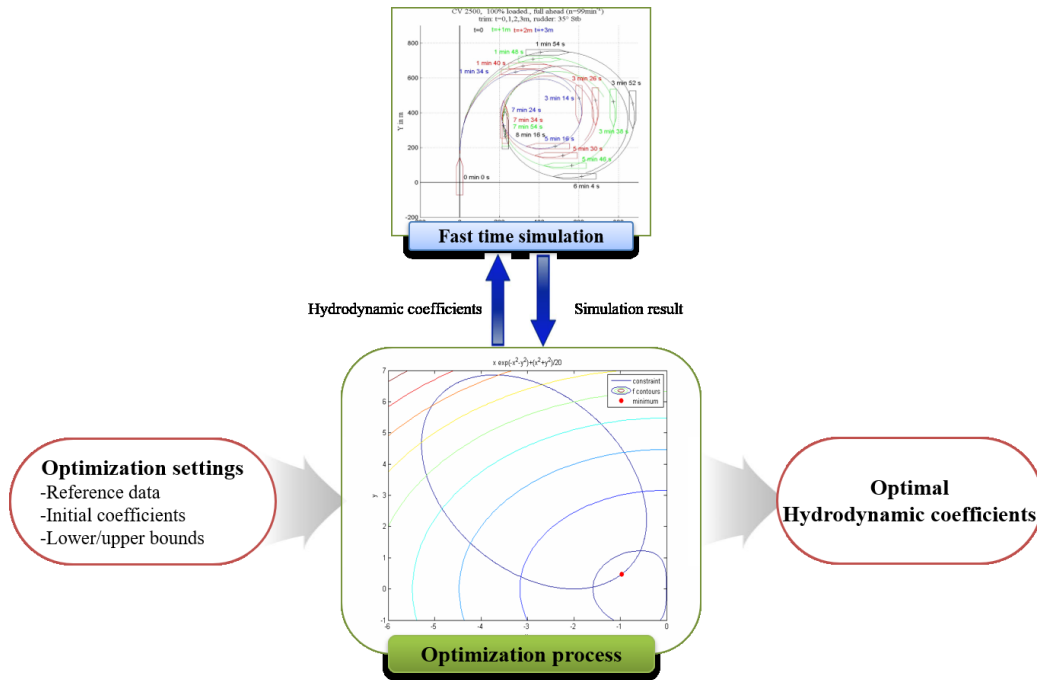


Figure 4.1 Concept of optimization process to estimate hydrodynamic coefficients

### 4.3 Setting of optimization problems

Solvers and corresponding algorithms in the optimization toolbox of the MATLAB are used for the estimation of hydrodynamic coefficients. Also, the fast-time simulation software SIMOPT is used for the simulation in the optimization procedure. This software is suitable for the optimization process because it allows to perform a large number of simulations in a short time. In addition, users can control parameters of a ship from the outside of the software. This is suitable for the optimization process which must change hydrodynamic coefficients and manoeuvre simulations at each iteration.

Equation (20) in Chapter 2 have too many hydrodynamic coefficients to conduct optimization at once. Thus, applying strict standards to select hydrodynamic coefficients are required for effective optimization. For this, a sensitivity analysis for selecting proper manoeuvres and corresponding coefficients should be performed prior to start the optimization procedure.

A general definition of the sensitivity analysis is a process of checking how the change of the input information affects the output change. The sensitivity analysis enables figuring out proper variables, a set of hydrodynamic coefficients for this study, for the optimization. Normally this can be divided into two types: global sensitivity and local sensitivity. In most cases, a term ‘sensitivity’ refers to the local sensitivity and it can also be divided into direct method, indirect method and green function method, and this study applies the indirect method for the sensitivity analysis [18].

The indirect method is the simplest way to find sensitivity, and it calculates correlation between a parameter and corresponding function using finite difference approximation:

$$\left| \frac{\partial f}{\partial x_i} \right| \approx \left| \frac{f(x_i + \Delta x_i) - f(x_i)}{\Delta x_i} \right|, \quad \text{with } i = 1, \dots, n. \quad (59)$$

This study applies three manoeuvres: straight motion with constant speed, zig-zag manoeuvre and turning manoeuvre. Sensitivity is calculated from changes of manoeuvre characteristics according to the change of each parameter in a certain range.

The calculated sensitivities may differ due to size or unit of corresponding parameters. Thus, it is required to conduct normalization to compare them at once. The normalization means adjusting values measured on different scales to common scale. Z-scores, min-max method and normalization by decimal scaling are well known methods.

The min-max normalization performs a linear transformation of the original data. This method converts a value  $d$  of a group of parameters  $P$  to  $d'$  in the new range [new.min( $P$ ), new.max( $P$ )], as follows:

$$d' = \frac{(d - \min(P)) * (\text{new.max}(P) - \text{new.min}(P))}{\max(P) - \min(P)} + \text{new.min}(P). \quad (60)$$

If the desired range is from 0 to 1, Equation (60) can be converted simply as shown below:

$$d' = \frac{d - \min(p)}{\max(p) - \min(p)} \quad (61)$$

As described above, the sensitivity analysis and the normalization are divided into three steps for the stepwise optimization for estimating hydrodynamic coefficients. Target coefficients for each sensitivity analysis are chosen according to basic characteristics of

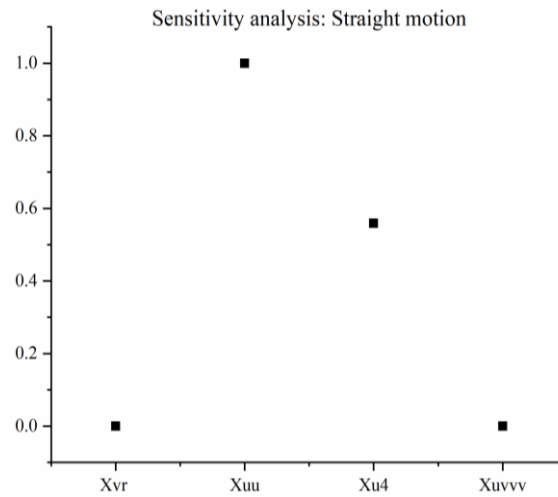
each manoeuvre: straight motion, steer a ship with small rudder angle and large rudder angle. Added mass which are combined with acceleration components in Equation (20) are excluded in the sensitivity analysis and corresponding normalization due to their complexity. Table 4.1 shows results of the sensitivity analysis and the normalization.

The first step compares only coefficients in the force acting on the X-axis, and coefficients  $X_{uu}$  and  $X_{u4}$  are the values of interest. For the second step, coefficients  $X_{vr}$  and linear components acting on Y- and Z-axis are compared with the small rudder angle. The result shows that the coefficient  $N_{uv}$  is the biggest influence on zig-zag manoeuvre and  $X_{vr}$  has no influence. The last step compares  $X_{vr}$  and the remaining nonlinear components acting on Y- and Z- axis. From this, coefficients  $X_{vr}$ ,  $Y_{vr}$ ,  $N_{rr}$  and  $N_{vv}$  are chosen as manipulate variables. Figure 4.2 shows corresponding results of the sensitivity analysis.

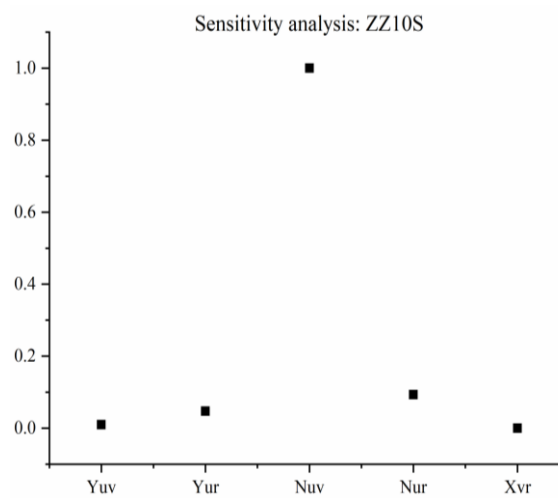
Table 4.1 Results of sensitivity analysis on hydrodynamic coefficients

Coefficients	Step 1 Straight motion	Step 2 Zig-zag, 10 deg.	Step 3 Turning, 35 deg.
$X_{vr}$	0	0	0.0890
$X_{uu}$	1.0000		
$X_{u4}$	0.5587		
$X_{uvvv}$	0		
$Y_{uv}$		0.0096	
$Y_{ur}$		0.0476	
$N_{uv}$		1.0000	
$N_{ur}$		0.0930	
$Y_{rr}$			0
$Y_{vv}$			0
$Y_{vrt}$			0
$Y_{vr}$			0.0675
$Y_{vvvr}$			0.0088
$Y_{rrt}$			0
$Y_{vvt}$			0
$Y_{4v2rt}$			0
$N_{vr}$			0
$N_{rrt}$			0
$N_{vvt}$			0
$N_{rr}$			1.0000
$N_{vv}$			0.2213
$N_{v4r2}$			0.0264
$N_{vrt}$			0
$N_{5v3rt}$			0

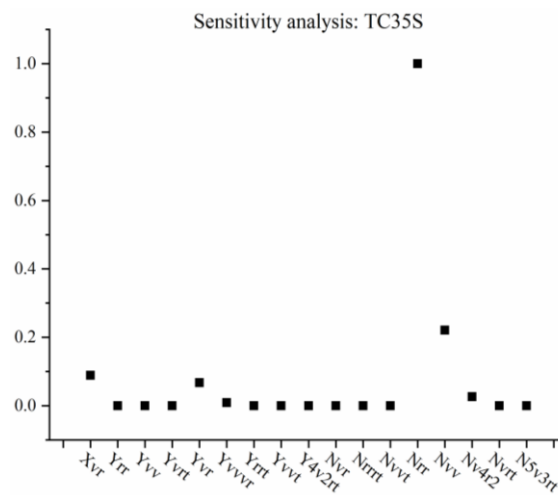




(a) Sensitivity analysis for straight motion



(b) Sensitivity analysis for zig-zag manoeuvre



(c) Sensitivity analysis for turning manoeuvre

Figure 4.2 Results of sensitivity analysis on hydrodynamic coefficients

Table 4.2 summarizes the variables for each optimization step.

Table 4.2 Variables on each optimization step

Step	Coefficients	Remarks
1	$X_{uu}, X_{u4}$	Straight motion
2	$Y_{uv}, Y_{ur}, N_{uv}, N_{ur}$	Zig-zag manoeuvre (10 deg.): Small rudder angle
3	$X_{vr}, Y_{vr}, N_{rr}, N_{vv}$	Turning manoeuvre (35 deg.): Large rudder angle

#### 4.4 Sea trial measurements and corrections for reference data

The objective function and constraints are written using reference data from sea trials, which were taken only for this thesis. The author planned and managed the whole process of the trials. The measurements are taken from a training ship of G/T 6,686t. The objective function compares trajectories of the reference data and trajectories of a simulation result which is based on calculated coefficients at each iteration. The constraint function compares manoeuvre characteristics of the same manoeuvre with the objective function. All of constraints are set as equality constraints. The biggest advantage of this idea is that optimization requires measurement data for ship's trajectories and this enables simple procedures during the sea trial measurements. Table 4.3 shows details of the reference vessel and equation (62) shows a concept of the objective function:

Table 4.3 Details of the reference vessel for comparing optimization algorithms

Type of vessel	Training ship
Length overall [m]	117.20
Length between perpendiculars [m]	104.42
Breadth [m]	17.80
Depth at upper deck [m]	10.85
Gross tonnage	6,686.00
Type of main engine	MAN B&W 6L42MC/ME
Maximum power [KW]	6,052.54
Maximum speed [kts]	18.40
Propeller	Single, right-handed, fixed-pitch
Draught forward (sea trial) [m]	6.10
Draught aft (sea trial) [m]	6.10
Displacement (sea trial) [ton]	6,741.70

$$f_{objective} = \sum_i |(pos.x_i^{reference} - pos.x_i^{iteration})| + \sum_i |(pos.y_i^{reference} - pos.y_i^{iteration})|. \quad (62)$$

Sea trials are carried out in accordance with recommendations of IMO and ITTC [23,27], as stated in the subchapter 2.2. Table 4.4 shows environmental conditions for sea trials. Time histories of position, heading, speed, rudder angle, propeller revolution and environmental information are measured during the sea trial. Table 4.5 and Table 4.6 show time histories for the zig-zag and turning manoeuvre, respectively.

Table 4.4 Summary of conditions for sea trials

	Data1	Data2
Manoeuvre	ZZ10	TC35
Latitude	34.98N	34.95N
Longitude	129.12E	129.09E
Heading [deg]	210	220
RPM [%]	681	681
Draught fore [m]	6.10	6.10
Draught mid [m]	6.10	6.10
Draught aft [m]	6.10	6.10
Wind direction [deg]	286	286
Wind speed [kts]	5.8	5.8
Current direction [deg]	225	225
Current speed [kts]	0.5	0.5
Water depth [m]	83	89

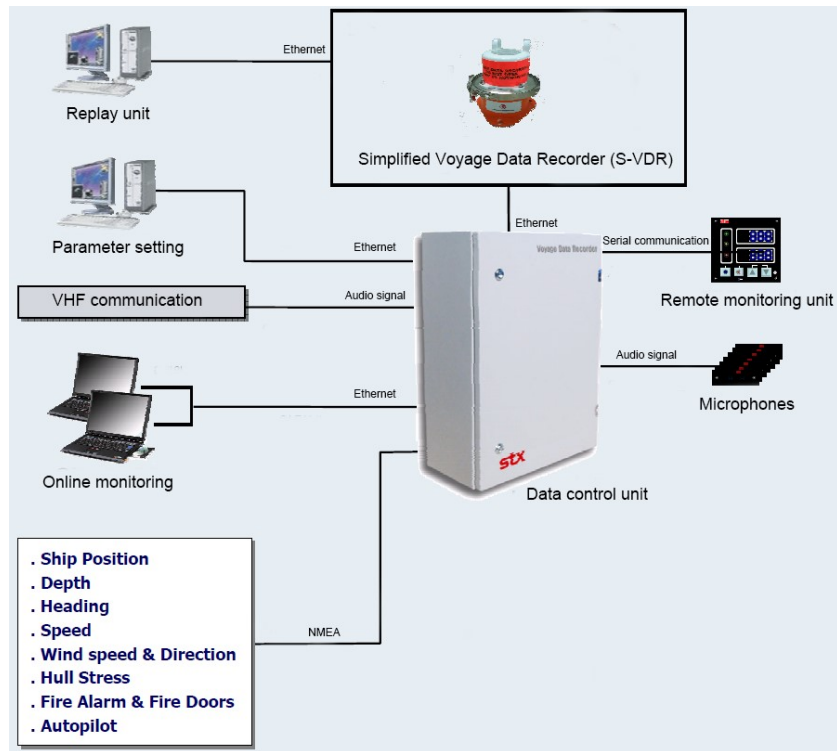
Table 4.5 Time history for zig-zag manoeuvre

Time (UTC)	Comments	Heading [deg]	Speed [kts]	Rudder [deg]	$\Delta$ Heading [deg]
07:39:23	Start recording	210	11.8	0	
07:39:33	Command, 10° Starboard	210	11.8	-	-
07:39:35	Rudder set to 10° Starboard	210	11.8	+10	-
07:40:02	Command, 10° Port	220	11.6	-	+10
07:40:06	Rudder set to 10° Port	220	11.6	-10	-
07:41:17	Command, 10° Starboard	200	10.6	-	-10
07:41:21	Rudder set to 10° Starboard	200	10.4	+10	-
07:42:35	Command, 10° Port	220	10.1	-	+10
07:42:39	Rudder set to 10° Port	220	10.1	-10	-
07:43:05	Terminate recording				

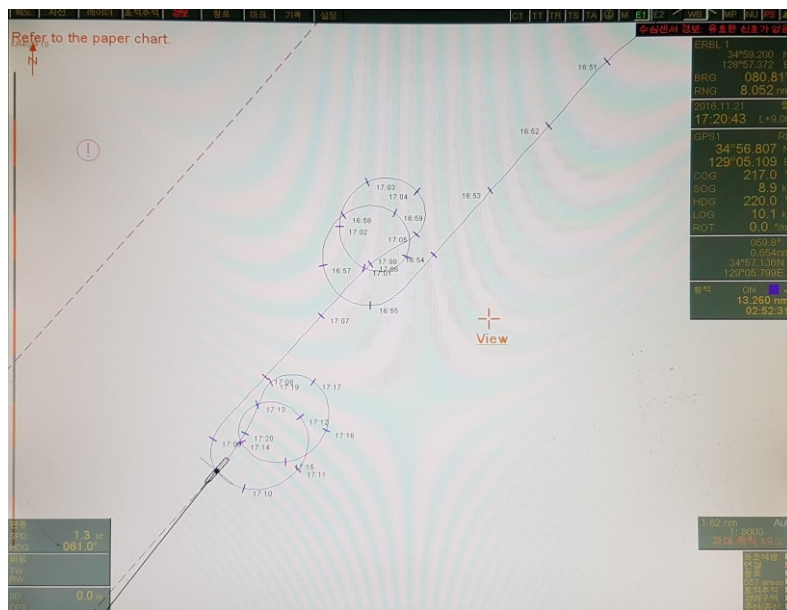
Table 4.6 Time history for turning manoeuvre

Time (UTC)	Comments	Heading [deg]	Speed [kts]	Rudder [deg]
07:54:55	Start recording	220	10.6	0
07:55:05	Command, 35° Starboard	220	10.6	-
07:55:15	Rudder set to 35° Starboard	220	10.6	+35
08:05:20	Terminate recording			

These data are taken from NMEA data in the voyage data recorder (VDR), provided by STX Engine – VDR 5000, and electronic chart display (ECDIS), provided by Marine Electronics – PM3D, in the reference vessel. The data of VDR are preferentially used, and data collected by other means are used as supplementation. Figure 4.3 introduces means of data acquisition for the measurement in this chapter.



(a) Simplified Voyage Data Recorder (S-VDR)



(b) Electronic Chart Display (ECDIS)

Figure 4.3 Means of data acquisition: S-VDR and ECDIS [65]

Sea trials should be carried out in calm weather conditions, as the situation allows. However, it is hard to conduct sea trials with desired weather conditions due to many reasons. In case of ship's manoeuvrability assessment, the trial results can be corrected, if the minimum weather conditions for the criteria requirements are not met. In this study, for

the purpose of comparing optimization algorithms, environmental effects on the measurement data are corrected according to the IMO recommendation [23].

This correction starts from the results of the turning manoeuvre. The turning circle test results are useful to measure the magnitude and direction of current. At the time of the sea trial, the ship's dynamic information, such as position and heading, should be collected until at least 720° of heading change. Two half circles which can be measured after 180° of heading change from the initial heading are used for estimating magnitude and direction of the environmental effect, especially for current. Equation (63) shows the local current velocity  $\underline{V}_i$  which can be defined by the two positions,  $(x_{1i}, y_{1i}, t_{1i})$  and  $(x_{2i}, y_{2i}, t_{2i})$ , from the half circles:

$$\underline{V}_i = \frac{(x_{2i} - x_{1i}, y_{2i} - y_{1i})}{(t_{2i} - t_{1i})}. \quad (63)$$

From sets of local velocity, the estimated current velocity can be calculated from Equation (64):

$$\underline{V}_c = \frac{1}{n} \sum_{i=1}^n \underline{V}_i = \frac{1}{n} \sum_{i=1}^n \frac{(x_{2i} - x_{1i}, y_{2i} - y_{1i})}{(t_{2i} - t_{1i})}. \quad (64)$$

The magnitude of the current velocity can be calculated as

$$V_c = |\underline{V}_c|. \quad (65)$$

The final corrected trajectories of the measurement data can be obtained from the following:

$$\underline{x}'(t) = \underline{x}(t) - \underline{V}_c t, \quad (66)$$

where  $\underline{x}(t)$  is the measured position vector and  $\underline{x}'(t)$  is the corrected position of the ship and  $\underline{x}'(t) = \underline{x}(t)$  at  $t = 0$ .

Figure 4.4 compares the measured sea trial trajectory and the corrected trajectory. Correction values are obtained from the measurement of turning manoeuvre, and they are

also applied to the measurement of the zig-zag manoeuvre. Both trajectories are corrected environmental effects which force the ship shift to the north-east direction.

Optimizations are carried out with six conditions using four algorithms: a solver ‘fmincon’ uses the interior point and the SQP algorithms, a solver ‘fminunc’ uses the Quasi-Newton algorithm and a solver ‘fminsearch’ uses the Nelder-Mead algorithm. Algorithms for constrained optimization, the interior point and the SQP are also be divided to optimizations with and without constraints. As mentioned in Table 4.2, stepwise optimization is carried out in the order of the straight motion, the zig-zag manoeuvre and the turning manoeuvre. Step 2 and Step 3 change coefficients which are already optimized in the previous step(s), prior to starting the main optimization process.

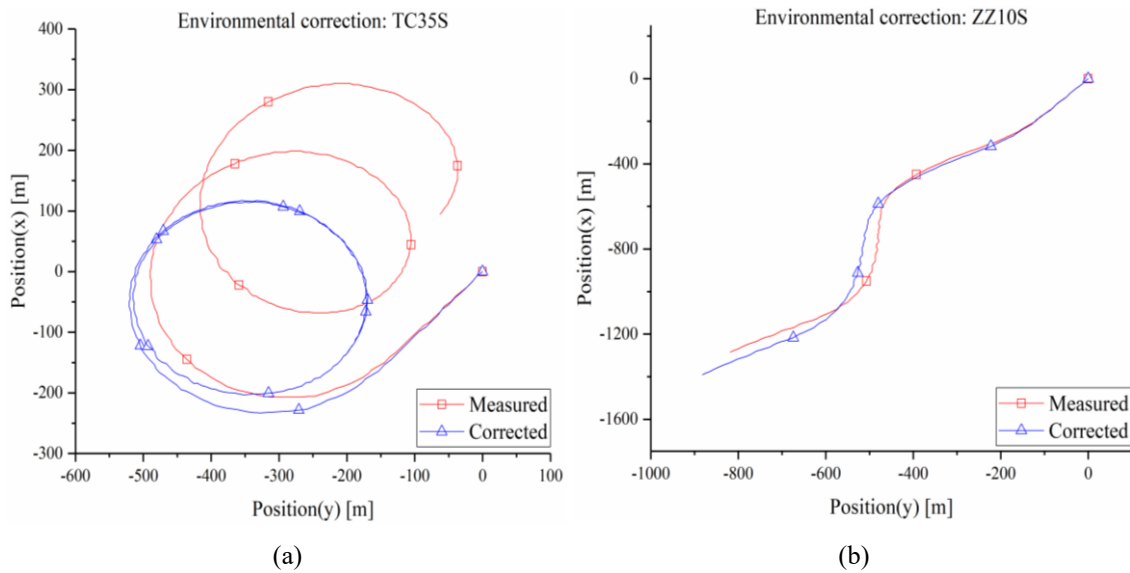


Figure 4.4 Comparisons of measurement data and corrected data

Table 4.7 shows detailed conditions of the optimization for this chapter. Initial values can be calculated from the Clarke estimation. Lower and upper bounds apply close value to 0 or 10 times greater than the initial value. Step 1 conducts optimization without constraints, due to simple manoeuvre and relatively small number of variables. Step 2 and 3 apply constraints using manoeuvre characteristics, such as overshoot angle and tactical diameter, if applicable.

Table 4.7 Detailed conditions of optimization

Step 1			Step 2		Step 3	
Solver (Algorithm)			fmincon (interior-point, SQP) fminunc (Quasi-Newton) fminsearch (Nelder-Mead)			
Initial values	$X_{uu}$	-0.0458	$Y_{uv}$	-1.5336	$X_{vr}$	1.0225
	$X_{u4}$	-0.3490	$Y_{ur}$	0.3245	$Y_{vr}$	1.7265
			$N_{uv}$	-0.5796	$N_{rr}$	0.1079
			$N_{ur}$	-0.2429	$N_{vv}$	0.8633
Lower bounds	$X_{uu}$	-0.4000	$Y_{uv}$	-15.3360	$X_{vr}$	0.0001
	$X_{u4}$	-3.0000	$Y_{ur}$	0.0001	$Y_{vr}$	0.0001
			$N_{uv}$	-5.7960	$N_{rr}$	0.0001
			$N_{ur}$	-0.2429	$N_{vv}$	0.0001
Upper bounds	$X_{uu}$	-0.0001	$Y_{uv}$	-0.0001	$X_{vr}$	10.0000
	$X_{u4}$	-0.0001	$Y_{ur}$	3.2450	$Y_{vr}$	17.0000
			$N_{uv}$	-0.0001	$N_{rr}$	1.0790
			$N_{ur}$	-0.0001	$N_{vv}$	8.6330
Objective function	Track difference					
	Straight motion		Zig-zag, 10 deg.		Turning, 35 deg.	
Constraints (if applicable)	-		First overshoot		Tactical diameter	

## 4.5 Optimization results

Table 4.8 shows Clarke coefficients, which are initial values in the optimization process and results of all optimizations at once. Optimized coefficients of step 1, constant speed with straight motion, are not different from the Clarke coefficients. In case of the step 2, the zig-zag manoeuvre with a rudder angle of 10 degrees, coefficients of yaw moment ( $N$ ) have more variation than coefficients of sway force ( $Y$ ). It relates to the results of the sensitivity analysis in the subchapter 4.2 that sensitivity for coefficients of yaw moment are greater than the others. Also, it is shown that the algorithms of constrained optimization, the interior point and the SQP, have different results according to the presence of constraints. This will be discussed later with simulation results using optimized coefficients. The results of step 3 also show that the coefficient  $N_{rr}$  which is the most sensible one has the biggest variation among variables.



Table 4.8 Summarization of Clarke coefficients and optimized coefficients

Coefficients	Clarke	IP (con)	IP (uncon)	SQP (con)	SQP (uncon)	QN	NM
$X_{uu}$	-0.0458	-0.0403	-0.0403	-0.0458	-0.0458	-0.0408	-0.0397
$X_{u4}$	-0.3490	-0.3490	-0.3490	-0.2323	-0.2323	-0.3480	-0.3575
$Y_{uv}$	-1.5336	-1.3006	-1.5283	-1.7185	-1.4252	-1.5257	-1.5188
$Y_{ur}$	0.3245	0.2888	0.2905	0.1780	0.3020	0.2970	0.2919
$N_{uv}$	-0.5796	-2.0583	-2.2262	-1.5637	-0.9484	-0.6141	-0.6293
$N_{ur}$	-0.2429	-0.7399	-0.7112	-0.4707	-0.2257	-0.1429	-0.1429
$X_{vr}$	1.0225	0.7680	0.4968	1.2000	0.0001	0.4167	1.0225
$Y_{vr}$	1.7265	2.4636	1.4223	1.6924	2.4582	1.8311	1.6099
$N_{rr}$	0.1079	0.0623	0.3461	0.1105	0.0172	0.3496	0.1079
$N_{vv}$	0.8633	0.6450	0.6232	1.0169	5.5060	0.6120	1.8633
Remarks	IP: Interior point SQP: Sequential quadratic programming QN: Quasi-Newton NM: Nelder-Mead			con: Constrained uncon: Unconstrained			

Table 4.9 shows manoeuvre characteristics of the reference data and simulations results using Clarke coefficients and optimized coefficients. Manoeuvre characteristics of the reference data are acquired from the measurement data which have been already corrected environmental effects. For the Clarke coefficients, simulation results are directly reflected in the results table. The simulation results using optimized coefficients are summarized step-by step to see the change of manoeuvring characteristics with step progress.

The selected manoeuvres for the simulation are the same as the optimization process: straight motion with constant speed, zig-zag manoeuvre with a rudder angle of 10 degrees and turning manoeuvre with a hard rudder. Manoeuvre characteristics are as follows: ratio of sailed distance for the straight motion to ship's length between perpendiculars (Way/LPP), first and second overshoot angles for the zig-zag manoeuvre and advance and tactical diameter for the turning manoeuvre.

Table 4.9 Manoeuvre characteristics of reference data and simulation results

	Straight	Zig-zag, 10 degrees		Turning, 35degrees	
	Way/LPP	Overshoot 1	Overshoot 2	Advance	Tactical dia.
Reference	23.4768	7.2	12.7	298.0000	399.5000
Clarke	23.0435	3.1	4.7	298.0729	430.2624
IP, step 1	23.4626	3.3	4.7	300.2329	433.8391
IP (con), step 2	23.4190	7.0	15.2	286.0168	353.8225
IP (con), step 3	23.4227	6.5	13.5	291.2115	389.6643
IP (uncon), step 2	23.4200	7.6	16.0	268.0846	336.7742
IP (uncon), step 3	23.4224	6.9	14.8	296.1285	393.6173
SQP, step 1	23.4435	3.3	4.6	299.8891	432.6124
SQP (con), step 2	23.1895	8.8	18.2	245.5009	300.8476
SQP (con), step 3	23.1896	8.6	17.9	247.0885	305.0851
SQP (uncon), step 2	22.6818	9.0	19.3	217.6083	270.2148
SQP (uncon), step 3	23.0396	5.9	8.7	329.6871	590.2585
QN, step 1	23.4268	3.3	4.6	299.9692	433.4675
QN, step 2	23.3352	7.3	13.0	222.3280	289.4011
QN, step 3	23.3541	5.6	8.8	285.9273	435.4688
NM, step 1	23.4787	3.3	4.6	300.3715	433.6262
NM, step 2	23.3100	7.9	14.1	219.6220	283.4635
NM, step 3	23.3281	6.8	11.0	246.2697	361.6117
Remarks	IP: Interior point SQP: Sequential quadratic programming QN: Quasi-Newton NM: Nelder-Mead				
				con: Constrained uncon: Unconstrained	

Figure 4.5 compares the manoeuvre characteristic, Way/LPP for the reference data and the simulation results. As shown in Table 4.9, Way/LPP for all simulations including results of Clarke coefficients are close to the reference data. Results for step 2 of the unconstrained SQP are the worst, and it is 3.38% lower than the reference data. It is shown that optimized coefficients of later steps can also affect a manoeuvrability of the straight motion.

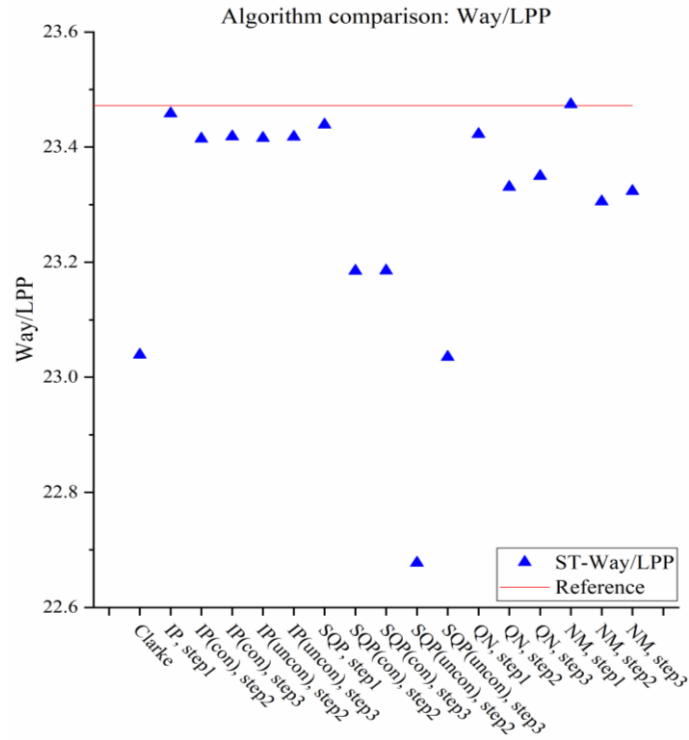


Figure 4.5 Comparison of optimization algorithms: straight motion

For step 2, as shown in Figure 4.6, the difference between the manoeuvre characteristics is larger than step 1. Results of the interior point and the Quasi-Newton algorithms are closer to the reference data than the rest results. In case of the interior point algorithm, the difference between constrained and unconstrained optimization is not large.

The results of step 3 show no significant difference from the results of step 2. The interior point and the Quasi-Newton algorithms have high similarity with the reference data, and in the order of the Nelder-Mead and the SQP algorithms. However, for the advance, the value for the Clarke coefficients is already close to the reference data. Because of this, advance values for the simulation using coefficients of step 1 are also close to the reference data. This means that the advance is not proper parameter to compare algorithms for this reference data. In addition, the advance should not be used as constraints.

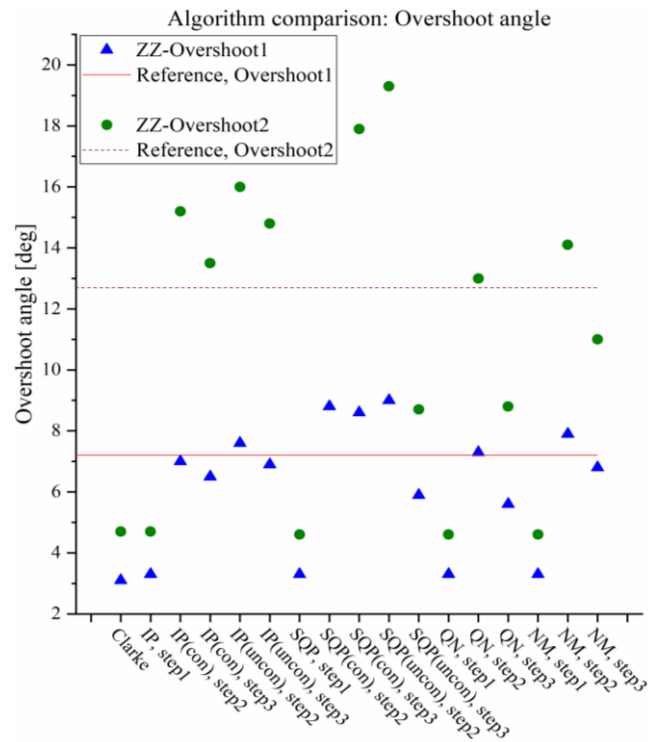


Figure 4.6 Comparison of optimization algorithms: zig-zag manoeuvre

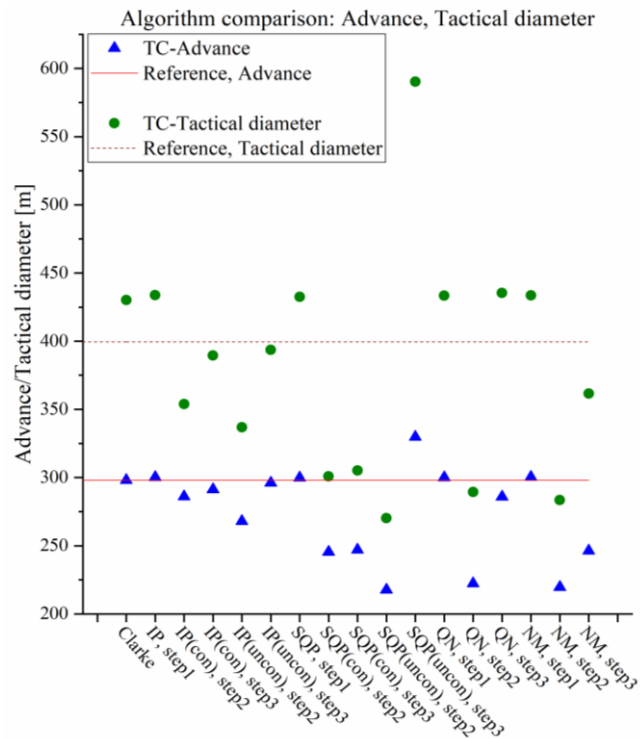


Figure 4.7 Comparison of optimization algorithms: turning manoeuvre

Following figures show trajectories for the straight motion and the turning manoeuvre, and time history of heading and rudder command, which are mentioned above. Figure 4.8 contains reference data, the simulation result using Clarke coefficients and simulation results using coefficients for all algorithms, only for step 1 results. Results of the straight motions are almost the similar with the reference data.

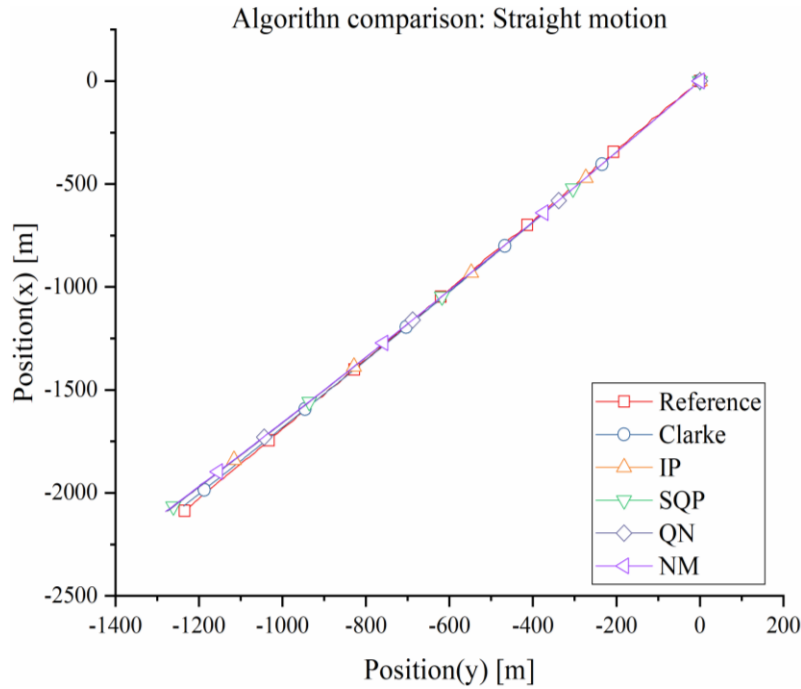


Figure 4.8 Comparison of trajectories: straight motion

Figure 4.9 and Figure 4.10 show results of the zig-zag simulation using coefficients of the step 2, excluding the results of the SQP and the QN which were worse than the others. The reference data and the result of Clarke coefficients are solid lines and the rest results are printed as dotted lines. The result of the Clarke coefficients shows clear difference from the reference data. In contrast to the first overshoot for optimized results, most second overshoot values are greater than the reference data. Simulation result of the interior point without constraints fits most well with the reference data.

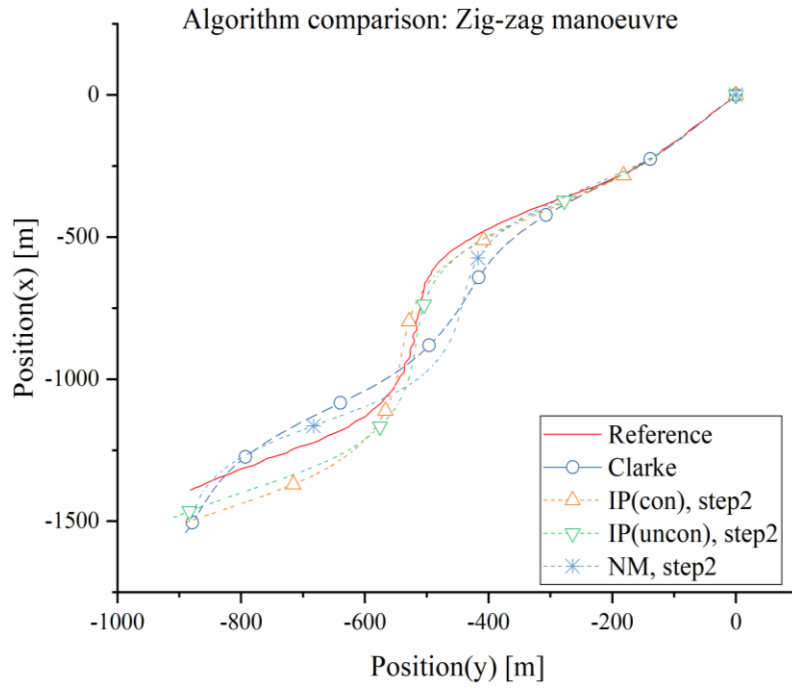


Figure 4.9 Comparison of trajectories: zig-zag motion

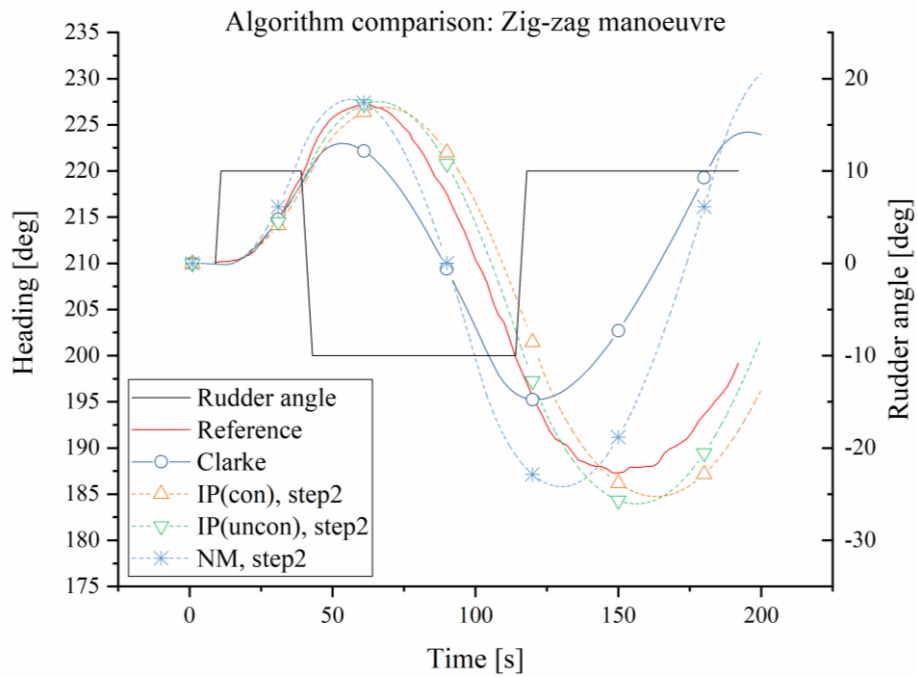


Figure 4.10 Comparison of heading change: zig-zag manoeuvre

Figure 4.11 shows results of the turning manoeuvre. Similar with the results of step 2, the circle of the SQP is significantly greater than both the reference data and other simulation

results. As mentioned above, values of the advance are similar with each other excluding the value of the SQP. For other algorithms, the shape and diameter of the circles are similar, but their positions differ.

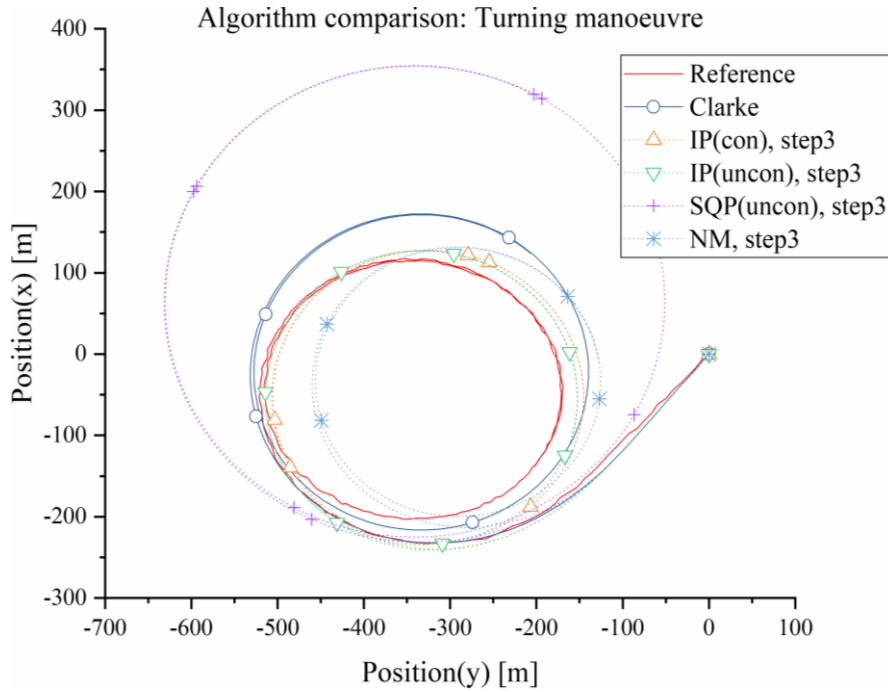


Figure 4.11 Comparison of trajectories: turning manoeuvre

Figure 4.12 to Figure 4.14 compare results of zig-zag manoeuvre using coefficients for the results of the optimization step 2 and 3, respectively. In every case, difference of the second overshoot angel from the reference from the simulation results for the step 3 is smaller than the ones for the step 2.

Considering the results, the interior point algorithm calculates the best solution for both constrained and unconstrained optimization. In the next chapter, unconstrained optimization with the interior point algorithm will be applied firstly; after that, if corresponding results are not satisfactory, constrained optimization will be tried.

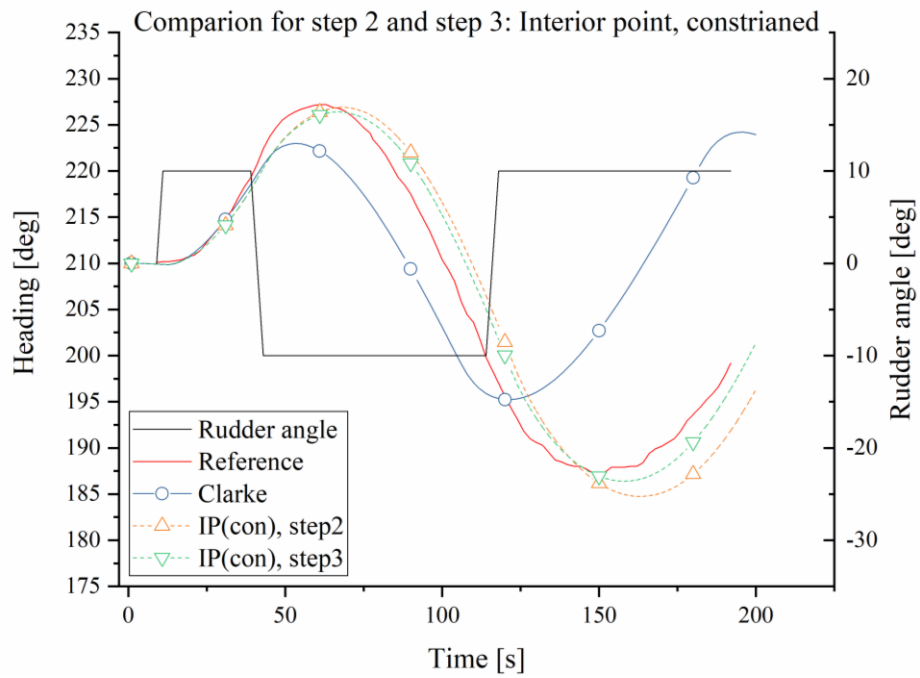


Figure 4.12 Comparison of heading change for optimization steps 2 and 3: Interior point algorithm with constraint

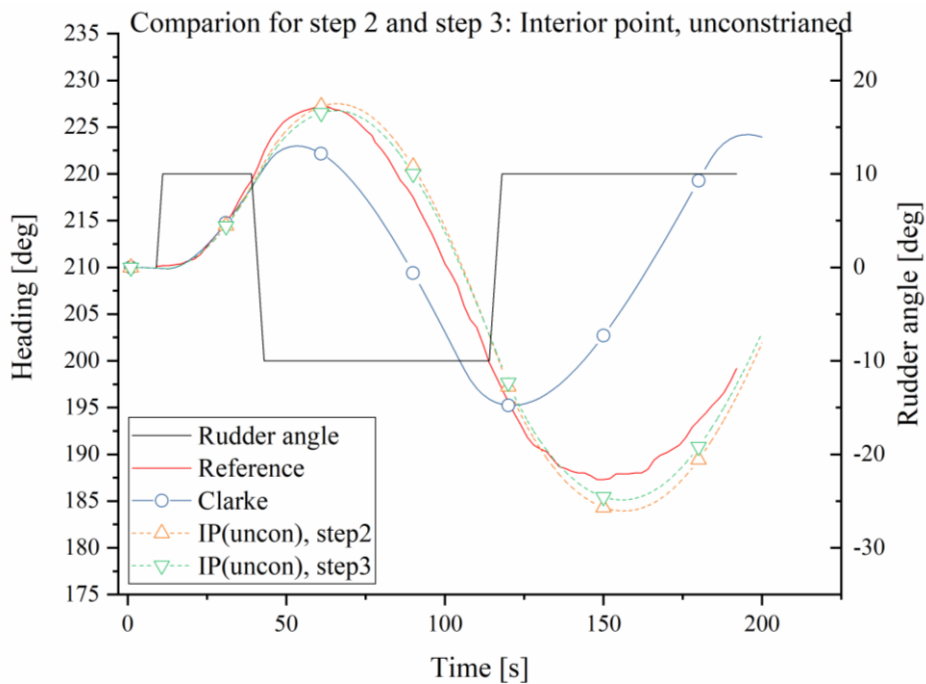


Figure 4.13 Comparison of heading change for optimization steps 2 and 3: Interior point algorithm without constraint



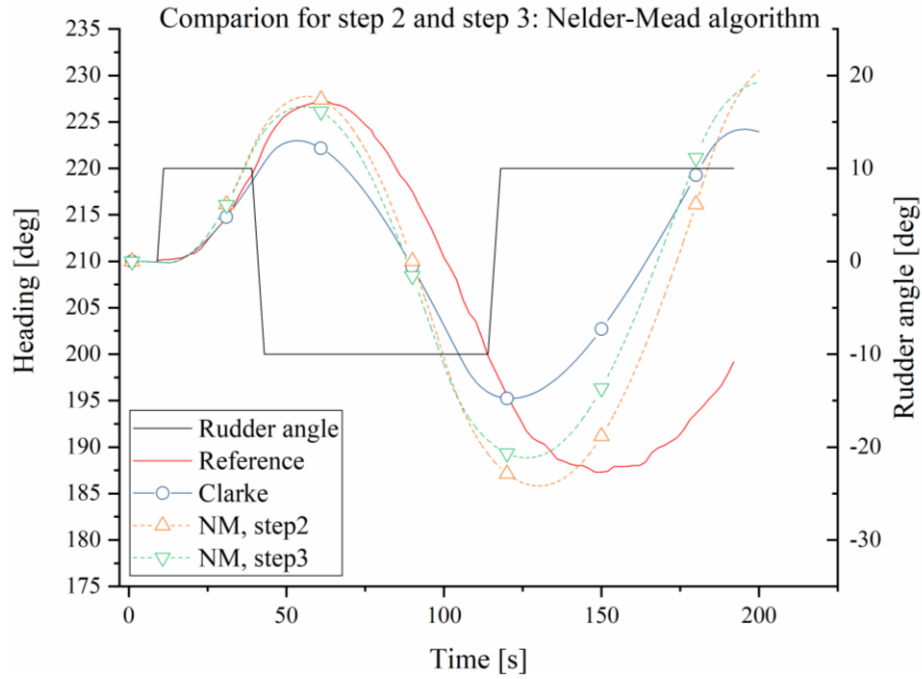


Figure 4.14 Comparison of heading change for optimization steps 2 and 3: Nelder-Mead algorithm

Figure 4.15 to Figure 4.17 show the history of iterations for each step. It seems that the ‘fmincon’ solver with the interior point algorithm has found optimal coefficients at the middle of the whole iterations. However, it takes more iterations to conclude them as a final solution. This is because of continuously descending gradients of the objective function. Regularly the algorithm starts an optimization for a certain coefficient from the lower or upper bound, prominent point in the iteration history, but soon the coefficient returns to the solution.

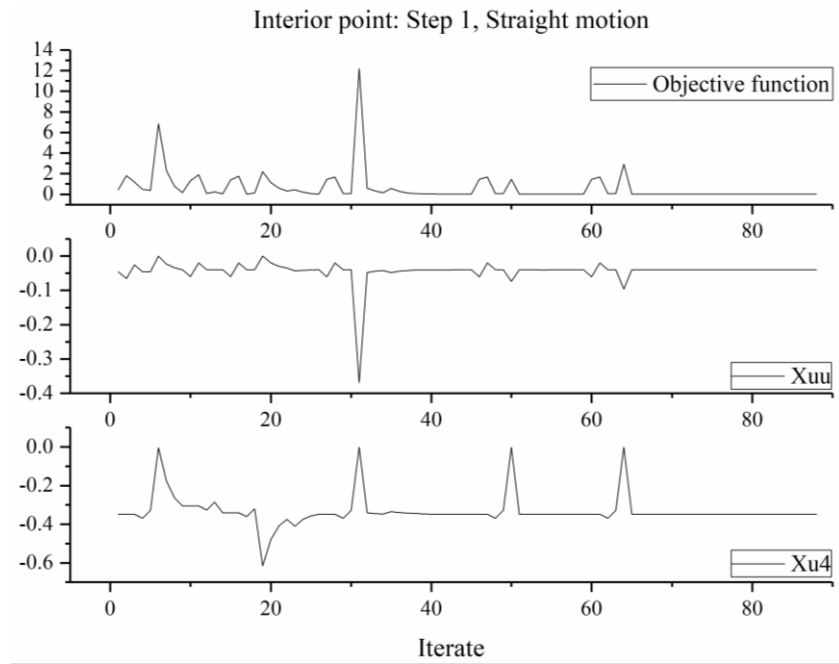


Figure 4.15 History of iteration: straight motion

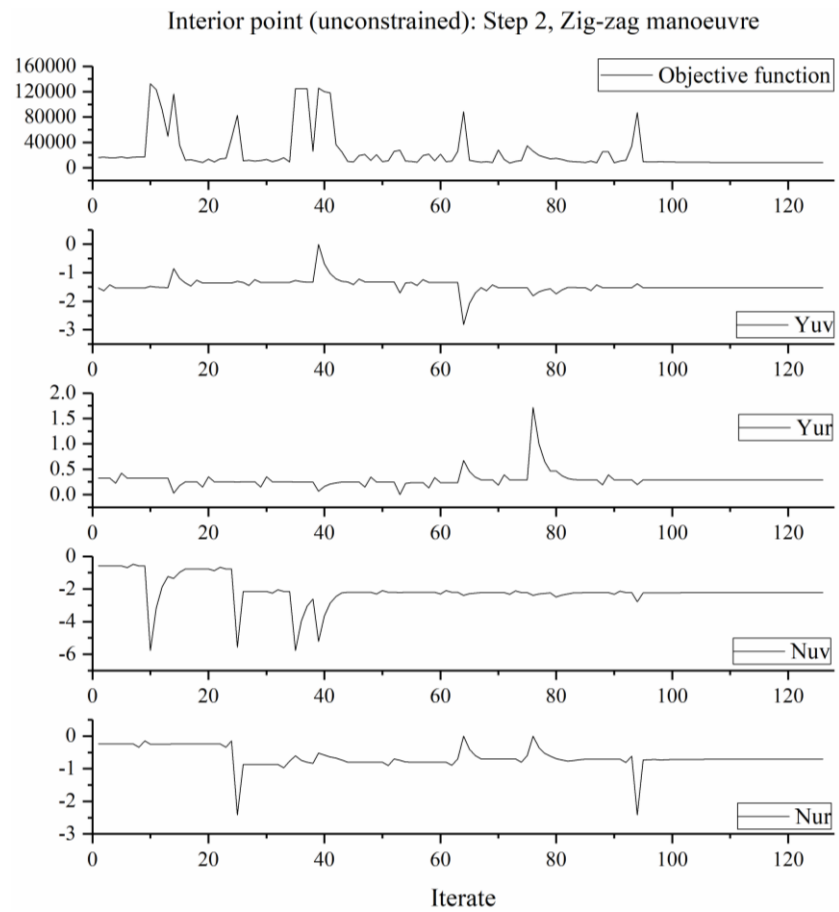


Figure 4.16 History of iteration: zig-zag manoeuvre

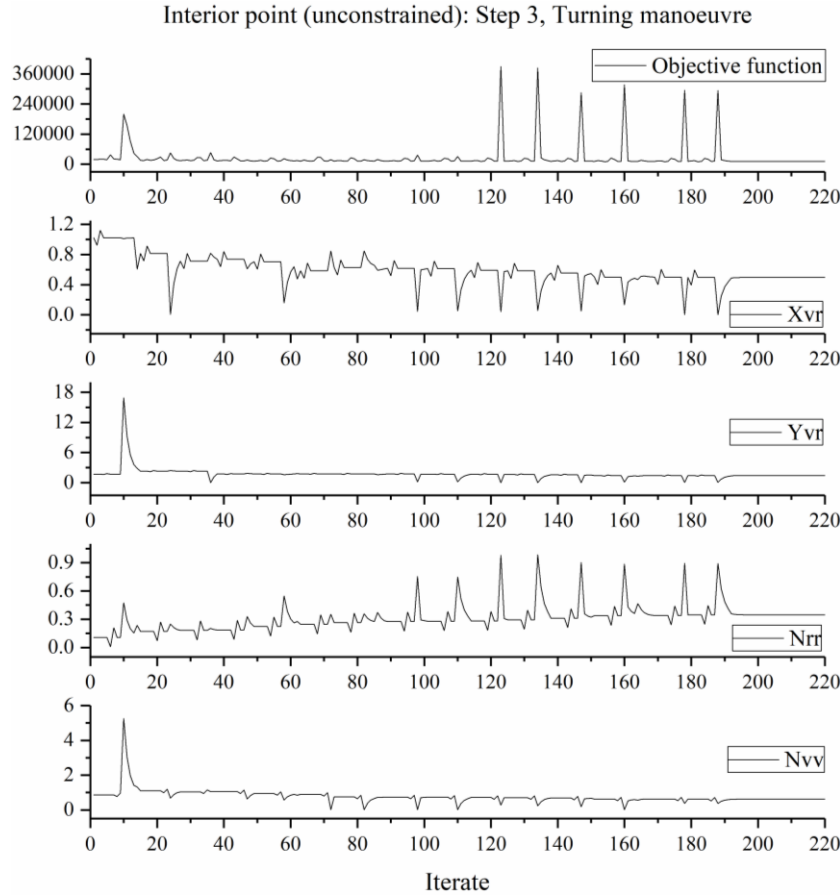


Figure 4.17 History of iterations: turning manoeuvre

## 4.6 Conclusion

In this chapter, an optimization problem was set up and its verification was carried out. Also, four optimization algorithms were compared to find the best algorithm for estimation of hydrodynamic coefficients.

The optimization problem consists of variables selection, reference selection for objective and constraint functions and optimization condition setting. Setting the optimal number of variables can help in making a more effective and faster optimization process. For this, optimal variables were selected through comparison of the hydrodynamic coefficients using sensitivity analysis and normalization. The reference data were borrowed from a set of sea trial data of a training ship, which were conducted and managed by author. The raw sea trial data were applied to the final reference data after applying the environmental influence correction formulas which are provided by IMO. The optimization conditions were set to six versions using four different algorithms. The optimizations were carried out stepwise according to the characteristics of each manoeuvre.

Most of the optimization results were similar with the reference. This seems to be the results of proper optimization problem setting and algorithm selection. Specifically, the optimization results fitted to the reference data in the order of the interior point, the Quasi-Newton, the Nelder-Mead and the SQP algorithms. In the next chapter, all the optimizations will be carried out using the interior-point algorithm.

## 5. Coefficients estimation for various trim and draught conditions

### 5.1 Introduction

This chapter estimates hydrodynamic coefficients considering various trim and draught conditions. Firstly, hydrodynamic coefficients are mathematically optimized using sea trial data with various trim and draught conditions. By utilizing those coefficients and corresponding trim and draught conditions, new coefficients which are for another trim and draught condition will be estimated, and simulation results using the new coefficients will also be compared with their reference data.

### 5.2 Optimization problems

Details of the reference vessel in this chapter are shown in Table 5.1. The vessel is a 4,500 TEU class container carrier with a length of 294 metres and a maximum draught of 13 metres. Sea trials were carried out in 2012 by Krüger [32].

Table 5.1 Details of the reference vessel

Type of vessel	4,500 TEU class container carrier
Length overall [m]	294.12
Length between perpendiculars [m]	283.20
Breadth, moulded [m]	32.20
Depth, moulded [m]	10.85
Design draught, moulded [m]	12.00
Scantling draught, moulded [m]	13.00
Gross tonnage	53,324.00
Deadweight [ton]	63,510.00
Full load displacement [ton]	82,496.00
Type of main engine	MAN B&W 9K90MC-C
Maximum power [KW]	41,040.00
Maximum speed [kts]	23.70
Propeller	Single, right-handed, fixed-pitch

Table 5.2 summarizes conditions of each sea trial. All five trials are zig-zag manoeuvres, and they can be divided into three trim and draught conditions: mean trim 9.35 metres

with trim 0.5 metres by stern, mean trim 10 metres with even keel and mean trim 12.875 metres with trim 0.25 metres by stern. Unlike Chapter 4, all simulations used in this chapter consider the environment influence, wind and currents at the time of sea trials. Time histories for each manoeuvre will be presented in 7.

Table 5.2 Summary of conditions for sea trials

	Data1	Data2	Data3	Data4	Data5
Manoeuvre	ZZ10P	ZZ10S	ZZ10S	ZZ10P	ZZ20S
Latitude	32.8N	32.0N	10.7N	9.7N	9.7N
Longitude	119.9W	117.3W	67.2W	79.6W	79.6W
Heading [deg]	110	110	260	250	250
RPM [‰]	843	620	676	422	422
Draught fore [m]	12.75	12.75	10.00	9.10	9.10
Draught mid [m]	12.55	12.55	10.00	-	-
Draught aft [m]	13.00	13.00	10.00	9.60	9.60
Wind direction [deg]	270	310	20	50	50
Wind speed [kts]	12	15	5	15	15
Current direction [deg]	160.47	251.56	169.50	23.62	23.62
Current speed [kts]	1.37	0.88	0.28	1.25	1.55
Water depth [m]	>1000	>1000	>1000	>1000	>1000

Table 5.3 shows selection of variables through sensitivity analysis and normalization, with the same process as in Chapter 4. However, coefficients for steering with a large rudder angle are excluded from variables because all the measurements are zig-zag manoeuvres. The selected variables are the same as those of Chapter 4.

Table 5.3 Variables on each optimization step

Step	Coefficients	Remarks
1	$X_{uu}, X_{u4}$	Straight motion
2	$Y_{uv}, Y_{ur}, N_{uv}, N_{ur}$	Zig-zag manoeuvre (10 deg.): Small rudder angle

Data 2, 3 and 4 in Table 5.2 which have different trim and draught conditions are optimized first. Table 5.4 summarizes optimization conditions of the data.

Table 5.4 Detailed conditions of optimization

		Data 2 (ZZ10S, draught=12.875m, trim=0.25m)				Data 3 (ZZ10S, draught=10.00m, trim=0)				Data 4 (ZZ10P, draught=9.35m, trim=0.5m)			
		Step 1		Step 2		Step 1		Step 2		Step 1		Step 2	
Solver (Algorithm)		fmincon (interior-point)											
Initial values	$X_{uu}$	-0.0280	$Y_{uv}$	-1.5857	$X_{uu}$	-0.0373	$Y_{uv}$	-1.3811	$X_{uu}$	-0.0407	$Y_{uv}$	-1.3947	
	$X_{u4}$	-0.3405	$Y_{ur}$	0.4281	$X_{u4}$	-0.4534	$Y_{ur}$	0.3820	$X_{u4}$	-0.4948	$Y_{ur}$	0.3934	
			$N_{uv}$	-0.5625			$N_{uv}$	-0.4401			$N_{uv}$	-0.3965	
			$N_{ur}$	-0.2675			$N_{ur}$	-0.2348			$N_{ur}$	-0.2339	
Lower bounds	$X_{uu}$	-0.2800	$Y_{uv}$	-15.8567	$X_{uu}$	-0.3700	$Y_{uv}$	-13.8110	$X_{uu}$	-0.4037	$Y_{uv}$	-13.9472	
	$X_{u4}$	-3.4050	$Y_{ur}$	0.0001	$X_{u4}$	-4.5000	$Y_{ur}$	0.0001	$X_{u4}$	-4.9485	$Y_{ur}$	0.0001	
			$N_{uv}$	-5.6252			$N_{uv}$	-4.4019			$N_{uv}$	-3.9654	
			$N_{ur}$	-2.6753			$N_{ur}$	-2.3480			$N_{ur}$	-2.3396	
Upper bounds	$X_{uu}$	-0.0001	$Y_{uv}$	-0.0001	$X_{uu}$	-0.0001	$Y_{uv}$	-0.0001	$X_{uu}$	-0.0001	$Y_{uv}$	-0.0001	
	$X_{u4}$	-0.0001	$Y_{ur}$	4.2813	$X_{u4}$	-0.0001	$Y_{ur}$	3.8201	$X_{u4}$	-0.0001	$Y_{ur}$	3.9344	
			$N_{uv}$	-0.0001			$N_{uv}$	-0.0001			$N_{uv}$	-0.0001	
			$N_{ur}$	-0.0001			$N_{ur}$	-0.0001			$N_{ur}$	-0.0001	
Objective function		Track difference											
		Straight motion		Zig-zag, 10 deg.		Straight motion		Zig-zag, 10 deg.		Straight motion		Zig-zag, 10 deg.	
Constraints		None											

Thereafter, in order to verify the optimization results, data 1 and 5 which have the same trim and draught condition with data 2 and 4, respectively.

### 5.3 Validation of optimization results using other sea trial data

Table 5.5 shows results of each mathematical optimization. In all the data, coefficients of step 1 do not show any significant change compared to the Clarke estimation coefficients. In contrast, in the case of the coefficients of step 2 which are acting on the y- and z-axis, some optimized coefficients have great differences compared to the Clarke estimation coefficients.

Table 5.5 Summarization of Clarke coefficients and optimized coefficients

Coefficients	Data 2		Data 3		Data 4	
	Clarke	Optimized	Clarke	Optimized	Clarke	Optimized
$X_{uu}$	-0.0280	-0.0250	-0.0373	-0.0515	-0.0407	-0.0665
$X_{u4}$	-0.3405	-0.2865	-0.4534	-0.5873	-0.4948	-0.4536
$Y_{uv}$	-1.5857	-1.9472	-1.3811	-2.2214	-1.3947	-2.2611
$Y_{ur}$	0.4281	0.3426	0.3820	0.4827	0.3934	0.3919
$N_{uv}$	-0.5625	-1.2354	-0.4401	-3.4181	-0.3965	-0.9541
$N_{ur}$	-0.2675	-0.2783	-0.2348	-0.6116	-0.2339	-0.2335
Remarks	Data 2: ZZ10S, draught=12.875m, trim=0.25m Data 3: ZZ10S, draught=10.00m, trim=0 Data 4: ZZ10P, draught=9.35m, trim=0.5m  Step 1: straight motion ( $X_{uu}, X_{u4}$ ), Step 2: zig-zag manoeuvre ( $Y_{uv}, Y_{ur}, N_{uv}, N_{ur}$ )					

Table 5.6 shows simulation results using the Clarke coefficients and the optimized coefficients together with the corresponding reference values. All simulation results of each step are shown in the table. For the straight motion with constant speed, as in Chapter 4, the comparison is based on the manoeuvring characteristic ‘way/LPP’. It is shown that the simulation results using the optimized coefficients are much closer to the reference data than the result using the Clarke coefficients.

In the zig-zag test, initial turning time and yaw check time are compared in addition to the overshoot angles. The initial turning time is an elapsed time of heading change by



initial steering order. The yaw check time can be taken from the point of the first steering command to the point of returning to the original heading after the second overshoot. Results of step 2 for all data are similar with the reference data compared to the result of the Clarke estimation. In the initial turning time and the yaw checking time, the distinction between results of the Clarke coefficients and the optimized ones cannot be clearly distinguished, but in the overshoot angles the difference between the two are obvious.

Table 5.6 Manoeuvre characteristics for reference data and simulation results

		Straight		Zig-zag, 10 degrees		
		Way/LPP	Init. turning	Yaw check	Overshoot 1	Overshoot 2
Data 2	Reference	3.53	58	370	6.70	11.80
	Clarke	3.33	82	366	1.87	2.73
	Step 1	3.52	79	319	1.99	2.55
	Step 2	3.52	69	378	5.31	9.66
Data 3	Reference	5.22	47	279	4.80	7.40
	Clarke	5.58	57	272	1.87	2.51
	Step 1	5.22	64	286	1.68	2.42
	Step 2	5.22	38	265	3.63	7.13
Data 4	Reference	3.52	78	398	3.20	4.60
	Clarke	3.89	89	414	1.71	1.79
	Step 1	3.50	93	438	1.53	1.72
	Step 2	3.51	87	423	2.98	3.90
		Data 2: ZZ10S, draught=12.875m, trim=0.25m				
		Data 3: ZZ10S, draught=10.00m, trim=0				
		Data 4: ZZ10P, draught=9.35m, trim=0.5m				
Remarks		Way/LPP: Distance from start point/LPP				
		Init. turning: Initial turning time [s]				
		Yaw check: Yaw checking time [s]				
		Overshoot 1: First overshoot angle [deg]				
		Overshoot 2: Second overshoot angle [deg]				

Figure 5.1 to Table 5.6 show both track difference and time history of heading for the results in the above table. As noted earlier, the simulation results using coefficients of the optimization step 2 are the most similar with the reference data. The simulation results using coefficients of the Clarke estimation and the optimization step 1 show no significant difference to each other in the zig-zag manoeuvre.

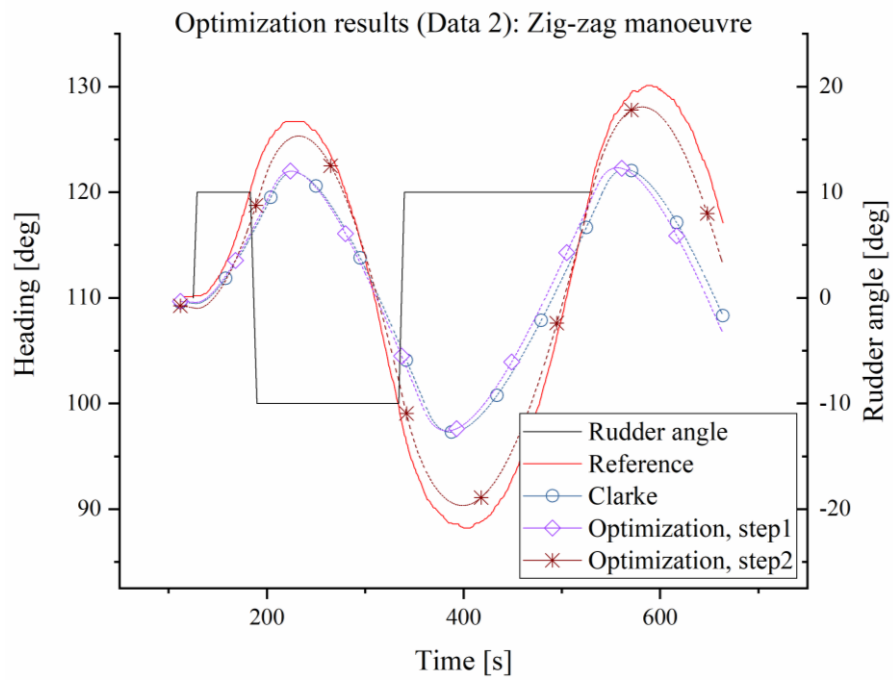


Figure 5.1 Comparison of heading change between sea trial data 2 and simulation results

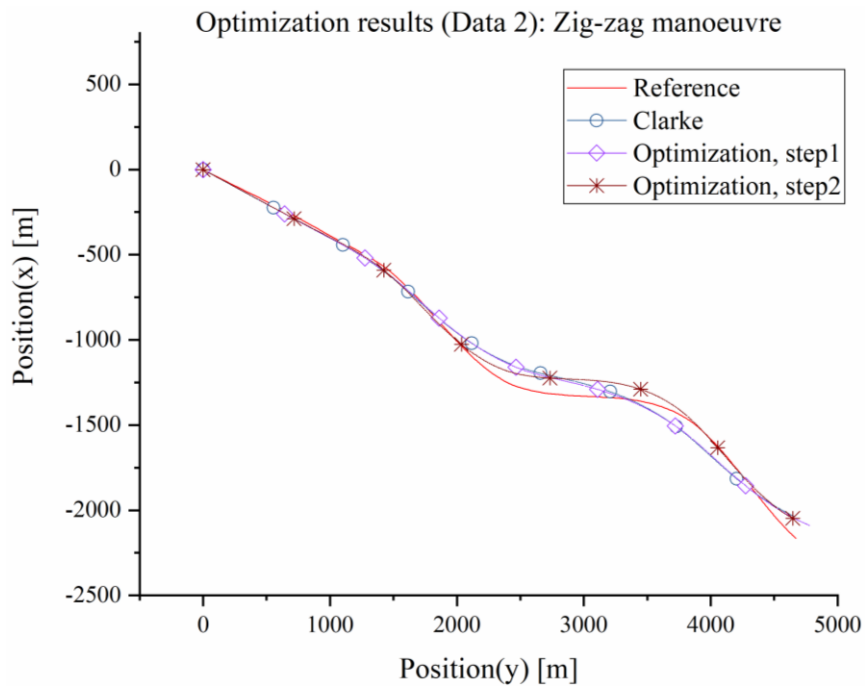


Figure 5.2 Comparison of trajectories between sea trial data 2 and simulation results

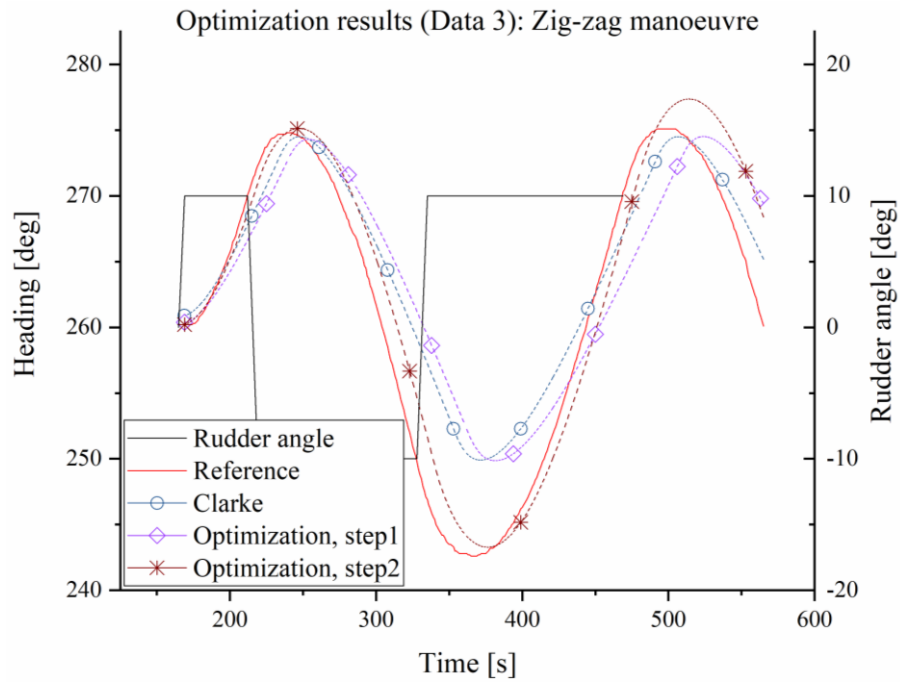


Figure 5.3 Comparison of heading change between sea trial data 3 and simulation results

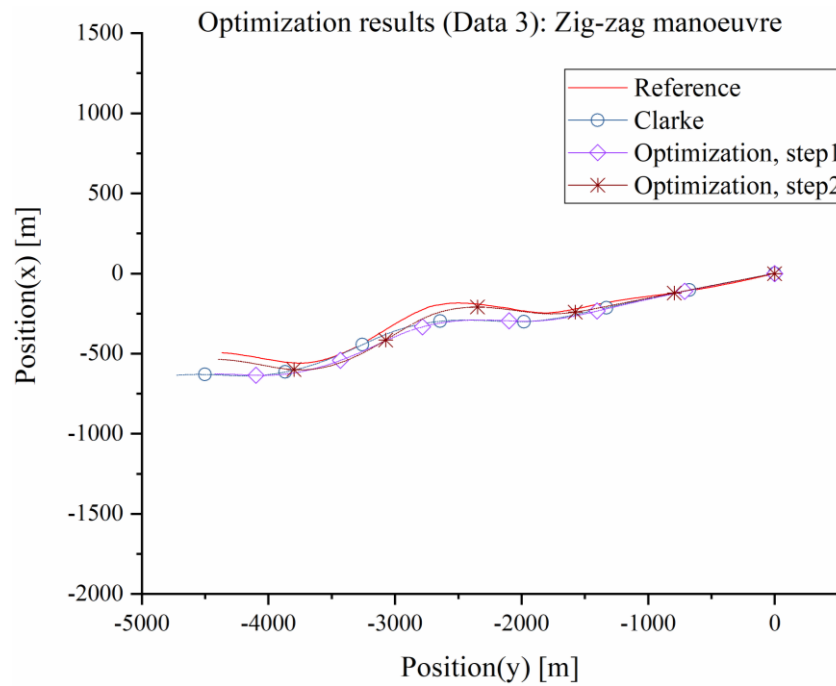


Figure 5.4 Comparison of trajectories between sea trial data 3 and simulation results

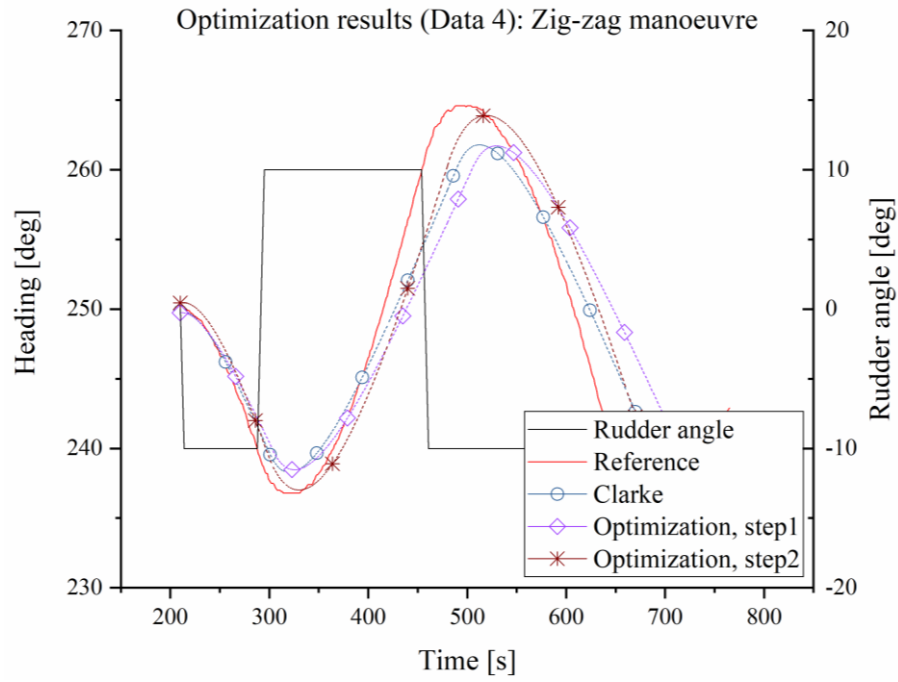


Figure 5.5 Comparison of heading change between sea trial data 4 and simulation results

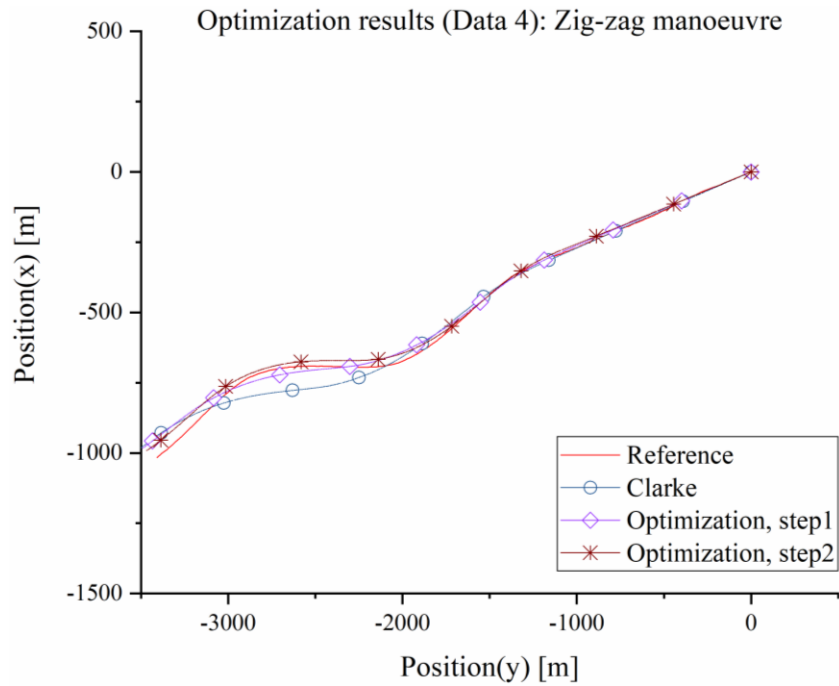


Figure 5.6 Comparison of trajectories between sea trial data 4 and simulation results

As mentioned in Table 5.2, the five sea trial data consist of three trim and draught conditions. The conditions of data 1 and data 2 are the same, and data 4 and 5 are the same.

Therefore, as a primary verification for the optimization results presented above, the tuned coefficients based on the data 2 and the data 4 are used in the simulations for the data 1 and 5, respectively. This verification is performed using the sea trial data 1 and 5, and each data is compared with three simulation results. The hydrodynamic coefficients used in the simulations are as follows:

- calculated coefficients by the formulas of Clarke estimation,
- tuned coefficients based on the data 2 and 4 (provided in Table 5.5) and
- tuned coefficients based on the data 1 and 5.

In other words, this procedure is to verify whether the tuned coefficients of the specific data can be applied to simulations for other data, if there is sea trial data for the same trim and draft conditions.

Table 5.7 and Table 5.8 present three sets of coefficients as mentioned above, respectively.  $X_{uu}$  for the optimization result of the data 1 differs from the Clarke coefficient, while the result of data 2 is close to the Clarke's.  $X_{u4}$ , on the other hand, showed that the result of data 1 is close to the Clarke coefficient. For the coefficients acting on the y- and z-axes, only  $N_{uv}$  for the both optimization results show a large difference with the Clarke coefficients; and for the remaining coefficients, the two optimization results are similar.

Table 5.7 Comparison of optimized coefficients for two sea trial data which have the same trim and draught condition (Case of the data 1 and 2)

Coefficients	Clarke	Optimization using	
		Data 1	Data 2
$X_{uu}$	-0.0280	-0.0412	-0.0250
$X_{u4}$	-0.3405	-0.3486	-0.2865
$Y_{uv}$	-1.5857	-1.6097	-1.9472
$Y_{ur}$	0.4281	0.4530	0.3426
$N_{uv}$	-0.5625	-1.3288	-1.2354
$N_{ur}$	-0.2675	-0.2740	-0.2783
Remarks	Data 1: ZZ10P, draught=12.875m, trim=0.25m		
	Data 2: ZZ10S, draught=12.875m, trim=0.25m		
	Step 1: straight motion ( $X_{uu}, X_{u4}$ ), Step 2: zig-zag manoeuvre ( $Y_{uv}, Y_{ur}, N_{uv}, N_{ur}$ )		

Table 5.8 Comparison of optimized coefficients for two sea trial data which have the same trim and draught condition (Case of the data 4 and 5)

Coefficients	Clarke	Optimization using	
		Data 4	Data 5
$X_{uu}$	-0.0407	-0.0665	-0.0598
$X_{u4}$	-0.4948	-0.4536	-0.8876
$Y_{uv}$	-1.3947	-2.2611	-2.3852
$Y_{ur}$	0.3934	0.3919	0.4110
$N_{uv}$	-0.3965	-0.9541	-1.2228
$N_{ur}$	-0.2339	-0.2335	-0.2548
Remarks	Data 4: ZZ10P, draught=9.35m, trim=0.50m		
	Data 5: ZZ20S, draught=9.35m, trim=0.50m		
	Step 1: straight motion ( $X_{uu}, X_{u4}$ ), Step 2: zig-zag manoeuvre ( $Y_{uv}, Y_{ur}, N_{uv}, N_{ur}$ )		

In case of the data 4 and 5, the  $X_{uu}$  for both optimization results are similar and differ from the Clarke coefficient.  $X_{u4}$  for the result of data 5 shows a large difference to the Clarke coefficient, whereas the coefficient for the result of data 4 is similar with the Clarke coefficient. The coefficients acting on the y- and z-axes for the both optimization results are close to each other. Among them,  $Y_{uv}$  and  $N_{uv}$  show a significant difference compared with the Clarke coefficients. Comparisons of the manoeuvre results according to these optimization results are shown in the following table and figures.

Table 5.9 compares manoeuvre characteristics for the simulation results using the coefficients presented above and for the reference data. Contents for the manoeuvre characteristics are the same as those in Table 5.6. Each term in the table means as follows:

- ‘Reference’ means manoeuvre characteristic of the sea trial for the data 1.
- ‘Clarke’ represents results of simulation using coefficients calculated by Clarke estimation.
- ‘Data 1’ shows results of simulation using optimized coefficients based on the data 1.
- ‘Data 2’ shows results of simulation using optimized coefficients based on the data 2.

All simulations are carried out under the same conditions as the sea trial data 1. The results of the straight motion with constant speed show that the simulation result of the data 1 is

closer to the reference data than the result of the data 2. This can be attributed to the difference in the optimized coefficients as shown in Table 5.7. In addition, since  $X_{uu}$  showed a higher sensitivity, the optimization result is much closer to the reference data. In the zig-zag manoeuvres, both the optimization and the validation results are similar with each other, and they are close to the reference data. As shown before, it is considered impossible to compare the simulation results using the initial turning time and the yaw checking time. The above results show that the change of coefficients acting on the x-axis do not have influence on the zig-zag manoeuvre. Also, the coefficients optimized with certain sea trial data are valid for other sea trials with the same trim and draught condition.

Table 5.9 Comparison of manoeuvre characteristics for simulation results and sea trial data  
(Case of the data 1 and 2)

	Straight		Zig-zag, 10 degrees		
	Way/LPP	Init. turning	Yaw check	Overshoot 1	Overshoot 2
Reference	4.42	46	293	6.00	12.30
Clarke	4.70	76	267	2.34	2.26
Data 1	4.42	48	290	6.51	8.45
Data 2	4.80	51	278	6.27	8.28
Remarks	Data 1: ZZ10P, draught=12.875m, trim=0.25m				
	Data 2: ZZ10S, draught=12.875m, trim=0.25m				
	Way/LPP: Distance from start point/LPP				
	Init. turning: Initial turning time [s]				
	Yaw check: Yaw checking time [s]				
	Overshoot 1: First overshoot angle [deg]				
	Overshoot 2: Second overshoot angle [deg]				

Table 5.10 also compares manoeuvre characteristics for the simulation results using the coefficients and for the sea trial data 5. Detailed conditions and definitions are the same as the Table 5.9. Comparison results show similar trend to those of data 1. In the case of the straight motion with constant speed, both the optimization result and the validation results have the same simulation results as the reference data. Each result has a different  $X_{u4}$ , but this coefficient does not have a large influence on the result of the straight motion. It can be confirmed again that the influence of  $X_{uu}$  is larger when the result of data 1 and the results of data 5 are considered together. In the case of zig-zag manoeuvre, it can be seen that the validation result is closer to the reference data than the optimization result.

Table 5.10 Comparison of manoeuvre characteristics for simulation results and sea trial data  
(Case of the data 4 and 5)

	Straight		Zig-zag, 20 degrees		
	Way/LPP	Init. turning	Yaw check	Overshoot 1	Overshoot 2
Reference	1.96	81	405	5.60	6.10
Clarke	2.15	93	441	3.21	3.25
Data 5	1.95	80	429	6.24	7.15
Data 4	1.93	84	436	5.59	6.26
Remarks	Data 4: ZZ10P, draught=9.35m, trim=0.50m				
	Data 5: ZZ20S, draught=9.35m, trim=0.50m				
	Way/LPP: Distance from start point/LPP				
	Init. turning: Initial turning time [s]				
	Yaw check: Yaw checking time [s]				
	Overshoot 1: First overshoot angle [deg]				
	Overshoot 2: Second overshoot angle [deg]				

Figure 5.7 to Figure 5.10 compare the time history of heading for the results from Table 5.9. For data 1, the first overshoot angle for both the optimization result and the validation result are similar with the reference data, while their second overshoot angle is smaller than the reference data. For data 5, both the first overshoot and second overshoot angles for all results are similar with the reference data.

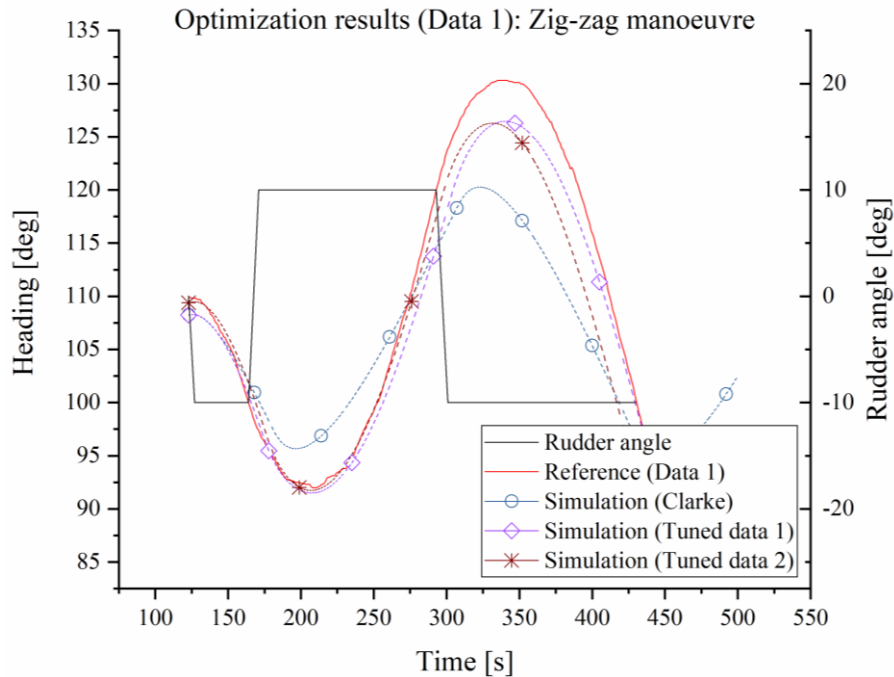


Figure 5.7 Comparison of heading change between sea trial data 1 and various simulations



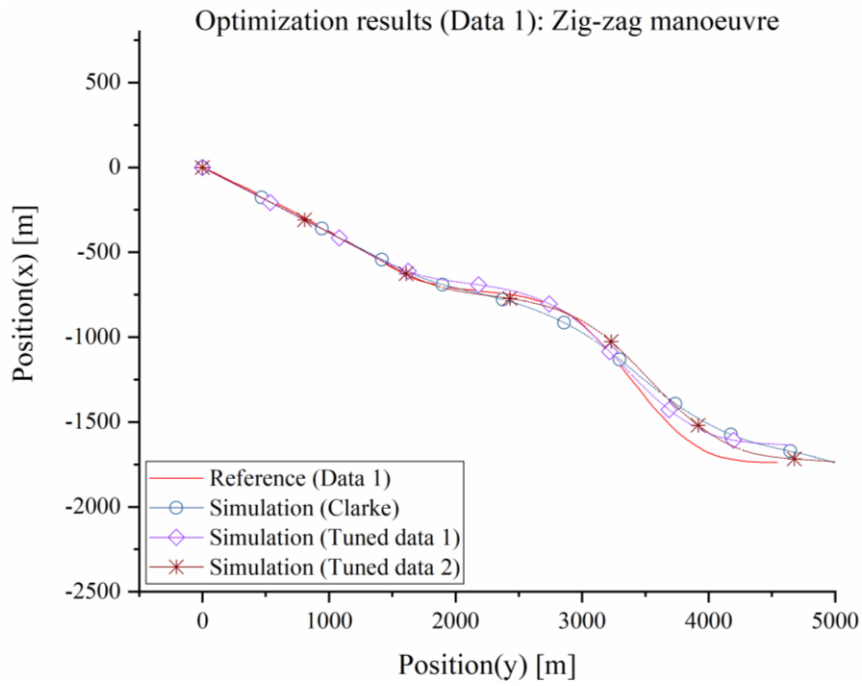


Figure 5.8 Comparison of trajectories between sea trial data 1 and various simulations

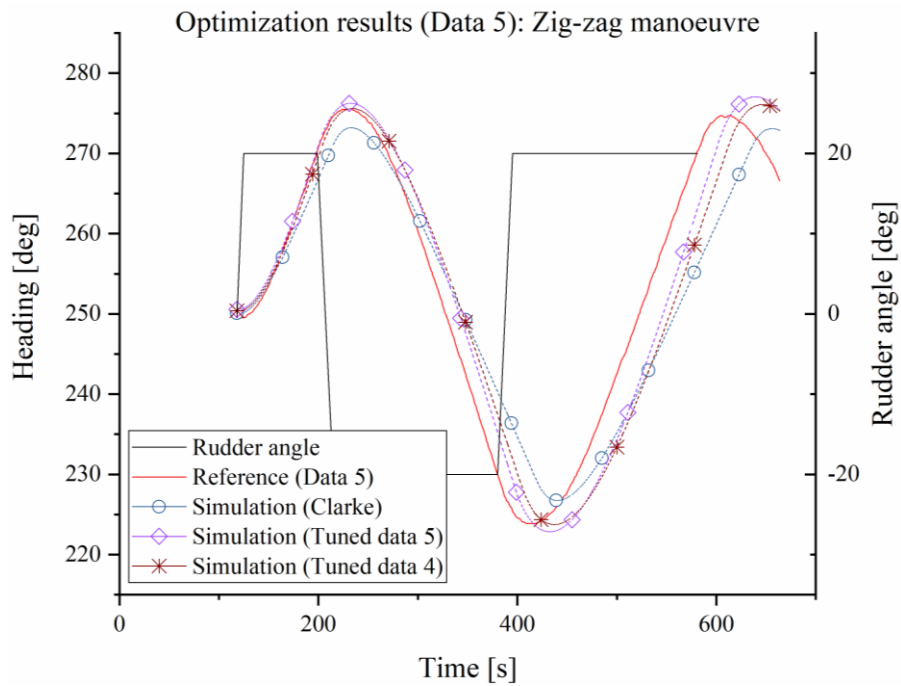


Figure 5.9 Comparison of heading change between sea trial data 5 and various simulations

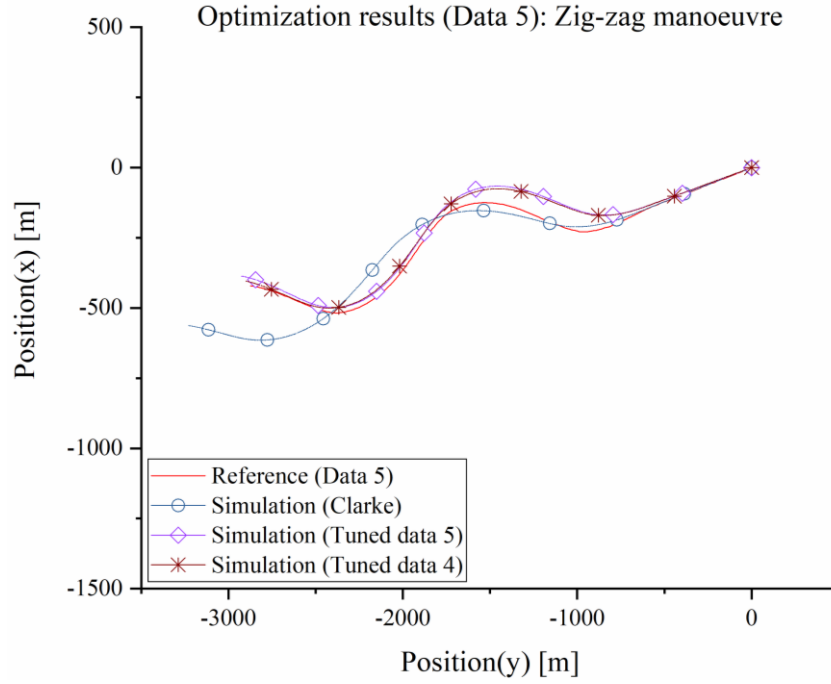


Figure 5.10 Comparison of trajectories between sea trial data 5 and various simulations

#### 5.4 Estimation of hydrodynamic coefficients considering various trim and draught conditions

Based on the optimization results obtained in Subchapter 5.3, estimation of the hydrodynamic coefficients for a certain trim and draught condition that are not included in the sea trial conditions are carried out. Also, a corresponding simulation results are compared with the reference data.

Estimation of the hydrodynamic coefficient considering various trim and draught conditions is basically based on the Clarke estimation formulas. In addition, final coefficients can be estimated by adding additional correction values using existing optimization results from sea trials. The validation of the estimated coefficients is performed by considering the data obtained in the sea trial booklet of the reference vessel.

The coefficients estimation formulas can be constructed as follows. First of all, the estimation formulas which can cope with various trim and draught conditions require a specific reference trim and draught condition.

In this study, the condition of the data 3 which is 10 metres of the mean draught and even keel condition is set as a reference condition. The new coefficients can be obtained by

adding correction values for differences of trim and draught between the desired and the reference condition.

$$C_{new} = C_{reference.tuned} + \Delta C_{draught} + \Delta C_{trim} \quad (67)$$

$$\Delta C_{draught} = (C_{reference.clarke} - C_{desired.draught}) * \gamma_{draught}$$

$$\Delta C_{trim} = (C_{reference.clarke} - C_{desired.trim}) * \gamma_{trim}$$

where

- $C_{new}$  is a finally tuned coefficient;
- $C_{reference.tuned}$  is a tuned coefficient by mathematical optimization process for the reference trim and draught condition;
- $C_{reference.clarke}$  is a calculated coefficient by the Clarke estimation formulas for the reference trim and draught condition;
- $C_{desired.draught}$  is a calculated coefficient by the Clarke estimation formulas for the desired draught condition, but trim is the same with the reference condition;
- $C_{desired.trim}$  is a calculated coefficient by the Clarke estimation formulas for the desired trim condition, but draught is the same with the reference condition;
- $\gamma_{draught}$  and  $\gamma_{trim}$  are correction values considering coefficients variation with draught and trim, respectively;
- $\Delta C_{draught}$  is difference between  $C_{standard.clarke}$  and  $C_{actual.draught}$ , with applying the correction value, and;
- $\Delta C_{trim}$  is difference between  $C_{standard.clarke}$  and  $C_{actual.trim}$ , with applying the correction value.

To comply with the form of equation (21), a correction value or a lookup table must be created that can consider trim and draught simultaneously. However, since the number of samples of the sea trial data used in this study is small, this study sets correction values for trim and draught separately.

Here states an example of application of equation (67) to a desired condition, 11.85m of mean draught ( $D$ ) and 0.1m of trim ( $t$ ) by the stern, which is a condition in the sea trial booklet of the model vessel. We have now three trim and draught conditions for the sea

trials -  $D=9.35m$   $t=0.5m$ ,  $D=10.00m$   $t=0m$  and  $D=12.875m$   $t=0.25m$  - and one of them should be the reference condition. The condition of  $10.00m$  of mean draught and even keel condition is chosen as the reference condition for this case. Thus equation (67) can be applied as follows:

$$C_{new,D=11.85m,t=0.1m} = C_{tuned,D=10.00m,t=0} + \Delta C_{draught} + \Delta C_{trim} \quad (68)$$

$$\Delta C_{draught} = (C_{Clarke,D=10.00m,t=0} - C_{Clarke,D=11.85m,t=0}) * \gamma_{draught}$$

$$\Delta C_{trim} = (C_{Clarke,D=10.00m,t=0} - C_{Clarke,D=10.00m,t=0.1m}) * \gamma_{trim}$$

$$\begin{bmatrix} \gamma_{draught} \\ \gamma_{trim} \end{bmatrix} = \begin{bmatrix} C_{Clarke \text{ difference } D1} & C_{Clarke \text{ difference } t1} \\ C_{Clarke \text{ difference } D2} & C_{Clarke \text{ difference } t2} \end{bmatrix}^{-1} * \begin{bmatrix} C_{tuned \ 1} \\ C_{tuned \ 2} \end{bmatrix}$$

$$C_{Clarke \text{ difference } D1} = C_{Clarke,D=10.00m,t=0} - C_{Clarke,D=9.35m,t=0}$$

$$C_{Clarke \text{ difference } D2} = C_{Clarke,D=10.00m,t=0} - C_{Clarke,D=12.875m,t=0}$$

$$C_{Clarke \text{ difference } t1} = C_{Clarke,D=10.00m,t=0} - C_{Clarke,D=10.00m,t=0.5m}$$

$$C_{Clarke \text{ difference } t2} = C_{Clarke,D=10.00m,t=0} - C_{Clarke,D=10.00m,t=0.25m}$$

$$C_{tuned \ 1} = C_{tuned,D=10.00m,t=0} - C_{tuned,D=9.35m,t=0.5m}$$

$$C_{tuned \ 2} = C_{tuned,D=10.00m,t=0} - C_{tuned,D=12.875m,t=0.25m}$$

For the coefficients acting on the  $x$ -axis,  $X_{uu}$  and  $X_{u4}$ , are affected by nominal resistance and nominal speed, and estimation of them in this case can be provided by second order curve fitting from three sets of tuned coefficients. Figure 5.11 shows results of curve fitting and Table 5.11 presents calculated correction values for the coefficients to be estimated.

Table 5.11 Correction values for estimation formulae which are based on three sea trial measurements

	Correction value	Remarks
$X_{uu}$	[-0.0037, 0.0952, -0.6305]	Second order fitting [B2, B1, Intercept]
$X_{u4}$	[0.0955, -2.0531, 10.3964]	
$\gamma_{draught}$	[-1.3953, 0.8239, 15.4710, 10.0599]	for [ $\gamma_{uv}$ , $\gamma_{ur}$ , $N_{uv}$ , $N_{ur}$ ]
$\gamma_{trim}$	[-0.3713, -11.2893, 224.6883, -184.9057]	

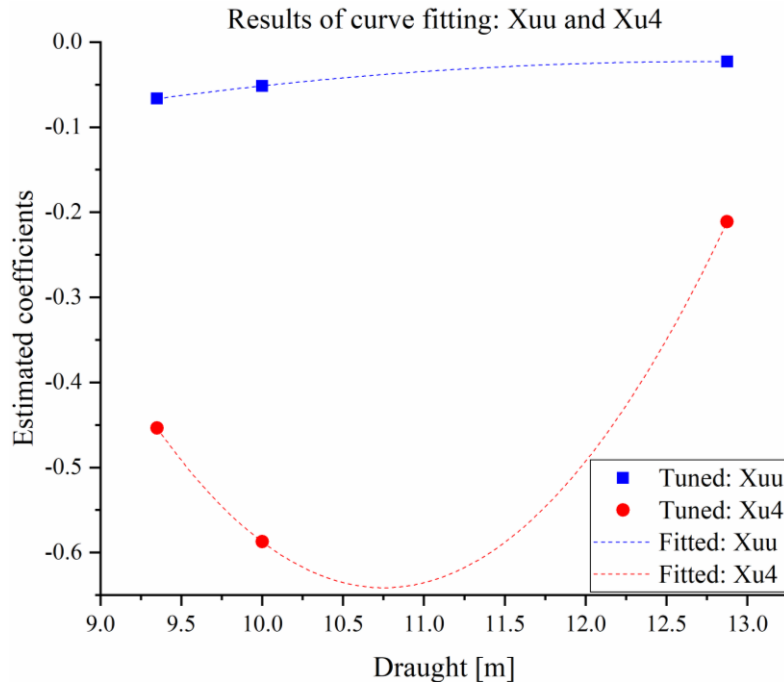


Figure 5.11 Results of curve fitting for  $X_{uu}$  and  $X_{u4}$

Table 5.12 presents environmental conditions for the corresponding sea trial for validation of the estimation formulae, and it is named as ‘Data 6’.

Table 5.12 Environmental conditions for the sea trial for validation of the estimation formulae

Data6	
Manoeuvre	ZZ20S
Heading [deg]	176.6
Draught fore [m]	11.80
Draught aft [m]	11.90
Wind direction [deg]	263.8
Wind speed [kts]	11.6
Current direction [deg]	181.4
Current speed [kts]	0.4
Water depth [m]	250

Table 5.13 compares the Clarke with the coefficients estimated by the above formulas. For the straight motion with constant speed, both estimation results differ from each other.

The coefficients acting on y- and z-axes also show a large difference for  $Y_{uv}$  and  $N_{uv}$ , as well as the results of the previous optimization.

Table 5.13 Comparison of coefficients between Clarke estimation and suggested formulas

$T_m=11.85\text{m}$ $t=0.1\text{m}$	Clarke	Estimation formula
$X_{uu}$	-0.0304	-0.0260
$X_{u4}$	-0.3699	-0.5263
$Y_{uv}$	-1.4991	-2.0650
$Y_{ur}$	0.4056	0.4649
$N_{uv}$	-0.5144	-3.7873
$N_{ur}$	-0.2527	-0.6562

Table 5.14 compares the simulation results for the Clarke coefficients and the estimated coefficients with the reference data. Because the results of the straight motion for the sea trial booklet cannot be obtained, only the results of the zig-zag manoeuvre of the reference data are compared with the two simulation results. In the straight motion, there was no difference between the two simulation results. In the case of the zig-zag manoeuvre, the initial turning time for the Clarke coefficient is closer to the reference data than the one of the estimation formulas, but this initial turning time cannot be given meaning that it is not suitable for comparison as shown in the previous results. In the case of the overshoot angles, the two simulation results show a significant difference. Compared to the simulation result for the Clarke coefficients, both the first and the second overshoot angles of the estimation formulas are quite similar with the reference data. On the basis of this, it can be seen that the coefficients using the newly proposed estimation formulas well reflect the reference data.

Figure 5.12 shows the results of the above table as time history of heading. Because there is no raw data for the reference, the figure combines two layers of the simulation results of both the Clarke coefficients and the estimated formulas and an image of the sea trial booklet, via synchronization of the x- and y-axes. As described above, the simulation result for the Clarke coefficients differs significantly from the reference data, while the results for the estimation formulas appear to have heading changes similar with the reference data.

Table 5.14 Comparison of manoeuvre characteristics for the simulation results of Clarke estimation and suggested formula

	Straight	Zig-zag, 20 degrees			
	Way/LPP	Init. turning	Yaw check	Overshoot 1	Overshoot 2
Reference	-	53	278	8.8	13.7
Clarke	28.5491	56	285	3.4	6.8
Estimation	28.6848	49	287	9.3	19.2
Remarks	Way/LPP: Distance from start point/LPP				
	Init. turning: Initial turning time [s]				
	Yaw check: Yaw checking time [s]				
	Overshoot 1: First overshoot angle [deg]				
	Overshoot 2: Second overshoot angle [deg]				
Estimation:		Hydrodynamic coefficients using suggested estimation formulas			

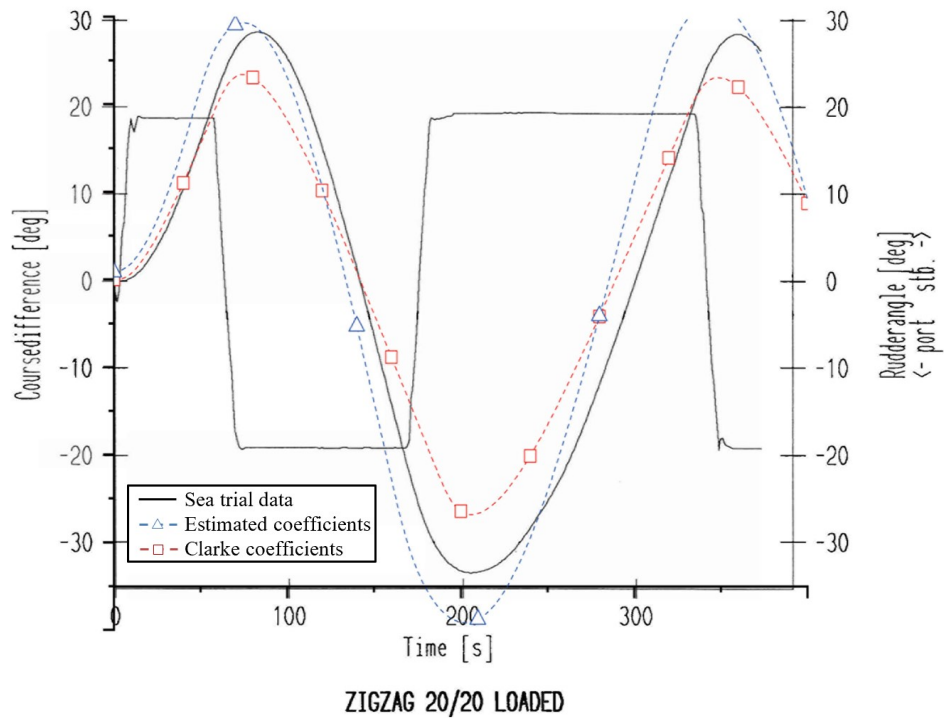


Figure 5.12 Comparison of heading change for the simulation results of Clarke estimation and suggested formula

## 5.5 Conclusion

In this chapter, five sea trial sets of data were optimized and they were mutually validated. Also, formulas for estimating the hydrodynamic coefficients for additional trim and draught conditions were proposed based on the optimized coefficients.

The sea trial data had three trim and draught conditions and the data 2,3, and 4, which have different trim and draught conditions, are firstly optimized. Optimization results for data 2 and 4 were verified using data 1 and the data 5, respectively. Validation results showed that any optimization results under the same trim and draught conditions can have mutually similar simulations results. As a result, the simulation results for both the ‘optimization’ result and the ‘validation’ result were much similar with the reference data than the result for the Clarke coefficients.

For estimating coefficients for additional trim and draught condition, formulas for correction values to be added to the existing Clarke estimation formulas were proposed. One of the sea trial conditions was set as the reference condition, and the correction values were obtained using all the optimization results. Then the difference of each trim and draught were added to obtain a new coefficient. Simulation results using the coefficient from the above process showed a similarity to the reference data by comparing the simulation results for Clarke estimation with the same conditions.

The experiment results were not possible to support the theoretical background of the correlation between the change of trim and draught conditions and ship’s manoeuvrability, as stated in the subchapter 2.3, due to the limitation of the sample data configuration. In addition, the proposed method is not yet complete because there was only one validation., Further validations using an additional reference vessel and its trials or more samples on an existing reference vessel are still required for higher reliability of this proposal.



## 6. Conclusion

In this paper, full-scale sea trials were performed and the system identification method were used to estimate the ship's hydrodynamic coefficients. Based on these results, this study proposed a new equation for estimating the coefficients considering various trim and draught conditions and this equation can supplement existing estimation formulas for the hydrodynamic coefficients.

Identification of appropriate hydrodynamic coefficients is an important and a fundamental element for predicting of analysing ship's manoeuvrability. Several experimental and theoretical researches for this have been conducted for decades.

Chinarro classified modelling techniques as priori, posteriori and intermediate modelling and he defined the system identification method as a posteriori or an intermediate method for a dynamic system which requires to observe input and output from experimental or measured data [66]. This method can also be applied to estimate the hydrodynamic coefficients for ship's equation of motions. Especially for the existing ships, which can conduct sea trial, this method is the most reasonable method to estimate the hydrodynamic coefficients. This is the biggest difference compared to the model test and CFD methods for the ships under construction, especially in the early design stage.

In this study, the optimization toolbox in MATLAB was used to get optimized hydrodynamic coefficients. In the preparation and verification phased for the setting of optimization problems, four algorithms with six versions were applied to figure out the best algorithm for this study. Those optimization results were utilized to the simulation and they were compared with reference data and simulation results using Clarke coefficients. The reference data for this phase were obtained from the sea trial using a training ship and these data were calibrated to consider environmental influence. The initial values for each optimization were set using the Clarke estimation. The optimization results showed that most results are similar with the reference. The optimization results fitted to the reference data in the order of the interior point, the Quasi-Newton, the Nelder Mead and the SQP algorithm.

Based on the above results, in the final validation phase, optimization and proposal of new estimation formula were conducted considering various trim and draught conditions. In this phase, the interior point algorithm was used for all optimization process according to the results of the previous phase.

The reference data, five zig-zag manoeuvres with three different trim and draught conditions, were acquired from the sea trials using a 4,500 TEU class container vessel. The optimization results showed that any optimization results under the same trim and draught condition could present mutually similar simulation results. Also, those simulation results fitted to their corresponding reference data better than the simulation results using Clarke coefficients.

Based on the optimization results, formulas for correction values to be added to the existing Clarke estimation formulas were proposed. One of the sea trial condition was set as the reference condition, and the correction values were obtained using all the optimization results. Then the difference of each trim and draught were added to obtain a new coefficient. Simulation results using the coefficient from the above process showed a similarity to the reference data by comparing the simulation results for Clarke estimation with the same conditions.

This study was conducted as a part of the modelling method for existing ships rather than ships under construction. For this purpose, the full-scale sea trial using a target vessel and following system identification method were used to estimate hydrodynamic coefficients. The overall results were satisfactory compared to the coefficients using existing empirical estimation method. Based on this an updated estimation formula was also suggested. However, this optimization procedure and suggested formula need more validation with additional sea trials and reference vessels. Through this, the reliability for the proposed idea will be increased.

## 7. References

- [1] Zou, Z.-j., “*Ship Manoeuvring and Seakeeping*”, Shanghai Jiao Tong University, 2006.
- [2] Kornev, N., “*Lectures on Ship Manoeuvrability*”, Bookboon.com, Rostock, Germany, 2013.
- [3] Abkowitz, M. A., “*Lectures on Ship Hydrodynamics: Steering and Maneuvrability*”, Hydro- and Aerodynamics Laboratory Report Hy-5, 1964.
- [4] Eloot, K., “*Selection, Experimental Determination and Evaluation of a Mathematical Model for Ship Manoeuvring in Shallow Water*”, Ph.D. thesis, Ghent University, 2006.
- [5] Norrbin, N. H., “*Theory and Observations on the Use of a Mathematical Model for Ship Manoeuvring in Deep and Confined Waters*”, SSPA Report, no. 68, 1971.
- [6] Yasukawa, H. and Y. Yoshimura, “*Introduction of MMG Standard Method for Ship Maneuvering Predictions*”, Journal of Marine Science and Technology, vol. 20, no. 1, pp. 37–52, 2015.
- [7] ITTC, International Towing Tank Conference, “*The Manoeuvring Committee: Final Report and Recommendation to the 25th ITTC*”, 2008.
- [8] Nomoto, K., “*Analysis of Kenpf’s Standard Manoeuvre Test and Proposed Steering Quality Indices*”, First Symposium on Ship Maneuverability, David Taylor Model Basin Report 1461, pp. 275–304, 1960.
- [9] Norrbin, N. H., “*Zig-zag Test Technique and Analysis with Preliminary Statistical Results*”, SSPA Report, no. 12, 1965.
- [10] Inoue, S., M. Hirano, K. Kijima, and J. Takashina, “*A Practical Calculation Method of Ship Maneuvering Motion*”, International Shipbuilding Progress, vol. 28, no. 325, pp. 207–222, 1981.
- [11] Crane, C. L., “*Maneuvering Trials of the 278,000 DWT Esso Osaka in Shallow and Deep Waters*”, Society of Naval Architects and Marine Engineers, vol. 87, pp. 251–283, 1979.
- [12] Clarke, D., P. Gedling, and G. Hine, “*The Application of Manoeuvring Criteria in Hull Design Using Linear Theory*”, RINA Transactions and Annual Report, pp. 45–68, 1983.
- [13] Kijima, K., Y. Nakiri, and Y. Furukawa, “*On the Prediction Method for Ship Manoeuvrability*”, Proceedings of the Internal Workshop on Ship Manoeuvrability, Hamburg Ship Model Basin, no. 7, 2000.

- [14] Kose, K., “*Studies on the Effect of Loading Condition on the Maneuverability of Ships*”, Journal of the Japan Society of Naval Architects and Ocean Engineers, no. 82, pp. 155–165, 1991.
- [15] Hess, J. L. and A.M.O. Smith, “*Calculation of Potential Flow about Arbitrary Bodies*”, Progress in Aerospace Sciences, vol. 8, pp. 1–138, 1967.
- [16] ZHANG, Z.-r., H. LIU, S.-p. ZHU, and F. ZHAO, “*Application of CFD in Ship Engineering Design Practice and Ship Hydrodynamics*”, Journal of Hydrodynamics, Ser. B, vol. 18, no. 3, pp. 315–322, 2006.
- [17] Abkowitz, M. A., “*Measurement of Hydrodynamic Characteristics from Ship Maneuvering Trials by System Identification*”, Society of Naval Architects and Marine Engineers, vol. 88, pp. 283–318, 1980.
- [18] Rhee, K.-P. and K.-h. Kim, “*A New Sea Trial Method for Estimating Hydrodynamic Derivatives*”, Journal of Ship and Ocean Technology, vol. 3, no. 3, pp. 25–44, 1999.
- [19] Zhang, X.-g. and Z.-j. Zou, “*Identification of Abkowitz Model for Ship Manoeuvring Motion Using  $\varepsilon$ -Support Vector Regression*”, Journal of Hydrodynamics, Ser. B, vol. 23, no. 3, pp. 353–360, 2011.
- [20] Tran, K. T., A. Ouahsine, F. Hissel, and P. Sergent, “*Identification of Hydrodynamic Coefficients from Sea Trials for Ship Maneuvering Simulation*”. Transport Research Arena (TRA) 5th Conference, Paris, 2014.
- [21] Kim, D., “*Optimisation Methods for Modelling Simulator Ship Models of a Ferry with Two Pairs of Azimuth Propellers*”, M.Sc. thesis, Hochschule Wismar, 2013.
- [22] Kim, D., K. Benedict, and M. Paschen, “*Estimation of Hydrodynamic Coefficients from Sea Trials Using a System Identification Method*”, Journal of the Korean Society of Marine Environment and Safety, vol. 23, no. 3, pp. 258–265, 2017.
- [23] IMO, International Maritime Organization, “*Explanatory Notes To The Standards For Ship Manoeuvrability: MSC/Circ. 1053*”, 2002.
- [24] Varyani, K. S., P. Krishnankutty, and R. C. McGregor, “*Effect of Rudder Size and Location on the Turning Performance of a High Speed SWATH Ferry*”, IFAC Proceedings Volumes, vol. 36, no. 21, pp. 61–66, 2003.
- [25] Sukselainen, J., “*On Ship Manoeuvring and Waterway Width*”, Ph.D. thesis, 1975.
- [26] Yoshimura, Y., K. Kose, and T. Hiraguchi, “*Criteria for Yaw-checking and Course-Keeping Abilities in IMO's Interim Standards for Ship Manoeuvrability*”, MARSIM 2000 Conference Proceedings, pp. 389–400, 2000.

- [27] ITTC, International Towing Tank Conference, “*Full Scale Measurements Manoeuvrability Full Scale Manoeuvring Trials Procedure: ITTC Recommended Procedures 7.5-04-02-01*”, 2002.
- [28] IMO, International Maritime Organization, “*Standards for Ship Manoeuvrability: Resolution MSC.137(76)*”, 2002.
- [29] Kijima, K., T. Katsuno, Y. Nakiri, and Y. Furukawa, “*On the Manoeuvring Performance of a Ship with the Parameter of Loading Condition*”, Journal of the Japan Society of Naval Architects and Ocean Engineers, no. 168, pp. 141–148, 1990.
- [30] Yasukawa, H., Y. Yoshimura, and K. Nakatake, “*Hydrodynamic Forces on a Ship Moving with Constant Rudder Angle: A Theoretical Treatment of Rudder Angle Test*”, Proceedings of MARSIM 1996, pp. 435–448, 1996.
- [31] Inoue, S., M. Hirano, and K. Kijima, “*Hydrodynamic Derivatives on Ship Manoeuvring*”, International Shipbuilding Progress, vol. 28, no. 321, pp. 112–125, 1981.
- [32] Krüger, C.-M. C., “*Untersuchung zum Effekt verschiedener Tiefgänge und Trimm-lagen auf das Manövrierverhalten anhand der Auswertung von Messdaten*”, Bachelor thesis, 2013.
- [33] Benedict, K., “*Nomoto Equation of 1st Order as Simplified Approach for Automatic Course Keeping and Track Control*”, Hochschule Wismar, 2006.
- [34] Seo, S. G. and M. Mishu, “*The Use of Pivot Point in Ship Handling for Safer and More Accurate Ship Manoeuvring*” in International Conference IMLA 19, 2011.
- [35] House, D. J., “*Ship Handling: Theory and Practice / D.J. House*”, Elsevier Butterworth-Heinemann, Amsterdam, London, 2007.
- [36] Hochschule Wismar, “*Final Report of Project ISSTES: Integrative Simulationsanwendung unter Beachtung von Trimm- und Tiefgangänderungen zur effektiven Schiffssteuerung und Verbesserung der Handlungssicherheit in Gefahrensituation*”, 2017.
- [37] Nocedal, J. and S. J. Wright, “*Numerical Optimization*”, Springer, New York, 2006.
- [38] Snyman, J. A., “*Practical Mathematical Optimization: An Introduction to Basic Optimization Theory and Classical and New Gradient-Based Algorithms*”, Springer, New York, 2005.
- [39] Cartis, C., N. I. M. Gould, and P. L. Toint, “*On the Complexity of Steepest Descent, Newton's and Regularized Newton's Methods for Nonconvex Unconstrained*

- Optimization Problems*”, SIAM Journal on Optimization, vol. 20, no. 6, pp. 2833–2852, 2010.
- [40] Martens, J., “*Deep Learning via Hessian-Free Optimization*”, ICML 2010 - Proceedings, 27th International Conference on Machine Learning, 2010.
  - [41] ACME, “*Newton and Quasi-Newton Methods*”, Brigham Young University, <http://www.acme.byu.edu/wp-content/uploads/2017/02/Vol2B-QuasiNewton.pdf>, 2017.
  - [42] Hennig, P. and M. Kiefel, “*Quasi-Newton Method: A New Direction*”, Journal of Machine Learning Research, vol. 14, pp. 843–865, 2013.
  - [43] Fletcher, R., “*Practical Methods of Optimization*”, Wiley, Chichester, New York, 1987.
  - [44] Ding, Y., E. Lushi, and Q. Li, “*Investigation of Quasi-Newton Methods for Unconstrained Optimization*”, Simon Fraser University, 2004.
  - [45] Kramer, O., D. E. Ciaurri, and S. Koziel, “*Derivative-Free Optimization*” in Computational Optimization, Methods and Algorithms, S. Koziel and X.-S. Yang, Eds., vol. 356, pp. 61–83, Springer, Berlin, 2011.
  - [46] Rios, L. M. and N. V. Sahinidis, “*Derivative-Free Optimization: A Review of Algorithms and Comparison of Software Implementations*”, Journal of Global Optimization, vol. 56, no. 3, pp. 1247–1293, 2013.
  - [47] Conn, A. R., K. Scheinberg, and L. N. Vicente, “*Introduction to Derivative-Free Optimization*”, Society for Industrial and Applied Mathematics, 2009.
  - [48] Hooke, R. and T. A. Jeeves, “*Direct Search Solution of Numerical and Statistical Problems*”, Journal of the ACM, vol. 8, no. 2, pp. 212–229, 1961.
  - [49] Hicken, J., J. Alonso, and C. Farhat, “*Introduction to Multidisciplinary Design Optimization: Chapter 6: Gradient-Free Optimization*”, Stanford University, 2012.
  - [50] Nelder, J. A. and R. Mead, “*A Simplex Method for Function Minimization*”, The Computer Journal, vol. 7, no. 4, pp. 308–313, 1965.
  - [51] Lagarias, J. C., J. A. Reeds, M. H. Wright, and P. E. Wright, “*Convergence Properties of the Nelder--Mead Simplex Method in Low Dimensions*”, SIAM Journal on Optimization, vol. 9, no. 1, pp. 112–147, 1998.
  - [52] Antoniou, A. and W. Lu, “*Practical Optimization: Algorithms and engineering applications*”, Springer, New York, 2007.
  - [53] Dantzig, G. B. and M. N. Thapa, “*Linear Programming: 2: Theory and Extensions*”, George B. Dantzig and Mukund N. Thapa, New York, NY, 2003.

- [54] Gondzio, J., “*Interior Point Methods 25 Years Later*”, European Journal of Operational Research, vol. 218, no. 3, pp. 587–601, 2012.
- [55] Karmarkar, N., “*A New Polynomial-Time Algorithm for Linear Programming*”, Combinatorica, vol. 4, no. 4, pp. 373–395, 1984.
- [56] Khachiyan, L. G., “*Polynomial Algorithms in Linear Programming*”, USSR Computational Mathematics and Mathematical Physics, vol. 20, no. 1, pp. 53–72, 1980.
- [57] Forsgren, A., P. E. Gill, and M. H. Wright, “*Interior Methods for Nonlinear Optimization*”, SIAM Review, vol. 44, no. 4, pp. 525–597, 2002.
- [58] Byrd, R. H., J. C. Gilbert, and J. Nocedal, “*A Trust Region Method Based on Interior Point Techniques for Nonlinear Programming*”, Mathematical Programming, vol. 89, no. 1, pp. 149–185, 2000.
- [59] Mathworks, “*Constrained Nonlinear Optimization Algorithms: fmincon Interior Point Algorithm*”, <https://kr.mathworks.com/help/optim/ug/constrained-nonlinear-optimization-algorithms.html>.
- [60] Conn, A. R., N.I.M. Gould, and P. L. Toint, “*Trust Region Methods*”, Society for Industrial and Applied Mathematics, 2000.
- [61] Boggs, P. T. and J. W. Tolle, “*Sequential Quadratic Programming*”, Acta Numerica, vol. 4, p. 1, 1995.
- [62] Gill, P. E. and E. Wong, “*Sequential Quadratic Programming Methods*” in Mixed Integer Nonlinear Programming, J. Lee and S. Leyffer, Eds., vol. 154, pp. 147–224, Springer, New York, London, 2012.
- [63] Morales, J. L., J. Nocedal, and Y. Wu, “*A Sequential Quadratic Programming Algorithm with an Additional Equality Constrained Phase*”, IMA Journal of Numerical Analysis, vol. 32, no. 2, pp. 553–579, 2011.
- [64] Hoppe, R. W., “*Optimization Theory: Chapter 4 Sequential Quadratic Programming*”, 2006.
- [65] STX Engine, “*Voyage Data Recorder*”, [http://www.stxen-gine.co.kr/eng/biz/elect\\_ship02.aspx](http://www.stxen-gine.co.kr/eng/biz/elect_ship02.aspx), 2006.
- [66] Chinarro, D., “*System Engineering Applied to Fuenmayor Karst Aquifer (San Julián de Banzo, Huesca) and Collins Glacier (King George Island, Antarctica)*”, Springer International Publishing, Cham, s.l., 2014.

## Appendix A. Details of manoeuvres for chapter 5

Time histories of five manoeuvres in the chapter 5 are presented in this appendix. All data are presented by Caspar M. Krüger.

### Appendix A.1 Time history for data 1

Time [sec]	Heading [deg]	Speed [kts]	Rudder [deg]	Comment	$\Delta$ Heading [deg]
17:20:00	110.0	19.70	0.0	initial conditions (UTC)	
+0	110.0	19.70	0.0	start manoeuvre, 10° to port	0.00
			-10.0	rudder is 10° to port	
+38	100.0	19.30	-10.0	counter rudder to starboard 10°	-10.00
			10.0	rudder is 10° to starboard	
+130	92.1	18.80	10.0	1. overshoot angle (ROT=0)	-17.90
+209	100.0	18.80	10.0	passing initial heading-10°	-10.00
+231	110.0	18.90	10.0	passing initial heading	0.00
+250	120.0	18.50	10.0	counter rudder to port 10°	10.00
			-10.0	rudder is 10° to port	
+336	130.3	18.20	-10.0	2. overshoot angle (ROT=0)	20.30
+430	120.0	18.40	-10.0	passing initial heading+10°	10.00
+448	110.0	18.00	-10.0	passing initial heading	0.00
+507	100.0	17.60	-10.0	counter rudder to starboard	-10.00
			10.0	rudder is 10° to starboard	
+602	86.8	17.0	10.0	3. overshoot angle (ROT=0)	23.20
			10.0	passing initial heading-10°	-10.00
			10.0	passing initial heading	0.00
			10.0	counter rudder to port	10.00
			-10.0	rudder is 10° to port	
			-10.0	4. overshoot angle (ROT=0)	
			-10.0	passing initial heading+10°	10.00
			-10.0	meet her	0.00



## Appendix A.2 Time history for data 2

Time [sec]	Heading [deg]	Speed [kts]	Rudder [deg]	Comment	$\Delta$ Heading [deg]
00:27:00			0.0	initial conditions (UTC)	
+0	110.0	15.8	0.0	start manoeuvre, 10° to starboard	0.0
+7	110.0	15.8	10.0	rudder is 10° to starboard	0.0
+58	120.0	15.8	10.0	counter rudder to port 10°	10.0
+106	120.0	15.8	-10.0	rudder is 10° to port	10.0
+140	126.7	15.6	-10.0	1. overshoot angle (ROT=0)	16.7
+236	120.0	15.5	-10.0	passing initial heading+10°	10.0
+304	110.0	15.3	-10.0	passing initial heading	0.0
+327	100.0	14.8	-10.0	counter rudder to starboard 10°	-10.0
+333	99.0	14.8	10.0	rudder is 10° to starboard	-11.0
+440	88.2	14.2	10.0	2. overshoot angle (ROT=0)	-21.8
+552	100.0	14.7	10.0	passing initial heading-10°	-10.0
+620	110.0	14.8	10.0	passing initial heading	0.0
+643	120.0	14.6	10.0	counter rudder to port	10.0
+648	121.0	14.6	-10.0	rudder is 10° to port	11.0
+750	130.1	14.6	-10.0	3. overshoot angle (ROT=0)	20.1
+850	120.0	14.8	-10.0	passing initial heading+10°	10.0
+917	110.0	14.6	-10.0	passing initial heading	0.0
+939	100.0	14.1	-10.0	counter rudder to starboard	-10.0
+946	96.0	14.1	10.0	rudder is 10° to starboard	-14.0
+1055	87.7	13.8	10.0	4. overshoot angle (ROT=0)	-22.3
+1212	100.0	14.4	10.0	passing initial heading-10°	-10.0
			10.0	meet her	

### Appendix A.3 Time history for data 3

Time [sec]	Heading [deg]	Speed [kts]	Rudder [deg]	Comment	$\Delta$ Heading [deg]
17:22:00			0.0	initial conditions (UTC)	
+0	260.0	16.50	0.0	start manoeuvre, 10° to starboard	0.0
+3	260.0	16.50	10.0	rudder is 10° to starboard	0.0
+46	270.0	16.50	10.0	counter rudder to port 10°	10.0
+52	272.0	16.40	-10.0	rudder is 10° to port	12.0
+113	274.9	16.20	-10.0	1. overshoot angle (ROT=0)	14.9
+148	270.0	16.10	-10.0	passing initial heading+10°	10.0
+218	260.0	15.70	-10.0	passing initial heading	0.0
+242	250.0	15.30	-10.0	counter rudder to starboard 10°	-10.0
+246	248.0	25.30	10.0	rudder is 10° to starboard	-12.0
+324	242.5	14.80	10.0	2. overshoot angle (ROT=0)	-17.5
+408	250.0	15.00	10.0	passing initial heading-10°	-10.0
+438	260.0	15.20	10.0	passing initial heading	0.0
+503	270.0	15.10	10.0	counter rudder to port	10.0
+508	272.0	15.10	-10.0	rudder is 10° to port	12.0
+534	275.1	15.00	-10.0	3. overshoot angle (ROT=0)	15.1
+611	270.0	15.10	-10.0	passing initial heading+10°	10.0
+640	260.0	15.00	-10.0	passing initial heading	0.0
+704	250.0	14.60	-10.0	counter rudder to starboard	-10.0
+709	247.0	14.50	10.0	rudder is 10° to starboard	-13.0
+745	242.7	14.20	10.0	4. overshoot angle (ROT=0)	-17.3
+831	250.0	15.10	10.0	passing initial heading-10°	-10.0
+900	260.0	14.90	10.0	meet her	0.0

## Appendix A.4 Time history for data 4

Time [sec]	Heading [deg]	Speed [kts]	Rudder [deg]	Comment	$\Delta$ Heading [deg]
17:36:57			0.0	initial conditions (UTC)	
+0	250.0	10.60	0.0	start manoeuvre, 10° to port	0.0
+4	250.0		-10.0	rudder is 10° to port	0.0
+117	240.0	10.50	-10.0	counter rudder to starboard 10°	-10.0
+121	240.0	10.40	10.0	rudder is 10° to starboard	-10.0
+200	236.8	10.30	10.0	1. overshoot angle (ROT=0)	-13.0
+234	240.0	10.20	10.0	passing initial heading-10°	-10.0
+324	250.0	10.20	10.0	passing initial heading	0.0
+405	260.0	10.00	10.0	counter rudder to port 10°	10.0
+409	262.0	10.00	-10.0	rudder is 10° to port	12.0
+446	264.6	9.90	-10.0	2. overshoot angle (ROT=0)	15.0
+545	260.0	9.90	-10.0	passing initial heading+10°	10.0
+637	250.0	9.70	-10.0	passing initial heading	0.0
+716	240.0	9.60	-10.0	counter rudder to starboard	-10.0
+720	239.0	9.40	10.0	rudder is 10° to starboard	-11.0
+807	234.9	9.50	10.0	3. overshoot angle (ROT=0)	-15.0
+858	240.0	9.60	10.0	passing initial heading-10°	-10.0
+945	250.0	9.70	10.0	passing initial heading	0.0
+1025	260.0	9.60	10.0	counter rudder to port	10.0
+1029	261.0	9.70	-10.0	rudder is 10° to port	11.0
+1111	264.3	9.50	-10.0	4. overshoot angle (ROT=0)	14.0
+1203	260.0	9.70	-10.0	passing initial heading+10°	10.0
+1255	250.0	9.70	-10.0	meet her	0.0

## Appendix A.5 Time history for data 5

Time [sec]	Heading [deg]	Speed [kts]	Rudder [deg]	Comment	$\Delta$ Heading [deg]
18:03:57			0.0	initial conditions (UTC)	
+0	250.0	10.50	0.0	start manoeuvre, 20° to starboard	0.0
+5	250.0	10.50	20.0	rudder is 20° to starboard	0.0
+121	270.0	10.00	20.0	counter rudder to port 20	20.0
+129	273.0	9.90	-20.0	rudder is 20° to port	23.0
+152	275.5	9.50	-20.0	1. overshoot angle (ROT=0)	25.5
+231	260.0	9.50	-20.0	passing initial heading+20°	10.0
+331	250.0	9.00	-20.0	passing initial heading	0.0
+419	230.0	8.40	-20.0	counter rudder to starboard 20°	-20.0
+430	227.0	8.40	20.0	rudder is 20° to starboard	-23.0
+500	223.9	8.20	20.0	2. overshoot angle (ROT=0)	-26.1
+542	230.0	8.30	20.0	passing initial heading-20°	-20.0
+644	250.0	8.50	20.0	passing initial heading	0.0
+742	270.0	8.20	20.0	counter rudder to port	20.0
+751	273.0	8.20	-20.0	rudder is 20° to port	23.0
+812	274.7	8.10	-20.0	3. overshoot angle (ROT=0)	24.7
+851	270.0	8.30	-20.0	passing initial heading+20°	20.0
+957	250.0	8.40	-20.0	passing initial heading	0.0
+1051	230.0	8.00	-20.0	counter rudder to starboard	-20.0
+1102	228.0	7.90	20.0	rudder is 20° to starboard	-22.0
+1128	224.2	7.80	20.0	4. overshoot angle (ROT=0)	-25.8
+1209	230.0	8.00	20.0	passing initial heading-20°	-20.0
+1313	250.0	8.40	20.0	meet her	0.0

# Lebenslauf

## Persönliche Daten

Name: Daewon Kim  
Geburtsdatum: 05.01.1983 in Daegu, Südkorea

## Beruflicher Werdegang

03.2005 – 07.2008 Hanjin Shipping & Keoyang Shipping  
- 2. Und 3. Nautische Offizier  
08.2008 – 07.2011 Korea Maritime University, Institute of Marine Traffic Safety  
- wissenschaftlicher Mitarbeiter  
10.2013 – 10.2015 Hochschule Wismar, Institute ISSIMS  
- wissenschaftlicher Mitarbeiter  
Seit 12.2018 Universität Rostock, Institut für Automatisierungstechnik  
- wissenschaftlicher Mitarbeiter

## Studium

03.2001 – 02.2005 Bachelor of Engineering  
Korea Maritime University, Department of Ship Operating System Engineering  
03.2009 – 02.2011 Master of Engineering  
Korea Maritime University, Department of Maritime Traffic Information  
Masterarbeit: „A Primary Study on the Development of Evaluation Model for Marine Traffic Safety Assessment“  
09.2011 – 08.2013 Master of Science  
Hochschule Wismar, Master Studiengang für Operation and Management of Maritime Systems  
Masterarbeit: „Optimization Methods for Modelling Simulator Ship Models of a Ferry with Two Pairs of Azimuth Propellers“